EFFECT OF BIOCERAMIC FUNCTIONAL GROUPS ON DRUG BINDING AND RELEASE KINETICS

by

Christopher Trujillo

A thesis submitted to the faculty of
The University of North Carolina at Charlotte
in partial fulfillment of the requirements
for the degree of Master of Science in
Mechanical Engineering

Charlotte

2015

Approved by:

_____
Dr. Ahmed El-Ghannam

_____
Dr. Qiuming Wei

_____
Dr. Didier Dreau

_____
Dr. Irina V Nesmelova

ABSTRACT

CHRISTOPHER TRUJILLO. Effect of bioceramic functional groups on drug binding and release kinetics.
(Under the direction of DR. AHMED EL-GHANNAM)

Bioceramics have been studied extensively as drug delivery systems (DDS). Those studies have aimed to tailor the drug binding and release kinetics to successfully treat infections and other diseases. This research suggests that the drug binding and release kinetics are predominantly driven by the functional groups available on the surface of a bioceramic. The goal of the present study is to explain the role of silicate and phosphate functional groups in drug binding to and release kinetics from bioceramics.

α-cristobalite (Cris; SiO_2) particles (90-150 μm) were prepared and doped with 0 μg (P-0), 39.1 μg (P-39.1), 78.2 μg (P-78.2), 165.5 μg (P-165.5) or 331 μg (P-331) of P_2O_5 per gram Cris, using 85% orthophosphoric (H_3PO_4) acid and thermal treatment. The material structure was analyzed using X-ray diffraction (XRD) with Rietveld Refinement and Fourier Transform Infrared (FTIR) spectroscopy with Gaussian fitting. XRD demonstrated an increase from sample P-0 (170.5373 $Å^3$) to P-331 (170.6466 $Å^3$) in the unit cell volume as the P_2O_5 concentration increased in the material confirming phosphate silicate substitution in Cris. Moreover, FTIR showed the characteristic bands of phosphate functional groups of v_4 PO4/O-P-O bending, P-O-P stretching, P-O-P bending, P=O stretching, and P-O-H bending in doped Cris indicating phosphate incorporation in the silicate structure. Furthermore, FTIR showed that the v_4 PO4/O-P-O bending band around 557.6 cm^{-1} and P=O stretching band around 1343.9 cm^{-1} increased in area for samples P-39.1 to P-331 from 3.5 to 10.5 and from 10.1 to 22.4, respectively due to

phosphate doping. In conjunction with the increase of the ν_4 PO4/O-P-O bending band and P=O stretching band, a decrease in area of the O-Si-O bending bands around 488.1 and 629.8 cm^{-1} was noticed for samples P-39.1 to P-331 from 5 to 2 and from 11.8 to 5.4, respectively. Furthermore, Cris samples (200 mg, n=5 for each sample) were immersed separately in DI water for 2 days and the concentrations of dissolved silicate and phosphate ions released from the surface of Cris were measured using Inductively Coupled Plasma – Optical Emission Spectrometry (ICP-OES). The phosphate ions released from the material activated the surface and exposed the silicate functional groups as indicated by the FTIR analysis. Pre-immersed Cris particles and control non-immersed samples (200 mg, n=5 for each sample) of particle size 90-150 μm were immersed in 2 mL of vancomycin (Vanc) solution (8 mg/ml) in PBS on an orbital shaker at 37^{o}C for 24 hours. The amount of drug bound to the material was measured by High Performance Liquid Chromatography (HPLC). Control non-immersed Cris samples P-0 and P-39.1 adsorbed a comparable amount of drug. While there was a statistically significant lower amount of drug adsorbed onto P-78.2 than that adsorbed onto P-39.1 ($p < 0.001$), comparable amounts of drug were adsorbed onto P-78.2, P-165.5, and P-331. Releasing phosphate ions from the material surface resulted in a significant increase in drug adsorption for pre-immersed samples. Higher Vanc adsorption was noticed for all pre-immersed Cris samples compared to their corresponding control non-immersed samples. Moreover, for pre-immersed samples the amount of drug adsorbed significantly increased from P-0 to P-78.2 (P-0 < P-39.1 < P-78.2; $p < 0.05$). However, at phosphate content higher than 78.2 μg per gram of Cris there was a significant decrease in drug adsorption (P-78.2 > P-165.5 > P-331; $p < 0.001$). ICP-OES analyses showed that the percent of

released phosphate ions during immersion decreased as the phosphate content in doped Cris increased (P-39.1 released 92±.08% and P-331 released 71±.05%). Therefore, the decrease in drug binding could be attributed to the presence of high phosphate content on the material surface. Comparison between the HPLC and FTIR analyses showed that ceramics that had higher content of O-Si-O bending (at ~498 cm^{-1} and ~620 cm^{-1}) bands facilitated Vanc adsorption. On the other hand surfaces with a higher content of v_4 PO_4/O-P-O bending (at ~557 cm^{-1}) and P=O stretching (at ~1343.9 cm^{-1}) bands did not enhance Vanc adsorption. Drug loaded pre-immersed and control non-immersed Cris samples (each 200 mg, n=5 for each sample) were immersed in 2 mL of PBS on an orbital shaker at 37^{o}C, and a 0.5 mL aliquot was removed from the solution and replenished at 1, 3, 6, 8, 24, and 48 hour, and every 48 hour intervals to 22 days thereafter. Drug concentration released from Cris samples after each time point was measured using HPLC. The drug release kinetics demonstrated a statistically significant decrease ($p < 0.05$) in the cumulative and percent of Vanc released from control non-immersed Cris samples P-0 (1.521 $\pm$ .026 mg; 37.66 ± .89 %) to P-331 (1.276 $\pm$ .016 mg; 33.46 ± .77 %) of Vanc, respectively. Additionally, release kinetics also demonstrated statistically significant increase ($p < 0.05$) in the cumulative and percent of Vanc released from pre-immersed samples P-0 (1.505 ± .014 mg; 33.59 ± 1.35 %) to P-331 (1.581 ± .057 mg; 42.27 ± 1.51 %) of Vanc, respectively. Furthermore, in the first 4 hours, the deceleration of drug release from sample P-0 to P-331 decreased from -66.92 to -34.07 µg of Vanc/mL /hr^2, for control non immersed Cris and from -72.60 to -46.04 µg of Vanc/mL/hr^2, for pre-immersed samples. Furthermore, during the first 4 hours of burst release the percentage of drug released from the total amount of drug loaded for non-immersed samples P-0 was

41 % and for P-331was 26 %. After the 4 hours of Vanc release the amount of Vanc available for release for samples P-0 and P-331 was .898 mg and .945 mg, respectively. The same relationship was found for pre-immersed samples during the first 4 hours of burst release the percentage of drug released from the total amount of drug loaded for samples P-0 was 42 % and for P-331 was 30 %. After the 4 hours of Vanc release the amount of Vanc available for release for samples P-0 and P-331 was .873 mg and 1.106 mg, respectively. These results indicated the effect of phosphate content on decreasing the drug release rate. The drug release kinetics study showed that the release of phosphate ions from the surface of Cris prior to drug loading exposed active silicate functional groups that enhanced drug binding by physisorption which in turn facilitated rapid release kinetics. On the other hand, a slower drug release rate was observed as the phosphate functional groups increased on the material surface due to chemisorption. Results from the present study indicate that it is possible to enhance the burst release stage of a bioceramic drug carrier by increasing the silicate functional groups. The sustained release profile can be engineered by controlling the phosphate content of the bioceramic drug carrier.

DEDICATION

I dedicate this thesis to my mom, Aniceta Castillo Rosales, and my brother, Yamil Edwin Castillo, for all their love and support that have motivated me through all my academic and non-academic endeavors.

I would also like to dedicate this thesis to my family, church family, and friends for who supported me throughout the entire process.

ACKNOWLEDGMENTS

I would like to profoundly thank my advisor, Dr. Ahmed El-Ghannam, for his support, motivation, and the wisdom he shared with me throughout the years of working in his lab. Dr. El-Ghannam's attention and passion to scientific research propelled me complete this work to the best of my abilities. I also would like to give thanks to Dr. Hernando Jose Pacheco Gomez, who also taught me how to properly conduct research in a lab, provided superb advice for my research, taught me how to operate equipment, and for his friendship. I would also like to thank Dr. Qiuming Wei, Dr. Didier Dreau, and Dr. Irina V Nesmelova for taking the time to serve on my graduate committee. Finally, I would like to thank all the professors and staff at the University of North Carolina at Charlotte that helped me with the completion of this thesis.

TABLE OF CONTENTS

LIST OF TABLES

LIST OF FIGURES

CHAPTER 1: BIOCERAMICS AS DDS

1.1 Introduction

Since the mid 1960's, when Judah Folkman and Alejandro Zaffaroni introduced the concept of controlled drug delivery system (DDS), a great amount of work has been committed to developing new and innovative ways to design DDS to deliver therapeutic agents [1]. The concept of controlled DDSs was a great step forward in medicine due to its ability to deliver a high dosage of drugs in a controlled manner to a specific site. In comparison to controlled DDSs, most traditional methods of drug delivery include injection, oral dosage, or intrusive surgeries which are effective methods, but are inefficient in delivering therapeutic agents to the targeted tissue. Traditional methods of drug delivery expose other tissues to the drug's toxicity, and second intrusive surgery may be needed to remove the implanted DDS. The difference between traditional methods of drug delivery in comparison to controlled DDS can be seen in Figure 1 (A-B) [2]. Figure 1A, is a representative graph of the drug concentration in plasma over time for traditional drug delivery methods. Multiple drug doses would be needed to keep an ideal drug concentration in the plasma thus causing a fluctuation in the drug concentration in plasma. Consequently, there would be insufficient drug for a therapeutic effect or a toxic amount of drug. In comparison, Figure 1B shows a controlled DDS which would provide a long sustained release of ideal drug dose for a determined amount of time,

which would negate the adverse effects of traditional drug delivery methods. These pressing issues with traditional drug delivery methods have spurred the interest of scientists in many fields to design new and innovative DDSs that can negate these current issues. One of these new DDS that is currently being implemented are bioceramics.

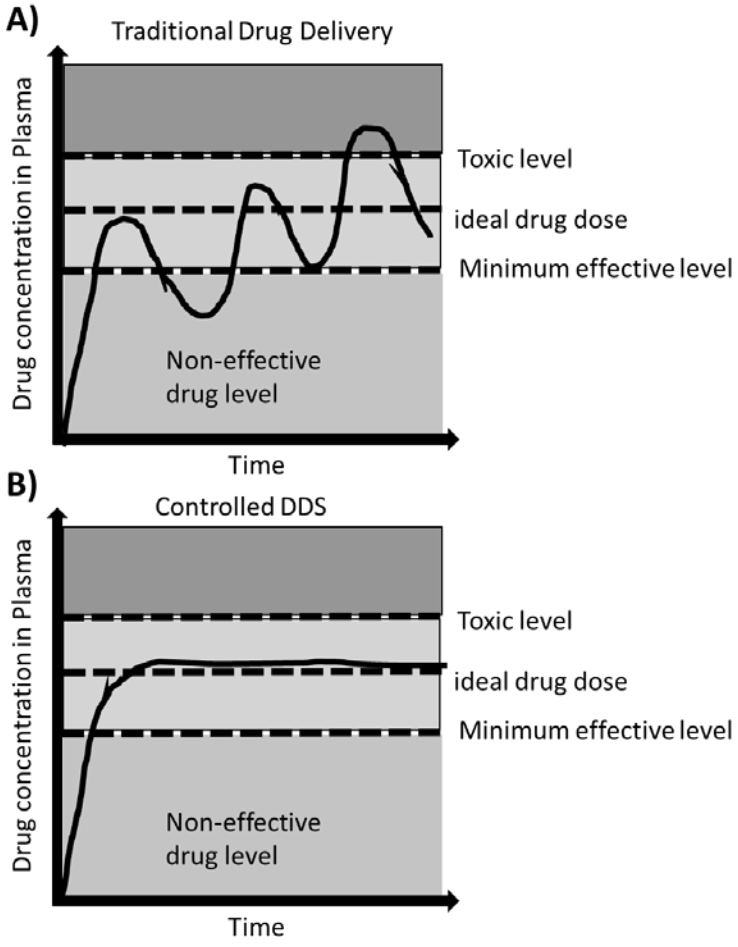

Figure 1: Representative comparison between traditional drug delivery methods and controlled DDS [2]

Current studies have focused on how bioceramics can be used as a DDS. Most of these studies concentrate on how the geometry, size, porosity and or drug loading techniques affect the adsorption and release kinetics of a therapeutic agent from a

bioceramic [3-9]. Previous studies have shown that by changing these parameters the loading and release profile of a drug by a bioceramic can be manipulated. This research although helpful does not explain how the drug and ceramic interact with each other at an atomic level. Knowing how the drug and ceramic interact at an atomic level is of utmost importance for researchers who want to tailor the drug adsorption and release to make customizable drug delivery systems. Very few researchers have explored what mechanism the functional groups on the surface of bioceramics play on the loading and release of therapeutic agents. Furthermore, through these studies it has been found that not every bioceramic and drug hybrid provides a sustained release of drug as is needed to promote a therapeutic effect. A review of current literature, was performed to give a representation of the lack of knowledge that is known on how surface functional groups contribute to the mechanism of drug adsorption and release within the field of bioceramics that are being implemented as DDSs.

1.2 Literature Review

Daculsi et. al., has completed extensive research with calcium phosphate as a DDS for Vancomycin (Vanc). The effects that different drug loading techniques such as wet granulation, isostatic compression, and dynamic compression on drug elution of Vanc from biphasic calcium phosphate (BCP) granules (200-500 μm) and calcium deficient apatite (CDA) granules (40-80, 80-200, or 200-500 μm) were analyzed [10-12]. Vanc was loaded onto all BCP samples in a 4.76 % w/w proportion. For the BCP (Ca/P= ~1.54) granules (250 mg) with wet granulation all Vanc was released in 3 days. The isostatic compression (100, 140, or 200 MPa for 2 minutes) and dynamic compaction (1.1, 1.5, or 1.9 MPa) of BCP (Ca/P= ~1.54) samples (250 mg, each) showed prolonged and complete Vancomycin release for 3 to 7 days and 4 to 6 days, respectively. It can be noted that there was not a significant change in the drug release for the samples that where compacted either by dynamic or isostatic pressure. The researchers attributed the change in drug release between the wet granulation and the compressed particles to an increase in porosity percentage for compressed particles. Although porosity plays an important role in drug release kinetics, it is curious to see how the isostatic compression samples were pressed at a much higher pressure than the dynamic compaction and a similar drug release curve was achieved.

Another study by Daculsi et. al., analyzed the effects of changing the granule size and using isostatic (150 MPa) or dynamic (2 MPa) compression would have on the release of Vancomycin from CDA (Ca/P= ~1.57) granules (2 grams). Vanc was loaded onto all CDA samples in a 5 % w/w proportion. The results show that the elution of Vanc from the CDA granules does not undergo significant changes regardless of which

compaction method was used (as in his previous studies with BCP) or the size of the granules. Furthermore the drug release only lasted 100 minutes for CDA which is an enormous difference in comparison to the previous studies done by Daculsi et. al. (even though .24 % w/w more Vanc was loaded onto CDA), where the same drug loading formulations were used on BCP and complete Vancomycin elution took 3-7 days. Interestingly, these results contradict theory which state that a smaller granule would have a greater surface area resulting in a higher drug release, and vice versa for large granules. Additionally the surface area was not measured for the BCP granules so no clear conclusion can be made if the surface area played a key role. Furthermore a greater mass of CDA-Vanc granules (2 grams) was used than for the BCP-Vanc granules (250 mg) and BCP still had a longer release of Vanc. Since these results contradict theory it signifies that there must be a different mechanism at work. In all these studies performed by Daculsi et. al., it was speculated that the nature of the bonds between the drug and ceramic played a significant role in the drug elution. XRD and FTIR analysis were used in these studies to confirm the presence of BCP and CDA phases before and after compaction had not been disrupted. However, XRD and FTIR analyses were not analyzed in such a fashion to prove their speculation, but it is assumed that the presence of phosphorous functional groups on the surface of the samples was responsible for the difference in elution of the Vanc drug from the CDA and BCP granules. This assumption could be true considering that the CDA (~1.57) sample was composed of a higher Ca/P ratio than BCP (~1.54). Which probably meant that the greater presence of phosphate functional groups in BCP was responsible for the prolonged release of Vanc.

Studies by Daculsi et. al., suggest that not every calcium phosphate material will provide the required drug elution or drug potency. For this reason it is important to study how the functional groups of a materials surface interact with different drug molecules for manipulating drug binding and elution as did Carmona et. al., in their research work. Carmona et. al., analyzed how modifying the surface functional groups of mesoporous silica samples (FBU-12 and SBA-15; 100 mg each) by adding the linkers of 3-mercaptopropyl trimethoxysilane (MPTS) or N-(2-aminoethyl)-aminopropyl dimethoxymethylsilane (APMS) affected the drug loading and release of the antibiotics of cefuroxime (5 g/L) or Vanc (5 g/L) [13]. Drug adsorption of both antibiotics onto samples with and without linkers is as follows: 1) FBU-12 and SBA-15 without any linkers had the same drug loading of cefuroxime (~5.0%); 2) The FBU-12 and SBA-15 without any linker was loaded with 18.5 and 6.0 % Vancomycin, respectively; 3) FBU-12 and SBA-15 with MPTS linker experienced the same drug loading of cefuroxime (~7%), while the Vanc drug loading was constant regardless of MPTS modification; (4) FBU-12 and SBA-15 with APMS linker loaded 12 and 13 % of cefuroxime, respectively; and (5) FDU-12 and SBA-15 with APMS linker loaded 31 and 23 % of Vanc, respectively. Inspection of the drug release curves for each sample reveal the following: 1) FDU-12 released 100% cefuroxime content in ~24 minutes, FDU-12 APMS released 8% cefuroxime in ~42 hours, and FDU-12 MPTS released 13% cefuroxime over ~75 hours; 2) FDU-12 released 100% Vanc in ~10 minutes, while FDU-12 APMS and FDU-12 MPTS materials released ~78% and ~53% Vancomycin over ~2 days, respectively; 3) SBA-15 released 100% Vanc over ~10 min and SBA-15 APMS materials released 35% cefuroxime over ~48 hours; and 4) SBA-15 released 100% Vanc in 10 mins and SBA-15

APMS released 100% Vanc over ~48 hours. The drug release of SBA-15 MPTS was not reported. The researchers attributed the increase in drug loading for the APMS and MPTS surface modified FBU-12 and SBA-15 samples to many factors including the functional groups present in the material and linker. Although there was no study of FTIR to fully explain how the functional groups of the bioceramic-linker-drug hybrid occurred. A trend is observed for all drug release profiles where the silica mesoporous bioceramic with no linker experiences a rapid drug release while the material with linker experiences a longer and more controlled drug release profile. The long term release profile as well as the drug binding can be attributed to the bond nature of the drug molecule in the presence of the carrier. In the absence of a linker the drug release is mainly governed by desorption (electrostatic) or physisorption. On the other hand the drug release in the presence of a linker is governed by chemisorption. The evidence provided by these studies strongly supports the idea that the drug release adsorption and release is highly dependent on the surface chemistry of a material. Furthermore, it is important to note that in the studies of Daculsi et. al., samples of CDA (Ca/P~1.57) and BCP (Ca/P~1.54) have a substantially longer drug elution (100 minutes, and 3 to 7 days, respectively) of Vanc in comparison to the rapid drug elution of mesoporous silica samples SBA-15 (~10 minutes) and FDU-12 (~ 10 minutes) without any linker found in the study by Carmona et. al.. The comparison of the results show that phosphate functional groups may play a role in the chemisorption of Vanc, while the silicate functional groups play a role in the physisorption of Vanc.

Doadrio et. al., studied the effect that changing the format of 0.1 g of mesoporous silica SBA-15 into a disk (13x3 mm; 3MPa) or calcined powder would have on the drug adsorption and delivery of gentamicin sulphate (GS) [14]. It was found that there was a

similar amount of drug adsorption by the powder and the disk format which was 20% and 17.5% wt, respectively. Interestingly, it was found that the release profiles for the disk and the powder had no significant difference because all the GS from both formats was released in 24 hours. Although the disk had a ~10% slower release of GS around 3 hours, but began increasing at a rate of ~1.15% per minute up to ~23 hours. The researchers attributed the difference in release rate to the smaller surface area to volume ratio of the disk in comparison to the SBA-15 powders. Curiously though the researchers only measured the surface area, and pore distribution and size of the powder and not the disk. Although this difference in drug elution could also have been attributed to a decrease in the pore size of the SBA-15 powder during isostatic compaction as noted in the previous studies done by Daculsi et. al which would also result in a slower drug elution. The results obtained from this study point out that the format of the drug delivery system did not change the drug adsorption or release significantly thus telling that the interaction between the drug molecule and the surface functional groups must play a pivotal function. It is also important to note how the SBA-15 sample in the study by Carmona et. al. released all Vanc within 10 min, and in this study by Doadrio et. al. complete GS elution is observed at 24 hours. The comparison between both studies shows that the drug elution is very much dependent on the bond made between the surface functional groups of the biomaterial and the drug, and furthermore shows that not every biomaterial-drug hybrid is ideal to deliver therapeutic agents in a controlled rate. Another study by Xia et. al., began to give an insight to how the surface functional groups may play a significant role in drug adsorption and elution.

Xia et. al., studied how changing the manufacturing technique, chemistry, and the drug release medium of a material effected the drug adsorption and delivery of gentamicin from a mesoporous bioactive glass (MBG) [15]. MBG powders of M58S (Si/Ca/P=58:23:9, weight ratio) and M77S (Si/Ca/P=77:23:9, weight ratio) were created using a two-step acid-catalyzed self-assembly process combined with a thermal treatment inorganic-organic system. The bioactive glass powder 58S (Si/Ca/P=58:23:9, weight ratio) was derived using the sol-gel method. It was found that the drug adsorption of 58S, M58S, and M77S was 10.3$\pm$3.7, 36.4$\pm$1.8, and 48.6$\pm$2.4 wt. %, respectively. It is important to notice how the drug adsorption increased as the silicate content increased in the samples. The drug release curves in water after 20 days for 58S, M58S, and M77S show that the cumulative release of GS was 56%, 47%, and 36%, respectively. For the samples 58S, M58S, and M77S of that were immersed in SBF for 20 days the cumulative release of GS was 85 %, 60%, and 69%, respectively. According to the authors, the drug adsorption and release of the different MBG powders was attributed to the surface area, pore volume, and pH of the medium in which the drug release occurred. It was noted that as the surface area and pore volume increased the drug adsorption and release increased. Furthermore it was found that as the pH value decreased the drug release increased.

XRD analysis, was used to verify the presence of the material phases, but did not perform any additional analysis on how the crystal structure may have changed due to the difference in composition between 58S, M58S, and M77S. Additionally the authors used FTIR to study the chemical composition of M58S with and without GS to give a qualitative explanation to how the surface functional groups of Si-OH and P-OH of tetraethyl orthosilicate and trithyl phosphate, respectively, interacted with the amino and

hydroxyl groups of GS. By analyzing the FTIR spectra the authors found that the silanol functional group band at 964cm^{-1} decreased significantly after the drug loading had been accomplished. Which meant that the drug was bonding to the silicate functional groups. From these results they concluded that the availability of the silanol functional groups on the surface of the material played a significant role for drug to material interaction. They speculated that the increase in surface area and silica content of M58S to M77S caused the increase in drug adsorption due to the higher availability and ease of access of the silanol functional groups on the surface to the GS drug molecules. It would have been helpful for the researchers to study M77S using FTIR to provide a stronger case for their speculation, and to measure the area under the Si-OH band in the FTIR to quantify the change in the area or shift in energy. Another study that reinforces the idea that the material to drug affinity plays a key role in drug binding and release is the study by Mir et.al., in which the drug adsorption and release of three different antiobotics (Amoxillicon, gentamicin, and Chloramphenicol) from CDA (Ca/P=~1.52) was studied. 0.4 mL of each antibiotic was loaded separately onto each batch of CDA powder [16]. The drug release profiles are highly similar regardless of what drug was loaded and in addition all CDA granules release the drug in 50 hours. The FTIR shows that even when the antibiotics were loaded there was no change or shift in the CDA peaks which meant there as little to no interaction between the CDA and the drug molecules as reported by the authors. Furthermore the XRD did not show any change in the peaks due to the drug loading. The surface area was not measured in this study, but because all the CDA powder is from the same batch it can be assumed that all the powder had the same area and pores size, which meant that all samples would follow a similar drug diffusion. This

drug release kinetics study indicates that the drug release is highly dependent on the surface functional groups present on the CDA, because all drug loaded materials experienced similar drug release regardless of which drug was loaded.

Additionally El-Ghannam, studied the effects that the chemical composition, thermal treatment on crystallization, and the mechanism of phase transformation on silica calcium phosphate nanocomposite (SCPC) would have on bone regeneration [17]. In this study El-Ghannam made SCPC samples containing different mole % of CaO, SiO_2, P_2O_5, and Na_2O. The SCPC samples synthesized were C1S3 (CaO= 10.1%, SiO_2= 63.7%, P_2O_5=5.0%, and Na_2O=21.1%), C1S1 (CaO= 23.2%, SiO_2= 49.0%, P_2O_5=11.5%, and Na_2O=16.3%), and C3S1 (CaO= 40.6%, SiO_2= 29.2%, P_2O_5=20.5%, and Na_2O=9.7%). All these samples were loaded with fetal bovine serum. As in the results of previous studies El-Ghannam's results showed that the amount of protein adsorbed onto SCPC samples C1S3, C1S1 and C3S1 decreased as the phosphate content increased (5.0%, 11.5%, and 20.5%, respectively) and vice versa for silicate content (63.7%, 49.0%, and 29.2%, respectively) [10-12, 15]. The studies reviewed strongly support the idea that the surface functional groups play a major role in the ability of a material to adsorb and release therapeutic agents.

1.3 α-cristobalite (Cris)

Cris, a ceramic with a white to yellowish color, was first discovered in Cerro San Cristobal, Mexico and is naturally found in vesicles and lithophysae, as a late-crystallizing phase in basaltic to rhyolitic volcanic rocks, acid-sulfate-type hydrothermal alteration of volcanic rocks, precipitation of hot springs, contact metamorphism of sandstone, and siliceous sedimentary rocks which have recrystallized [18]. Cris is formed when β-cristobalite, a high temperature (≥1470^{o}C) and low pressure polymorph of silicon dioxide (SiO_2), under goes a phase transition at 275^{o}C or upon cooling to metastable Cris. Cris consists of a three-dimensional framework of corner-bonded tetrahedra and a tetragonal unit cell structure [19]. The space group of the Cris tetragonal unit cell is $P4_12_12$ and the lattice parameters of Cris a, b, c, α, β, and γ are ~4.98 Å , ~4.98 Å , ~6.95 Å , 90^{o}, 90^{o}, and 90^{o}, respectively (Figure 2) [19]. Furthermore, Cris is also a brittle material with a hardness of 6-7 on the Mohs Hardness Scale [18]. The lattice parameters and other information regarding the crystallographic structure of Cris can be found on the PDF card # 00-039-1425.

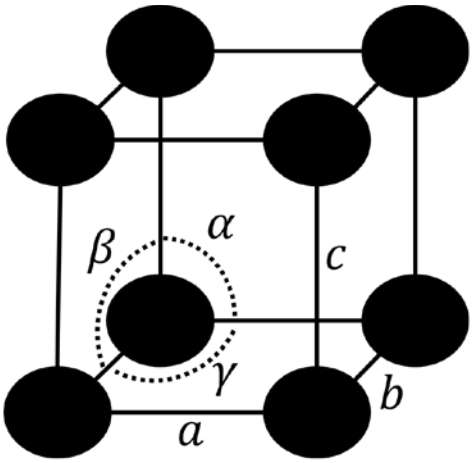

$$a = b = \sim 4.98\,\text{Å}; c = \sim 6.95\,\text{Å}$$
$$\alpha = \beta = \gamma = 90^{o}$$

Figure 2: Unit cell with unit cell parameters of Cris

1.4 Hypothesis

The silicate surface functional groups of Cris ceramic can be modified via phosphate doping to modify the drug adsorption and release kinetics of Vanc.

1.5 Objectives

The purpose of the present study is to analyze the effects that silicate and phosphate functional groups have on the drug adsorption and release of Vanc. Cris, was selected for this study because of its high chemical stability, and simple crystalline structure which makes it an ideal candidate to analyze the effects of silicate and phosphate functional groups on drug adsorption and release kinetics. Furthermore, silicate (base material) and phosphate (dopant) functional groups are commonly found in other biomaterials (calcium phosphate, silica mesoporous, bioactive glass, and many more) making this study relevant to the field of bioceramics used as DDSs as a whole. Additionally, both silicate and phosphate ions obey the Hume-Rothery rules of substitutional solid solution formation because they have a similar atomic radius, same crystal structures, similar valency, and electronegativity. Vanc, a trycyclic glycopeptide antibiotic that was developed and released in the 1950's, was selected because it is commonly used to treat aerobic gram-positive infections that are difficult to treat [20-22]. There has been many studies that speculate the importance of surface functional groups on drug adsorption and release, but have not shown the required depth of analysis to explain how the material and drug interaction occur when explaining the drug adsorption and release kinetics. In this study, highly stable porous Cris particles (90-150μm) were prepared and doped with 0 μg (P-0), 39.1 μg (P-39.1), 78.2 μg (P-78.2), 165.5 μg (P-165.5) or 331 μg (P-331) of P_2O_5 per gram Cris, using 85% orthophosphoric (H_3PO_4) acid and heat treatment at 1000^oC/3hr to promote silicate phosphate ionic substitution. X-ray Diffraction (XRD) with Rietveld Refinement was used to analyze the crystalline structure of Cris before and after doping. Fourier Transform Infrared spectrometry (FTIR) with Gaussian fitting was used to study surface chemistry

after doping. Cris samples were immersed separately in DI water and the concentrations of Si and P ions in the immersing solution were measured using inductively coupled plasma optical emission spectroscopy (ICP-OES) after 2 days. FTIR was used to study the surface chemistry of the Cris samples after immersion. Pre-immersed Cris particles and control non-immersed samples (200 mg, n=5 of each sample) of particle size 90-150 μm were immersed in 2 mL of Vanc solution (8 mg/ml) in PBS on an orbital shaker at 37^{o}C for 24 hours. The drug concentration was measured by HPLC for control non-immersed and pre-immersed Cris samples, and the amount of drug adsorbed on the material surface was calculated. The affect that drug binding had on the surface chemistry of non-immersed and pre-immersed Cris samples was analyzed using FTIR. Drug loaded control non-immersed and pre-immersed Cris samples (each 200 mg, n=5 for each sample) were immersed in 2 mL of PBS on an orbital shaker at 37^{o}C, and a 0.5 mL aliquot was removed from the solution and replenished at 1, 3, 6, 8, 24, and 48 hr, and every 48 hour intervals to 22 days thereafter. Statistical analysis was completed using the student's t-test, and all p values below 0.05 were considered statistically significant. The role that the surface functional groups of silicate and phosphate play on drug adsorption and release of Vanc from bioceramics was analyzed experimentally.

CHAPTER 2: MATERIALS AND METHODS

2.1 Ceramic Material Preparation

Commercial crystalline quartz (Geleste, INC.) was mixed with DI water to make a quartz powder slurry. The slurry was placed in 50 mL test tubes and dried in a Thermocenter TC160 oven (SalvisLab) at 80^{o}C. The dried quartz ceramic was then removed from the test tubes and placed into an alumina crucible and heat treated in a Thermo Scientific Thermolyne furnace at 1150^{o}C, holding for 6 hours (Figure 3). Quartz ceramic was then heated in a high temperature tubular furnace at 1500^{o}C holding for 8hrs to transform quartz to Cris. Cris was grinded using an agate mortar and pestle and sifted to obtain a granule size of 90-150 μm. The 90-150 μm particle size was used for all studies in this work.

Figure 3: Thermo Scientific furnace used to synthesize quartz and dope Cris

2.2 Rationale for Selecting the Phosphate Doping Dose in Cris Samples

The objective of Cris doping was to induce silicate and phosphate ionic substitution to create a substitutional solid solution without forming a secondary phase. The ideal temperature for heat treatment and content of phosphate dopant needed to be verified. 9 grams of Cris (250-150 μm) were blended with 9 ml of 85% orthophosphoric acid aqueous solution (Alfa Aesar, H_3PO_4) and left under a vented hood to dry. The calculated amount of P_2O_5 to be doped in cristobalite was 8.39 mg of P_2O_5 per gram of Cris. Next, 3 gm of Cris-dried Phosphoric acid mixture were pressed into disks (1" dia x .25" height) using a 1" carbide (440 stainless steel) die and Carver hydraulic press by applying 52 MPa. Each disk was heated at different thermal treatments of 600^{o}C/3hr, 800^{o}C/3hr, and 1000^{o}C/3hr, respectively. The crystal structure of doped Cris was analyzed using XRD analysis and the phases present were verified using the PDF cards for silicon phosphate (SiP_2O_7; PDF card # 00-039-0189) and Cris (PDF card # 00-039-1425). The sample heated at 600^{o}C/3hr showed peaks belonging to the secondary crystalline phase of (SiP_2O_7) at ~24 and ~28^o (Figure 4A). The sample heated at 800^{o}C/3hr also showed peaks belonging to the secondary crystalline phase SiP_2O_7 at ~24, ~28, ~38 and ~48^o (Figure 4B). The sample heated at 1000^{o}C/3hr showed the formation of an amorphous phase hump from ~15 to ~35^o but no peaks belonging to SiP_2O_7 (Figure 4C). From the XRD analysis the following observations were made: 1) thermal treatment of 1000^{o}C/3hr should be used to dope Cris, due to the disappearance of the crystalline SiP_2O_7 phase; and 2) The content of phosphate should significantly be decreased to avoid the formation of crystalline or amorphous secondary phases. To conclude this section it was decided that the thermal treatment for doping would be 1000^{o}C/3hr, surface area of

the particles was going to be increased by using a different Cris particle size (90-150 μm) to further promote silicate to phosphate ionic substation, and Cris samples would contain 0 μg (P-0), 39.1 μg (P-39.1), 78.2 μg (P-78.2), 165.5 μg (P-165.5) or 331 μg (P-331) of P_2O_5 per gram Cris to avoid the formation of a secondary phase.

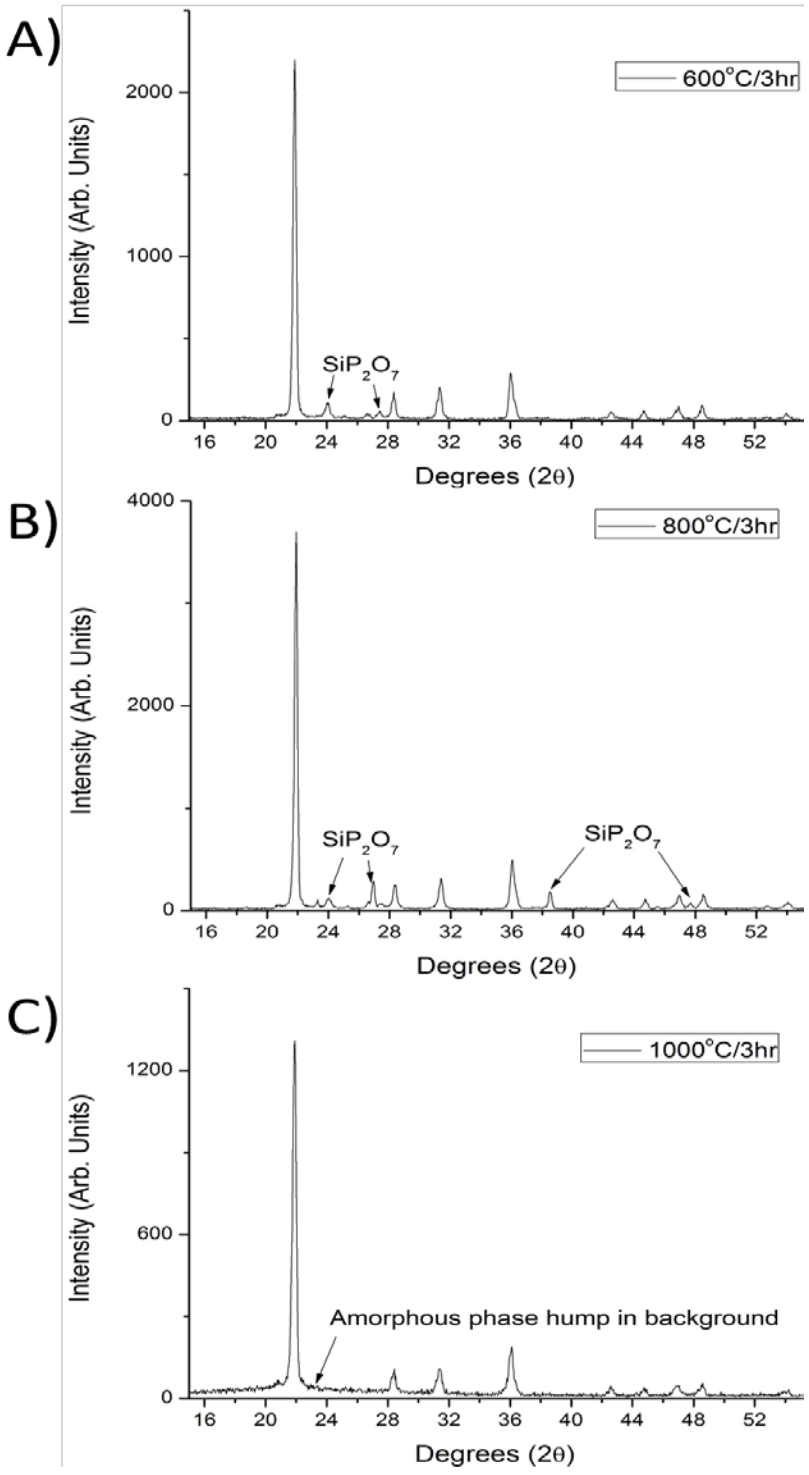

Figure 4: Cris doped with 8.39 mg of P_2O_5 per gram of Cris and thermally treated at A) 600°C/3hr, B) 800°C/3hr, and C) 1000°C/3hr

2.2 Preparation of Doped Cris

Four, 6 gram batches of Cris granules (90-150 μm) were blended with 6 mL of 85% orthophosphoric acid aqueous solution (Alfa Aesar, H_3PO_4) via direct impregnation with 0 μg (P-0), 39.1 μg (P-39.1), 78.2 μg (P-78.2), 165.5 μg (P-165.5) or 331 μg (P-331) of P_2O_5 per gram of Cris and left under a vented hood to dry. After each batch of Cris and P_2O_5 mixture had dried 2 three gram disks were made of each sample by pressing the ceramic into 1" disks in a Carver hydraulic press (Figure 5) by applying 52 MPa and using a 1" carbide die (as in section 2.1). The Cris and orthophosphoric acid disks were heat treated at 1000^{o}C holding for 3 hours to promote silicate and phosphate ion substitution in the Cris lattice structure.

Figure 5: Carver hydraulic press

2.3 Ceramic Material Structure Analysis Before and After Phosphate Doping

2.3.1 X-ray Diffraction (XRD) Analysis

The crystalline phases and modification of the crystalline structure of Cris before and after P doping was analyzed by XRD using PANalytical's X'Pert PRO Materials Research Diffractometer (PANalytical, Westborough, MA) (Figure 6). The XRD copper radiation (λ=1.54059 Å) was set to a current of 45 kV and tension of 40 mA. Doped and non-doped Cris particles in the size range of 90-150 um were ground down separately in an agate mortar and pestle into a fine powder. The powder of each sample was loaded onto a silica disk zero background holder and pressed into the holder using a flat surface. The sample loaded into the zero background disk was then locked into the XRD sample stage. The triple-beam axis analyzer setting was used for the analysis of all samples. The following optics settings were used to ensure the highest signal to noise ratio of the diffraction spectra: 1) incident beam optics used a Ni 0.02mm attenuator and a 1^{o} divergence fixed slit; 2) The diffracted beam optics had no receiving slit but did have a 0.04 rad soller slit. Cris samples were analyzed between the 2θ range of 15^{o} to 55^{o} with a step size of 0.02^{o}, time step of 2 seconds, and a scan speed of 0.01 ^{o}/s. The synthesis of Cris was verified using PDF card # 00-039-1425. The X'Pert HighScore Plus program was used to perform the Rietveld Refinement method to analyze the lattice parameters of the XRD patterns. The XRD diffractogram of each sample was fitted with the low Cris standard. Pseudo-Voigt was used as the profile function to fit the peaks and the Newton-Raphson method for least squares fit was implemented. Statistical R-indices lower than 10 were taken as acceptable data [23].

Figure 6: PANalytical's X'Pert PRO materials research diffractometer

2.3.2 Surface Chemistry Analysis

FTIR was utilized to study the changes in surface chemistry of non-doped and doped Cris samples due to phosphate doping by the diffuse reflectance mode with FTIR grade KBr using a Nicolet 6700 FTIR (Figure 7). KBr, was grinded to a fine powder then loaded into the sample holder using a spatula to make a flat consistent medium inside the sample holder. The KBr was used as the background and collected from 400 to 4000 cm^{-1} range after 64 scans at a 2 cm^{-1} resolution. To analyze the samples FTIR grade KBr was grinded in an agate mortar and pestle and loaded into the sample holder using a spatula. Afterwards the sample (not grinded) was loaded on top of the KBr already present in the sample holder. Infrared spectra for each sample was collected in the 400 to 4000 cm^{-1} after 200 scans at a 2 cm^{-1} resolution range. Omnic software was used to measure the position and area under the silicate and phosphate functional characteristic bands. Also the Omnic software's Gaussian fitting method was used to reveal and verify all silicate and phosphate functional band positions and area in the FTIR spectra of each sample to obtain a better understanding of the change in the silicate structure due to phosphate doping. The parameters applied on the Gaussian fitting were as follows: 1) a full width half height (FWHH) of 15; 2) no baseline; 3) low sensitivity; 4) noise target of 10; and 5) find peaks set to Gaussian. A standard error value near 0.05 was taken as acceptable data.

Figure 7: Nicolet 6700 FTIR

2.3.3 Surface Morphology Analysis

Cris particles of each sample were spread onto separate pieces of copper tape on top of separate JEOL, aluminum specimen mounts (Ø 12.2 x 10 mm). Each sample was then coated with a 10 nm thick coat of gold (Au) using the Denton Desk IV Sputter Coater. The rotation and sputter set point for the Denton Desk IV Sputter Coater were 30 and 15 %, respectively. The surface morphology of samples before and after phosphate doping were analyzed using the JEOL JSM 6480 scanning electron microscopy by taking images at 2500x and 4kV.

2.4 Corrosion Analysis Before and After Phosphate Doping

Dissolution kinetics of doped and non-doped Cris in DI water were analyzed using the Perkin Elmer ICP-OES Optima 2100 (Figure 8). 200 mg of each ceramic sample and its replicates (n=5) were placed into a 15 mL test tube and immersed in 10 mL of DI water. Samples were then placed on an orbital shaker inside an incubator at 37^{o}C. The samples were left in the incubator for a period of 2 days. DI water was removed from the samples after the 2 day immersion period and used to measure the silica and phosphorous ion concentration at wavelengths of 251.611 and 213.617 nm, respectively. The peristaltic pump was set at a flowrate of 1.5 mL/min. Commercial standards of silica (Aldrich; 10000 ppm silicon ICP/DCP standard solution) and phosphorous (Aldrich; 10000 ppm phosphorous ICP/DCP standard solution) were diluted with 1% nitric acid to make standards for the corrosion analysis. Standards for silica were made at the following concentrations: 10, 5, 2.5, 0.5, 0.25, 0.125, 0.05, 0.025, 0.0125, 0.005, 0.0025, 0.000125, 0.000025, and 0.000013 ppm. Standards for phosphorous were made at the following concentrations: 100, 10, 5, 2.5, 1, 0.5, 0.25, 0.05, 0.025, 0.005, 0.0025, 0.0005, and 0.00025 ppm. Samples were prepared by using a 1:5 dilution factor using 1% nitric acid.

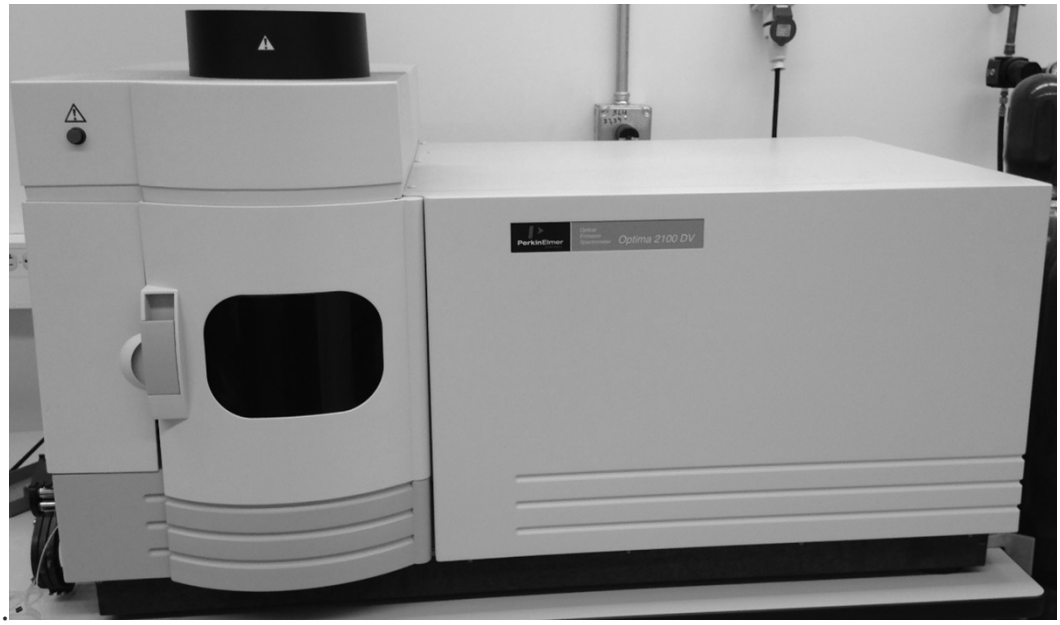

Figure 8: Perkin Elmer optical emission spectrometer Optima 2100 DV

2.5 Surface Chemistry Analysis for Pre-Immersed Cris

FTIR analysis was performed on all pre-immersed Cris samples by the diffuse reflectance mode with FTIR grade KBr using the Nicolet 6700 FTIR to study the effects of releasing the phosphate from the surface of the Cris particles after immersion in DI water. The KBr standard and samples were analyzed as previously mentioned in section 2.3.2. Furthermore, Gaussian fitting was performed as in section 2.3.2.

2.6 Drug Adsorption and Release Kinetics of Non-Immersed and Pre-Immersed Cris

Each sample (non-immersed and pre-immersed samples of P-0, P-39.1, P-78.2, P-165.5, and P-331) had 5 replicates for the drug loading and drug release kinetics study.

2.6.1 Vancomycin Adsorption onto Cris Surface

216 mg of Vanc were dissolved in 27 mL of phosphate buffered solution (PBS; pH 7.4; 1X) and stirred in a magnetic stirrer to make an 8 mg/mL solution of Vanc. PBS was composed of the inorganic salts of potassium phosphate monobasic (KH_2PO_4), sodium chloride (NaCl), and sodium phosphate dibasic (Na_2HPO_4-$7H_2O$) at the concentrations of 144, 9000, and 795 mg/L, respectively. Next, 200mg of each non-immersed and pre-immersed Cris sample was immersed into 2 mL of 8mg/mL Vanc for 24 hours. After the immersion period the remaining drug solution was removed and stored in a snap cap micro centrifuge tube and the Cris particles were left under a vented hood to dry. Micro centrifuge tubes containing the drug aliquot from each sample were centrifuged in the Eppendorf Centrifuge 5424 for 3 minutes at 5000 rpm. The samples were then diluted at a 1:2 dilution factor using a 5% mM KH_2PO_4 aqueous solution. Standards were prepared by reconstituting HPLC grade Vancomycin with PBS to make an 8 mg/ml Vancomycin solution. The following standards were made by using the 8 mg/ml Vancomycin solution by dilution with PBS: 6 mg/ml, 4mg/ml, 2 mg/ml, 1 mg/ml, 0.5 mg/ml, 0.25 mg/ml, 0.125 mg/ml, 0.0625 mg/ml, and 0.03125 mg/ml. The standards were used to create a calibration curve of Vanc concentration versus area under the curve. All sample concentrations were determined by using the calibration curve. Drug loading was measured using the Agilent Technologies 1200 Series HPLC (Figure 9). Mobile Phase A, was a 5% mM KH_2PO_4 aqueous solution, and mobile phase B was 100%

acetonitrile. The needle sampler was set to remove 50 μL of all samples with a needle wash in between samples. The column used was an Eclipse XDB-C18 column (4.6 X 150 mm; 5 um). The drug molecule was detected with UV absorbance at 282 nm. The pump was set at a flow rate of 1.5 ml/min with the following gradient conditions as seen in Table 1.

Figure 9: Agilent Technologies 1200 series HPLC

Table 1: Pump setup for HPLC analysis

Time (min)	**Flow rate (mL/min)**	**% of Mobile Phase A (5% mM KH_2PO_4 solution)**	**% of Mobile Phase B (100% HPLC grade acetonitrile)**
0	1.5	80	20
4.0	1.5	80	20
4.5	1.5	0	100
7.0	1.5	0	100
7.5	1.5	80	20
9.0	1.5	80	20

2.6.2 Vancomycin Drug Release Kinetics

200 mg of each drug loaded non-immersed and pre-immersed Cris sample was immersed in 2 mL of PBS and placed on an orbital shaker inside an incubator at 37^{o}C. A .5 mL aliquot was removed from the samples and replenished at 1, 3, 6, 8, 24, 48, and at 48 hour intervals to 22 days thereafter. Drug release kinetics were measured using Agilent Technologies 1200 Series HPLC using the same method and pump settings described in section 2.6.1 and Table 1, respectively.

2.7 Surface Chemistry Analysis after Drug Adsorption

FTIR analysis was performed on all non-immersed and pre-immersed Cris samples that were Vanc loaded by the diffuse reflectance mode with FTIR grade KBr using a Nicolet 6700 FTIR to study the mechanism of drug binding between Vanc and the silicate and phosphate functional groups. The KBr standard and samples were analyzed as previously mentioned in section 2.3.2. Furthermore, Gaussian fitting was performed as in section 2.3.2.

2.8 Statistical Analysis

A p-value of <0.05 was considered statistically significant for all work performed in this research.

CHAPTER 3: RESULTS

3.1 Ceramic Material Structure Analysis Before and After Phosphate Doping

XRD, FTIR, and SEM was used to characterize Cris and verify any changes that may have occurred to the silicate structure due to phosphate doping. XRD was used to study the modification of the crystallographic structure of Cris before and after doping. FTIR was used to analyze changes in the silicate chemical structure of Cris that may have occurred. SEM was used to study the surface morphology of samples before and after doping.

3.1.1 X-ray Diffraction Analysis

Analysis of the XRD pattern in Figure 10, using PDF card # 00-039-1425, confirmed that Cris had been synthesized using the processes described in section 2.1.

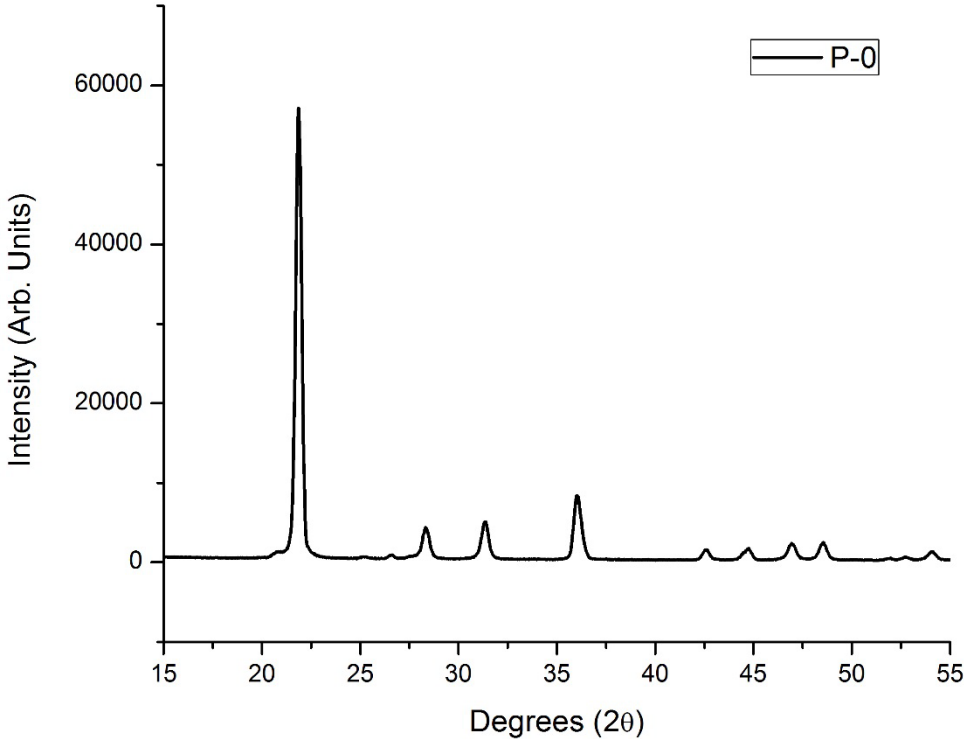

Figure 10: XRD pattern of P-0

The XRD pattern of Cris samples non-doped and doped with phosphate are depicted in Figure 11. Normally changes in the crystal lattice structure can be verified by shifting that occurs in the XRD pattern, but due to the miniscule dopant that was introduced in all the samples, Rietveld Refinement was used to verify the miniscule changes in the crystal structure by calculating the crystal lattice parameters (a, b, and c) and unit cell volume of non-doped and doped Cris to see if any changes occurred due to silicate phosphate ion substitution.

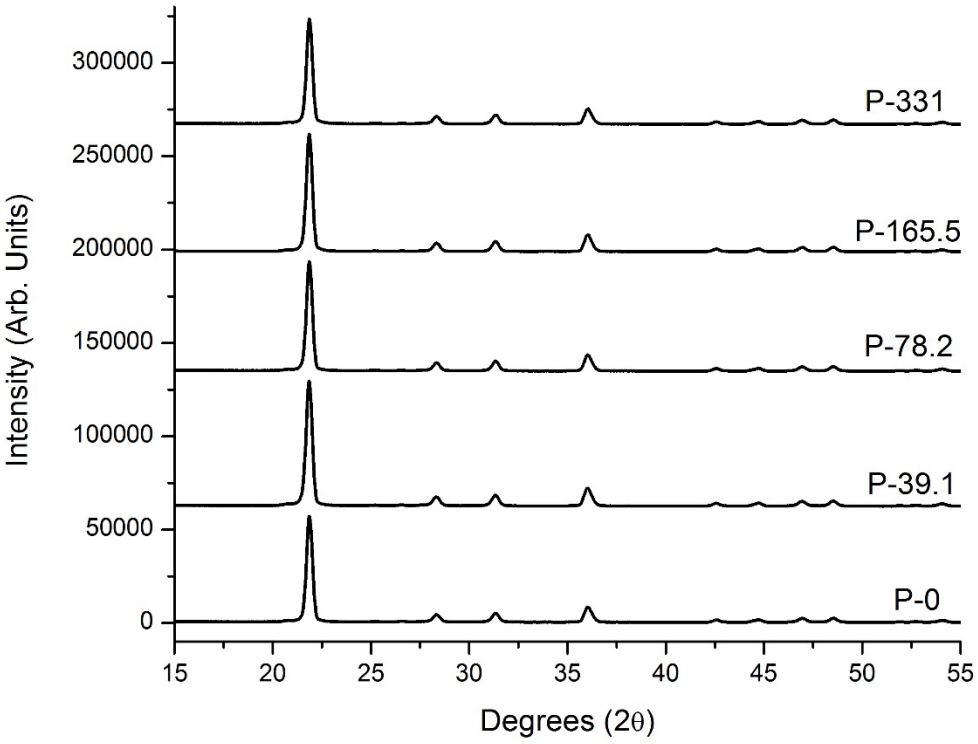

Figure 11: XRD patterns of Cris samples P-0, P-39.1, P-78.2, P-165.5, and P-331

The crystal lattice parameters (a, b, and c) and unit cell volume of the Rietveld Refinement for Cris samples can be found in Table 2. The statistical R factors of the Rietveld refinement can be found in Table 3. XRD demonstrated an increase from sample P-0 (170.5373 $Å^3$) to P-331 (170.6466 $Å^3$) in the unit cell volume as the P_2O_5 concentration increased in the material confirming phosphate silicate substitution in Cris. The change in the unit cell volume can be accounted to the difference in size ionic radii of phosphate (P^{-3}; 2.12 Å) and silicate ($Si^{+}4$; 0.4 Å) ions [24]. The values of unit cell volume for the samples in this study that were grinded and pressed at 52 MPa are viable, because they are between the values of unit cell volume found in the studies by R.L. withers et. al. and J.B. Parise et. al. in which no pressure was applied and 60 MPa were applied, respectively [19, 25]. The change in the crystal lattice parameters and unit cell

volume for the samples of Cris proves that a silicate and phosphate ionic substitution occurred.

Table 2: Pressure applied, crystal lattice parameters, and unit cell volume of Cris samples

Sample	**Pressure Applied (MPa)**	**a (Å)**	**b (Å)**	**c (Å)**	**Volume ($Å^3$)**
Cris [19]	0	4.98	4.98	6.95	172.36
Cris [25]	60	4.9226	4.9226	6.8173	165.199
P-0	0	4.96359	4.96359	6.92193	170.5373
P-39.1	52	4.96339	4.96339	6.92200	170.5212
P-78.2	52	4.96389	4.96389	6.92267	170.5764
P-165.5	52	4.96418	4.96418	6.92321	170.6086
P-331	52	4.96473	4.96473	6.92316	170.6466

Table 3: Statistical R factors of Rietveld Refinement of non-doped and doped Cris

Sample	**R_{wp}**	**$R_{expected}$**	**$R_{profile}$**
P-0	9.12512	2.69640	6.36517
P-39.1	9.73720	2.47484	6.68548
P-78.2	9.09439	2.67744	6.03247
P-165.5	8.71943	2.56755	6.12625
P-331	8.72384	2.66819	6.10139

3.1.2 Surface Chemistry Analysis

Figure 12, below shows a representative FTIR spectra of Cris samples before immersion in DI water. Lines (1), (2), (3), and (4) are areas with visible changes due to the increase in phosphate content in the samples P-0 to P-331. Line (1) shows a decrease in the intensity and area of the O-Si-O bending band at 488 cm^{-1}. Line (2) shows the increase in intensity and area of the ν_4 PO_4/O-P-O bending band located at 588 cm^{-1}. Line (3) shows a decrease in the intensity and area of the Si-O-Si symmetric and asymmetric stretching bands located at 1017and 1119 cm^{-1}, and 1192 cm^{-1}, respectively. Line (4) shows an increase in intensity and area of the P=O stretching bands at 1331 cm^{-1}.

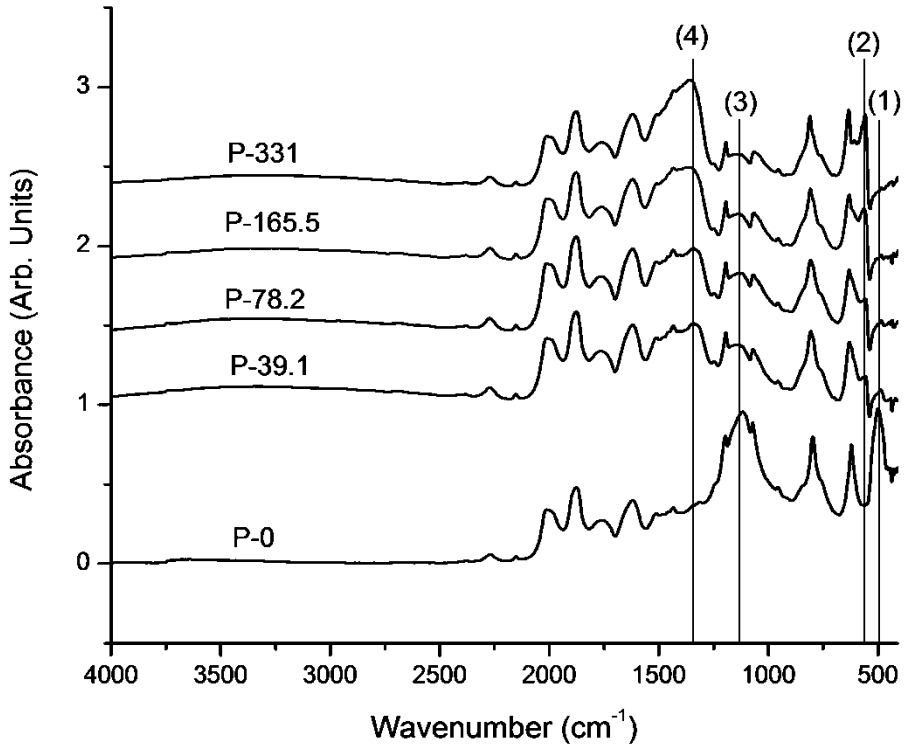

Figure 12: Stacked FTIR spectra normalized to the highest peak intensity and base line corrected of all Cris samples showing changes in the silicate structure due to phosphate doping

Figure 13 (A-E) and 14 (A-E) show the Gaussian fitting of the FTIR spectra found in Figure 12 from 1230-470 cm^{-1} and 1560-1185 cm^{-1}, respectively.

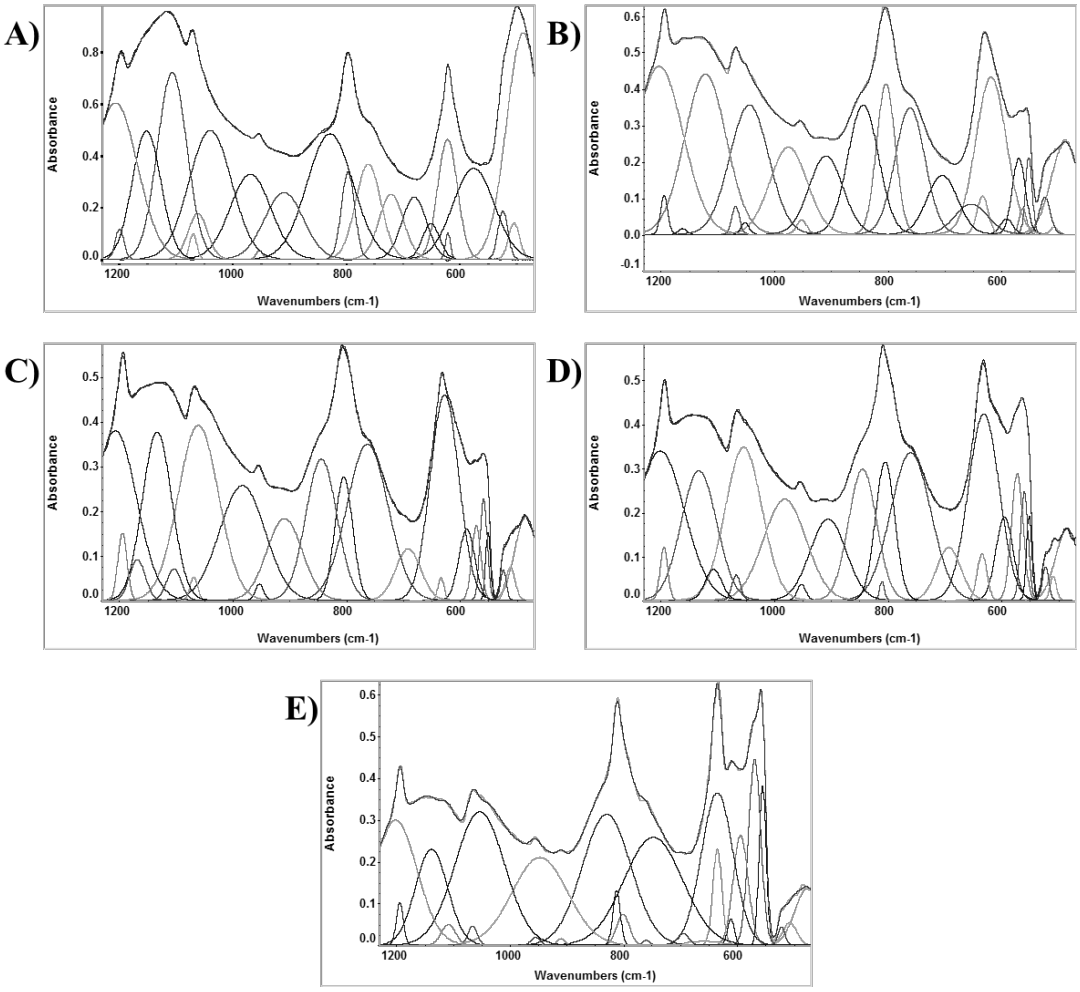

Figure 13: Gaussian peak fitting normalized to the highest peak intensity and base line corrected FTIR Spectra of A) P-0, B) P-39.1, C) P-78.2, D) P-165.5, and E) P-331 from 1230 to 470 cm^{-1}

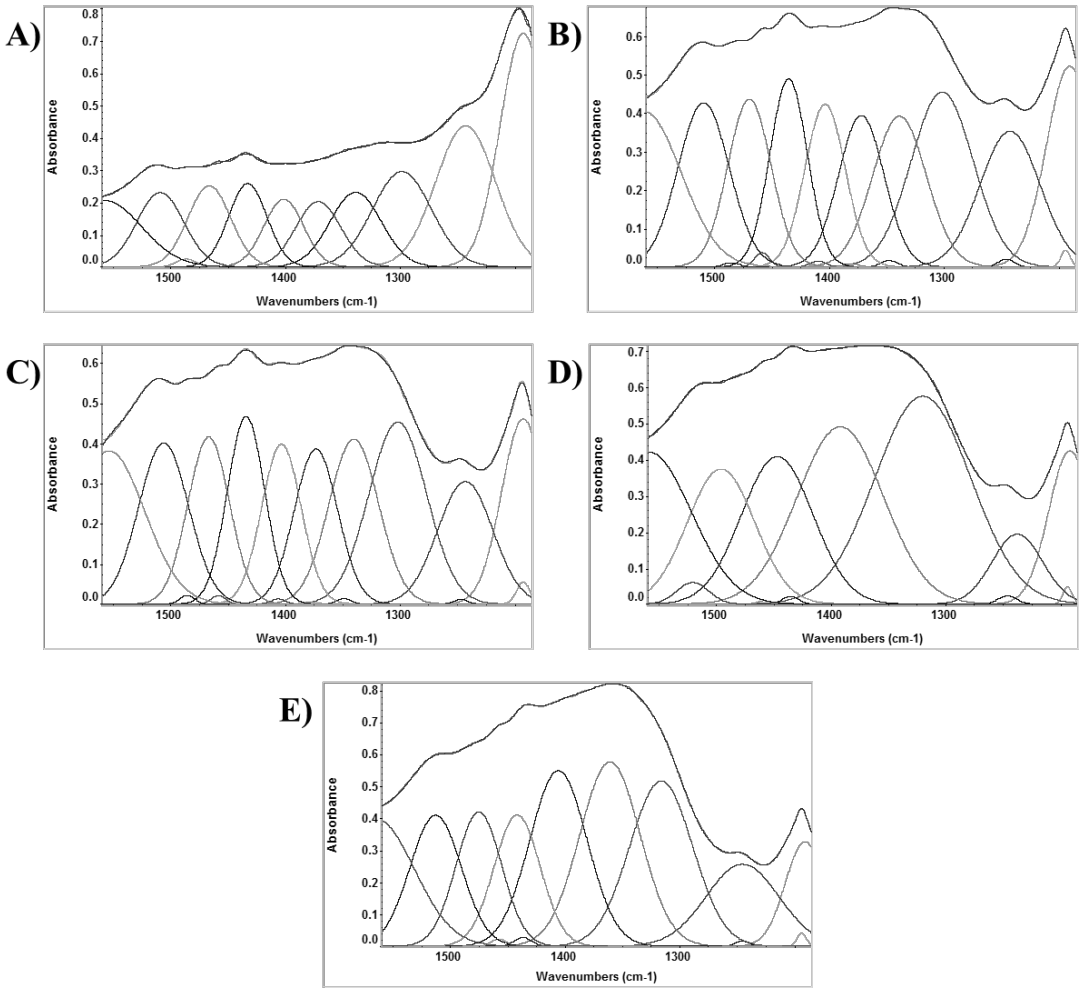

Figure 14: Gaussian peak fitting normalized to the highest peak intensity and base line corrected FTIR Spectra of A) P-0, B) P-39.1, C) P-78.2, D) P-165.5, and E) P-331 from 1560 to 1185 cm^{-1}

The peak positions and areas before (no G-fit) and after (G-fit) Gaussian Peak fitting for samples P-0, P-39.1, and P-78.2 before immersion in DI water are documented in Table 4. The peak positions and areas before and after Gaussian Peak fitting for samples P-165.5 and P-331 before immersion in DI water are documented in Table 5.

Table 4: Peak positions and areas before and after Gaussian peak fitting for samples P-0, P-39.1, and P-78.2

		Wavenumbers (cm^{-1})					
		band position/area					
Functional Group	**Assignment**	**P-0 (no G-fit)**	**P-0 (G-fit)**	**P-39.1 (no G-fit)**	**P-39.1 (G-fit)**	**P-78.2 (no G-fit)**	**P-78.2 (G-fit)**
O-Si-O bending	490, 500 [26-28]	498.4/23.6	488.8/64.3, 504.9/3.3, 524.6/4	488.1/5	487.9/15.8, 508/0.2, 524/2.4	486.6/3.8	484.3/9, 511.4/1.5, 523.9/0.8
HPO_4	551 [29-31]	none	none	none	552.2/3	none	550.8/1.5
$v_4 PO_4$/ O-P-O bending	567, 572, 602 [29-31]/ 577,597 [32]; 560 [33, 34]	none	none	557.6/3.5	562.7/1.1, 569.9/6.0 591.4/1.1	560.1/4.0	558.6/3.5, 571.5/3.3, 588.2/5.5
O-Si-O bending	620 [26-28]	621.6/13.7	576.1/31.9, 621.5/1.1, 622.1/20.1, 651.3/5.1, 680.8/13	629.8/11.8	618.6/28.8, 653.6/5.9	631.4/10.4	627.4/28.8
P-O-P stretching	758.9 [32]; ~650, ~700 [33]	none	none	698.6/.02, 756.9/.5	633.6/2.5, 704.6/10.8	757.4/0.5	633.7/0.6, 691.5/6.4
Si-O-Si symmetric stretching	798[27], 797 [26, 28], 860-940 [35]	798/28.6	721.4/13.4, 761.8/20.4, 797.5/9.7, 829.2/49.1	807.6/7.1	761.6/22.7, 803.9/16.9, 844/23.9	808.1/8.7	763.2/31.7, 804.9/10.7, 844.5/21.6
Si-O-H stretching	~950 [32]	951.7/.4	910.3/21.9, 953.6/0.4, 969.5/29.3	956.2/.4	909.6/15.9, 952.4/0.8, 975.6/19.6	955.9/0.6	909.4/14.2,9 53.5/0.6, 983.7/25.7
Si-O-Si stretching	1025, 1050[32]	1072.3/2	1040.2/46.6, 1062.3/7.5, 1070.5/1.5	1069.8/3.1	1044.9/30.6, 1052.2/0.5, 1068.8/1.2	1068.7/4.1	1061.2/34.9, 1069.2/0.8
Si-O-Si Asymmetric Stretching	1144, 1196, 1100 [28], 1120-1162 [32], 1160 [36]	1117.4/10.1, 1196.7/2.5	1107.4/46.8, 1152.6/31.3, 1200.1/2.2 1207.5/58.6	1143.9/3.4, 1193.7/2.3	1122.0/40.3, 1162.3/.2, 1194.8/1.6, 1203.7/48.4	1123.2/3.4, 1193.8/2.4	1104.2/2.2, 1168.7/3.1, 1195.1/3 1207.7/35.6
P=O stretching	1230-1300, 1390 [33]	none	none	1248.3/0.3, 1343.9/10. 1	1245.6/.3, 1347.8/.2, 1381/.1	1245.3/0.4, 1342.1/16. 3	1246.9/.1, 1348.9/.2, 1378.8/.06
P-O-H bending	1406 [32]	none	none	none	1409.8/.2, 1458.8/0.5	none	1406.4/.2, 1458.7/0.3
O-H vibrations	~1450 [34], ~1600 [33]	1434.9/0.5, 1458.3/0.07, 1482.6/0.03, 1509.8/0.9	1242.8/28.5, 1298.4/18.9, 1338.8/12.9, 1371.4/9.9, 1401.6/9, 1433/10.7, 1466.6/11.7, 1486.9/.4, 1509.3/11.7, 1557.9/16.5	1434.7/0.6, 1456.9/0.1, 1480/0.03, 1510.6/1.4	1242.3/23.1, 1301.5/30.8, 1338.8/23, 1372.2/19.6, 1403.8/18.6, 1435.6/19.9, 1469.8/20.6, 1485.7/0.1, 1509.8/23.9, 1561.6/32.6	1434.8/0.6, 1456.9/0.0 8, 1481.3/0.0 1, 1509.8/1.3	1243.9/18.3, 1302/28.5, 1340.4/22.3, 1373.4/18.2, 1403.6/17.1, 1434.5/19, 1467/18.8, 1485.9/0.3, 1506.4/21.8, 1554.2/29.8

Table 5: Peak positions and areas before and after Gaussian peak fitting for samples P-165.5 and P-331

		Wavenumbers (cm^{-1})			
		band position/area			
Functional Group	**Assignment**	**P-165.5 (no G-fit)**	**P-165.5 (G-fit)**	**P-331 (no G-fit)**	**P-331 (G-fit)**
O-Si-O bending	490, 500 [26-28]	484.8/2.8	484.6/8.2, 509.2/0.7, 522.8/1	484.6/2	476.1/7.5, 507.6/1.6, 522.2/0.6
HPO_4	551 [29-31]	none	551.6/2.2	none	555.3/5.8
v_4 PO_4/O-P-O bending	567, 572, 602 [29-31]/ 577,597 [32]; 560 [33, 34]	564.1/7.5	560.1/4.1, 572.6/7.3, 595/7.1	559.5/10.5	569.4/12, 594.1/8.5, 611.3/0.9
O-Si-O bending	620 [26-28]	631.8/8.5	631.5/28.9	633.4/5.4	635.2/25.4
P-O-P stretching	758.9 [32]; ~650, ~700 [33]	690.4/0.01, 754.5/0.4	634.5/2.2, 693.2/6.4	759.6/0.3	635.2/4.5, 695.3/0.6
P-O-P bending	800-870, ~780 [33]	none	810.8/0.4	none	812.6/2, 748/33.3
Si-O-Si symmetric stretching	798[27], 797 [26, 28], 860-940 [35]	809.2/6.4	760.3/29.6, 805.4/13.3, 845.1/18.3	810.7/5.6	760.4/.1 801.3/2, 830.2/33.4
Si-O-H stretching	~950 [32]	956.1/0.3	905.7/14.6, 952.7/0.6, 982.2/21.5	955.9/0.3	910.2/0.2, 955.6/0.3, 947.8/25.6
Si-O-Si stretching	1025, 1050[32]	1066.6/5.4	1054.7/27.9, 1067.7/1	1065.8/4.5	1053.7/34.9, 1066.5/0.9
Si-O-Si Asymmetric Stretching	1144, 1196, 1100 [28], 1120-1162 [32], 1160 [36]	1143/3.1, 1193.8/2.4	1107.8/2.5, 1133.5/22.9, 1195.1/2, 1201.8/35.9	1149/2.2, 1193.6/2	1109/1.5, 1138.8/16.1, 1194.7/1.5
P=O stretching	1230-1300, 1390 [33]	1245.6/0.2, 1355.9/15.9	1237.5/10.6, 1320/60.2, 1392/46.2	1249.4/0.2, 1358.8/22.4	1316.2/35.4, 1360.9/37.9
P-O-H bending	1406 [32]	none	1447.1/31.9, 1458.6/0.1, 1496.2/27.5, 1520.9/2	none	1405.9/34.3, 1441.9/20.6, 1458.1/0.3, 1475.4/20.8, 1513/22.8
O-H vibrations	~1450 [34], ~1600 [33]	1433.8/0.4, 1459/0.7, 1483.6/0.03, 1510.9/0.8	1246.1//0.4, 1435.5/0.3, 1520.9/2, 1559.2/39.1	1432.1/0.4, 1458.3/0.06, 1480/0.01, 1511.2/0.8	1245.3/20.3, 1245.3/0.2, 1436.8/0.4, 1565/33.1

The main changes in Tables 4 and 5 of the silicate and phosphate functional groups due to phosphate doping are illustrated in Figures 15-21. Figure 15A, shows a decrease in the area of the O-Si-O bending band at 498 cm^{-1} before Gaussian fitting as phosphate content increased from samples P-0 to P-331. Gaussian fitting (Figure 15B and 15C) revealed that this decrease in area was due to the decrease of the O-Si-O bending bands located at ~488.8 cm^{-1} with symmetry *E* and ~524.6 cm^{-1} with symmetry A_2.

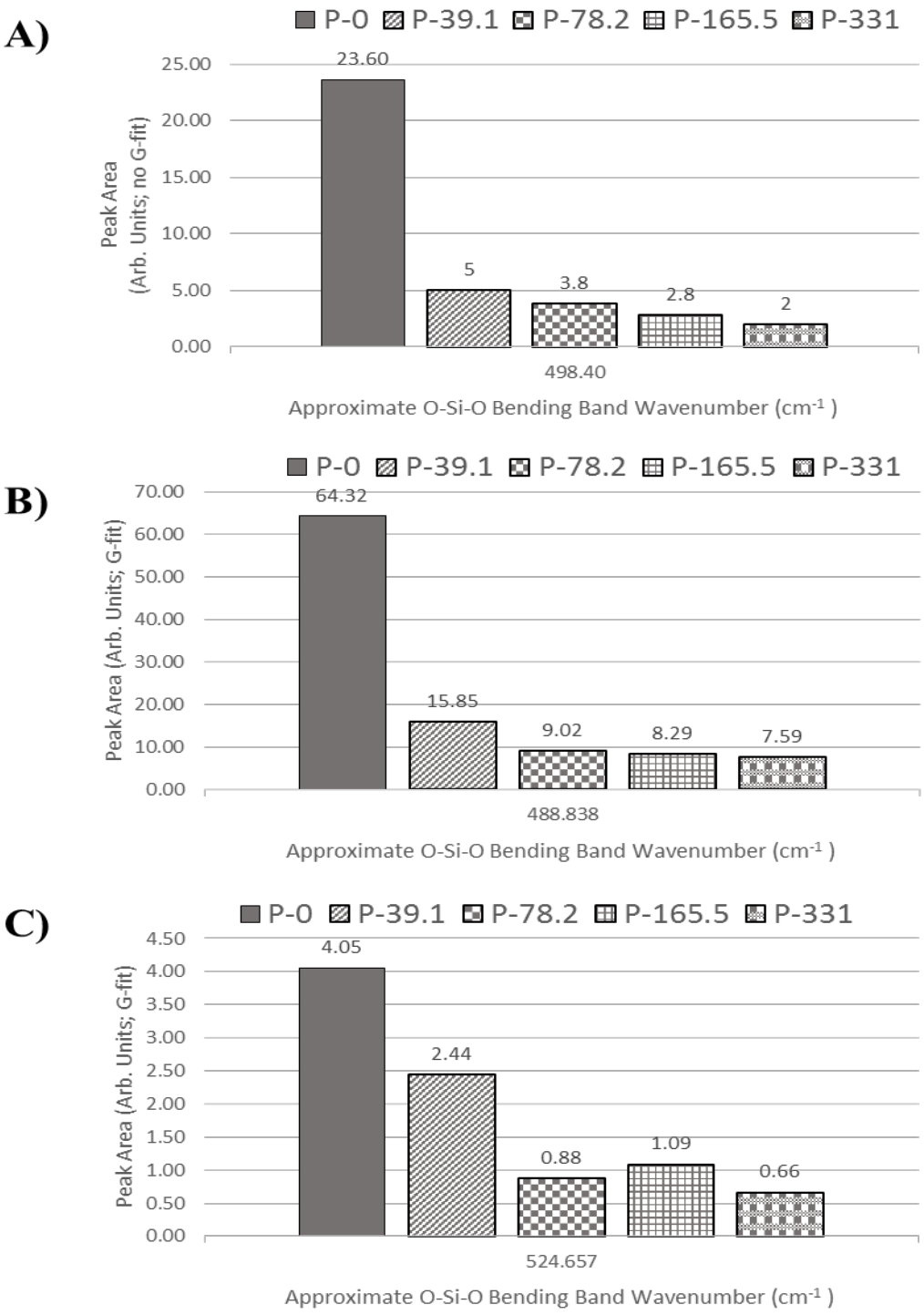

Figure 15: O-Si-O bending band area before (15A) and after Gaussian fitting with symmetry *E* (15B) and symmetry A_2 (15C) showing a decrease in area as phosphate content increases

Addition of phosphate into the silicate structure was responsible for the appearance and increase in area of the v_4 PO_4/O-P-O bending band at ~557.6 cm^{-1} as phosphate content increased from sample P-0 to P-331 (Figure 16A). Gaussian fitting, revealed that the increase in area was due to the increase of the v_4 PO_4/O-P-O bending bands at ~552, ~562, and ~591 cm^{-1} (Figure 16B).

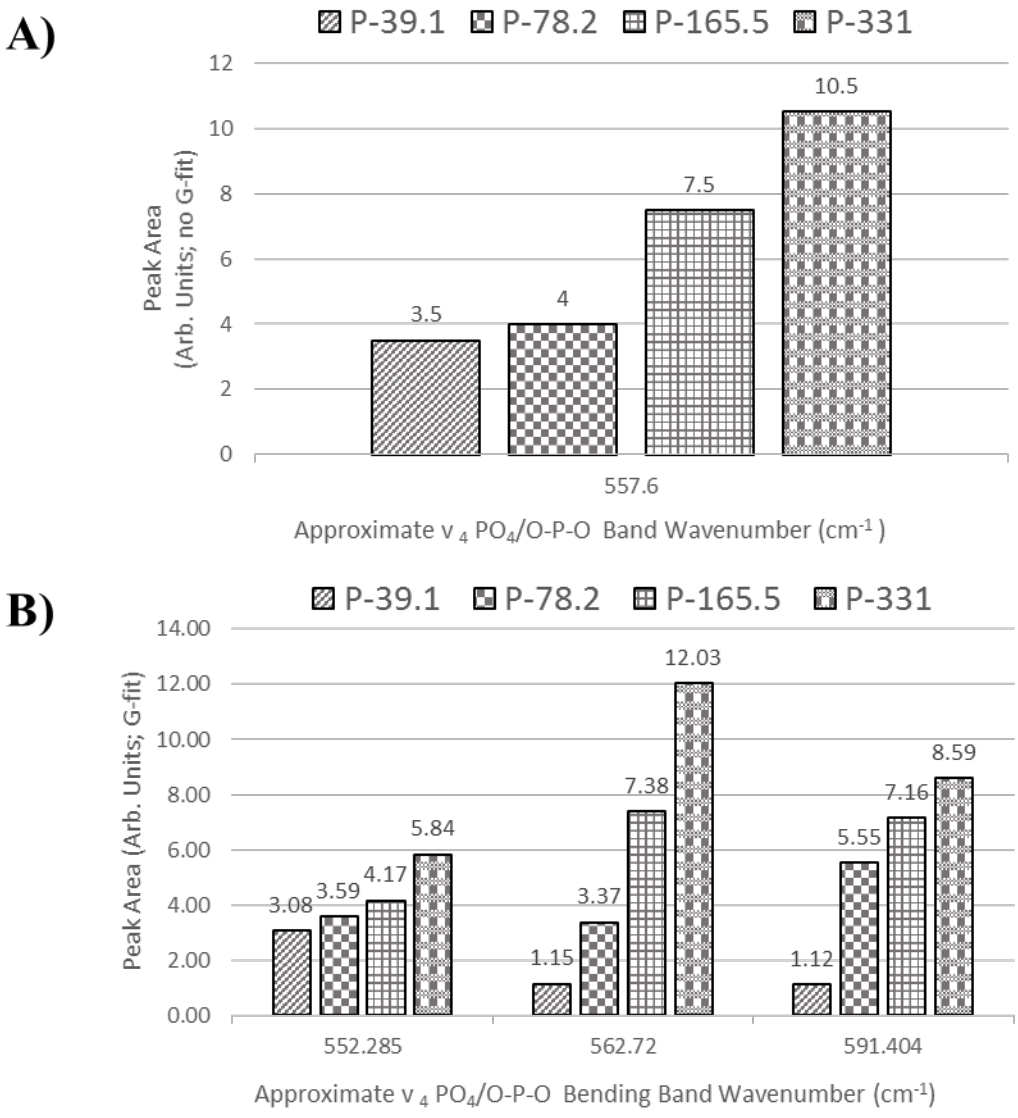

Figure 16: v_4 PO_4/O-P-O bending bands before (16A) and after (16B) Gaussian fitting showing an increase in area as phosphate content increased

Figure 17, shows a decrease in the area of the O-Si-O bending band located at 621.6 cm^{-1} before Gaussian fitting. Gaussian fitting revealed that the decrease in the area was due to the disappearance of the O-Si-O bending bands at 576.1, 621.5, 651.3, and 680.8 cm^{-1} as the P content increased from sample P-0 to P-331.

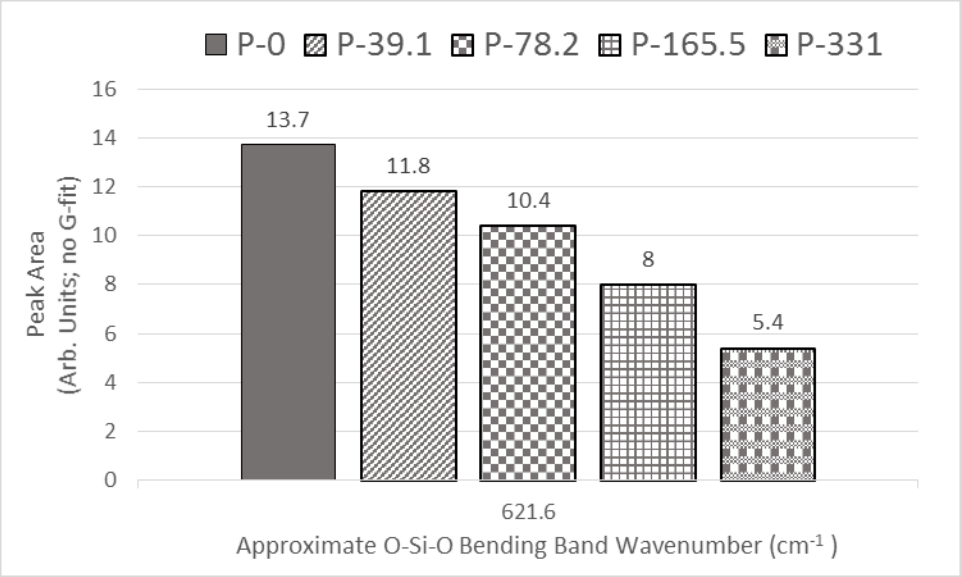

Figure 17: O-Si-O bending band at ~621.6 cm^{-1} decreasing in area as phosphate content increased

In addition, P-O-P stretching bands appeared before and after Gaussian fitting near 698.6 and 765.9 cm^{-1}, and 633.6 and 704.6 cm^{-1}, respectively regardless of the concentration of phosphate in the material. Furthermore, Gaussian fitting revealed the presence of P-O-P bending bands at 810 cm^{-1} for sample P-165.5, and at 812 and 748 cm^{-1} for sample P-331. In conjunction with the appearance of the P-O-P bands, a decrease in the Si-O-Si symmetric stretching band at 798 cm^{-1} before Gaussian fitting was seen (Figure 18). Gaussian fitting revealed that the decrease in area was due to the disappearance of a Si-O-Si symmetric stretching band at 721.4 cm^{-1} which disappeared for all doped samples.

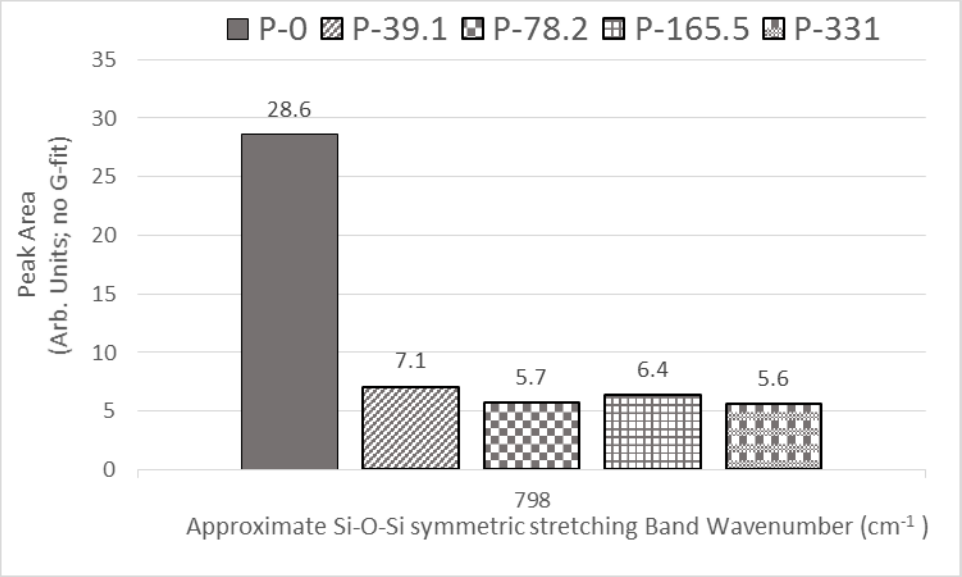

Figure 18: Si-O-Si symmetric stretching decreasing in area as phosphate content increases

Moreover, the incorporation of phosphate resulted in a decrease in the area under the peak in the Si-O-H stretching band at 951.7 cm^{-1} (Figure 19A). Gaussian fitting revealed that the decrease in area of the Si-O-H band was due to the decrease in the area of the Si-O-H band at ~953.6 cm^{-1} (Figure 19B).

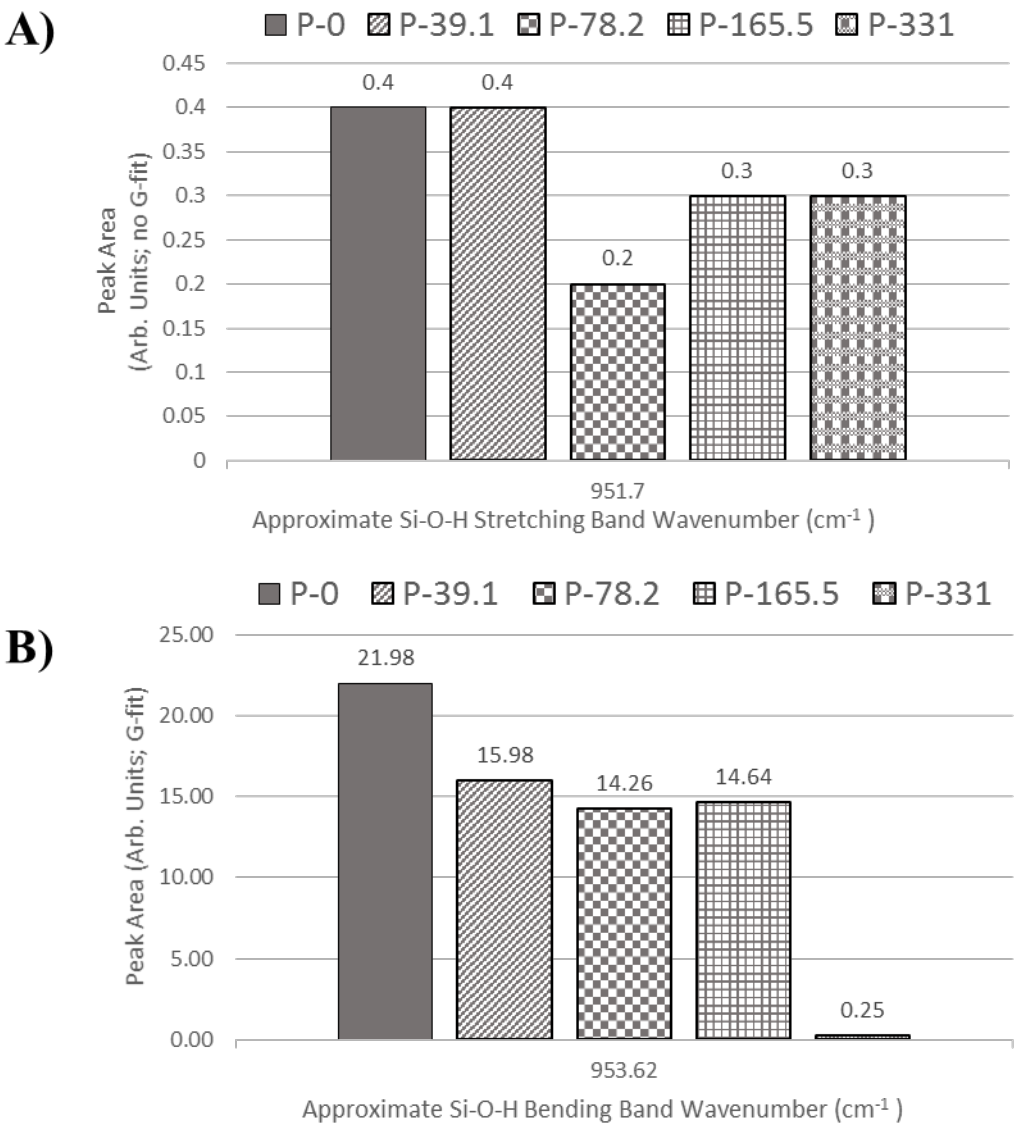

Figure 19: Si-O-H stretching bands decreasing in area as phosphate content increases before (Figure 19A) and after (Figure 19B) Gaussian fitting

A decrease in band area before Gaussian fitting is also noted for Si-O-Si asymmetric stretching bands at 1117.4 cm^{-1} as phosphate content increases (Figure 20A). Gaussian fitting revealed that the decrease in area was due to Si-O-Si asymmetric stretching bands at 1107.4 and 1207 cm^{-1} decreasing in area as phosphate content increased (Figure 20B). Additionally Gaussian fitting revealed there was also a disappearance of the band at 1207 cm^{-1} in the sample P-331.

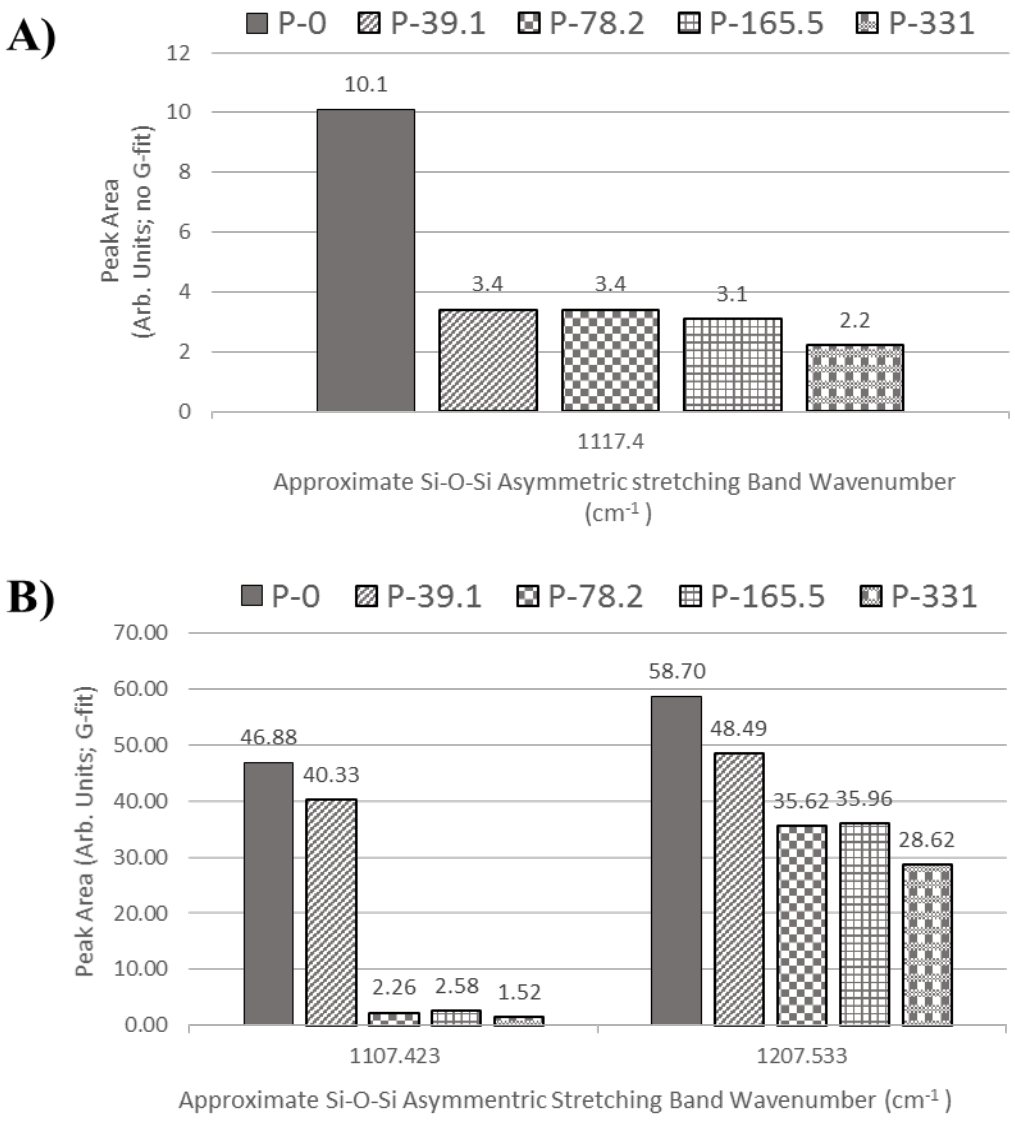

Figure 20: Si-O-Si asymmetric stretching bands decreasing in area as phosphate content increases before Gaussian fitting (Figure 20A) and after Gaussian fitting (Figure 20B)

Figure 21, shows the increase in the area of the P=O stretching band located at 1343.9 cm^{-1} before Gaussian fitting as phosphate content increased. Gaussian fitting revealed three bands under the P=O stretching band at 1245.6, 1347.8, and 1381 cm^{-1}, all of which increased in area up to sample P-165.5. At sample P-331, the band at 1245.6 cm^{-1} disappeared and the area under the bands near 1347.8 and 1381 cm^{-1} decreased in area, but still had a significantly higher area than the peaks in sample P-39.1.

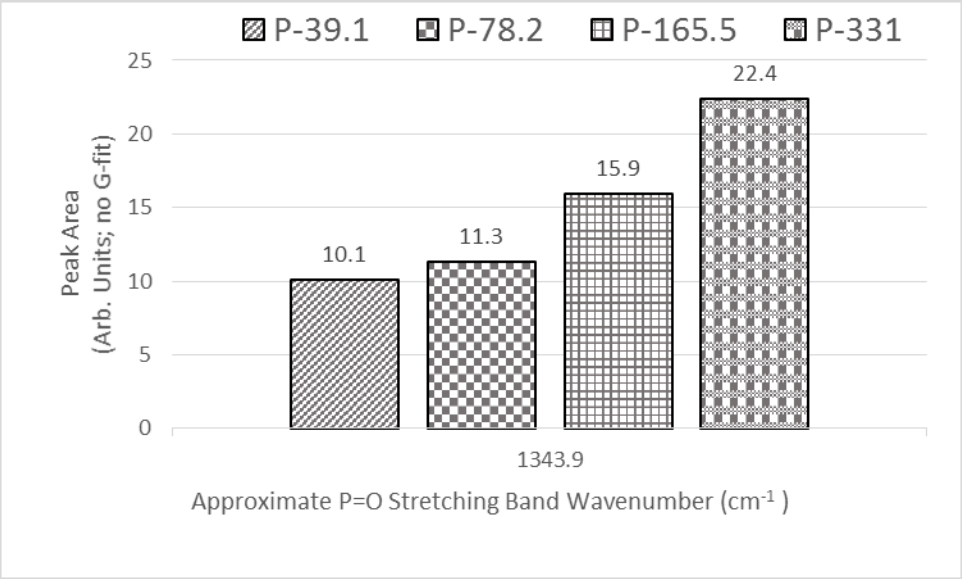

Figure 21: P=O stretching band increasing in area as phosphate content increases before Gaussian fitting

Other changes in the functional groups were also noted in the data found in Tables 4 and 5. Gaussian fitting revealed that O-H vibration bands in the sample P-0 were located at 1242.8, 1298.4, 1338.8, 1371.4, 1401.6, 1433, 1466.6, 1486.9, 1509.3, and 1557.9 cm^{-1}. As the phosphate content increased to the sample P-331, Gaussian fitting showed a disappearance of the O-H vibrations bands 1298.4, 1338.8, 1371.8, 1401.6, 1486.9, and 1509.3 cm^{-1}. In conjunction to the disappearance of the O-H bands, Gaussian fitting showed that there was an increase in the appearance of the P-O-H bending bands from sample P-39.1 to P-331. Gaussian fitting showed that P-39.1 and P-78.2 had bands belonging to P-O-H bending at 1409.8 and 1458.8 cm^{-1}. As P content increased, Gaussian fitting showed that sample P-165.5 had two new P-O-H bands at 1496.2 and 1520.9 cm^{-1} and that P-331 had three new peaks at 1441.9, 1475.4, and 1513 cm^{-1} in addition to the ones found in samples P-39.1 and P-78.2. For samples P-165.5 and P-331 it is also assumed that the peaks at 1447.1 and 1520.9 cm^{-1} belong to P-O-H, but there was not enough evidence from the literature to completely support this assumption.

3.1.3 Surface Morphology Analysis

Scanning Electron Microscopy helped determine that the microstructure for all samples was comparable. The SEM images of all samples at 2500x and 4kV are shown in Figures 22-26. As can be noted from the figures all samples had similar pore size and pore distribution. It is also assumed that these pores are interconnected which can serve as a reservoir for drug containment and provide a longer release of drug.

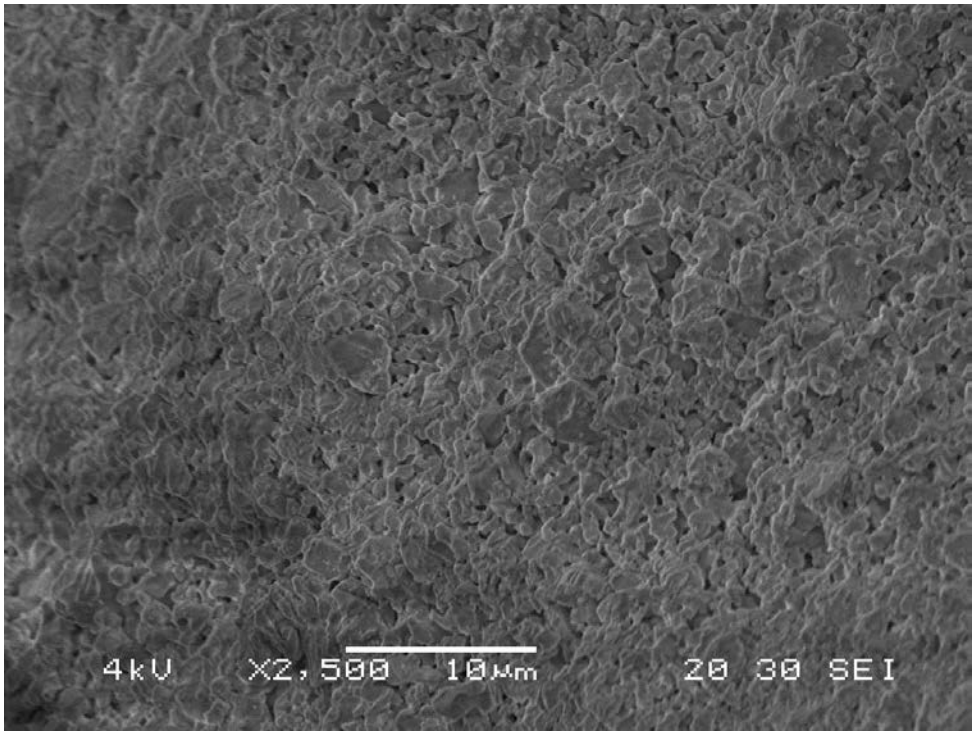

Figure 22: P-0 at 2500x and 4kV

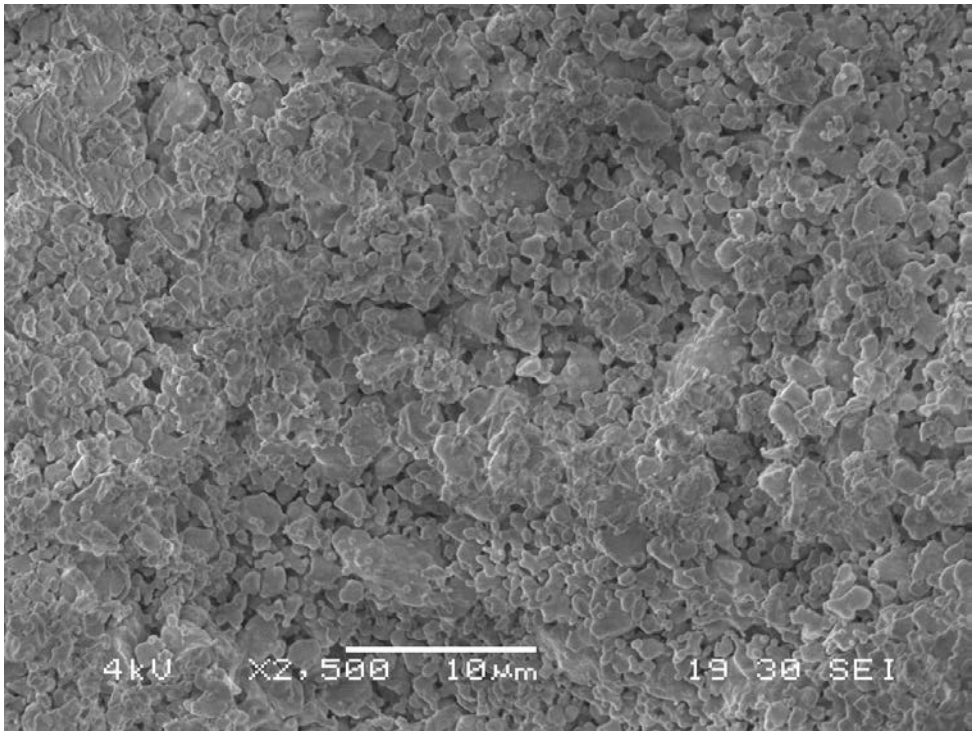

Figure 23: P-39.1 at 2500x and 4kV

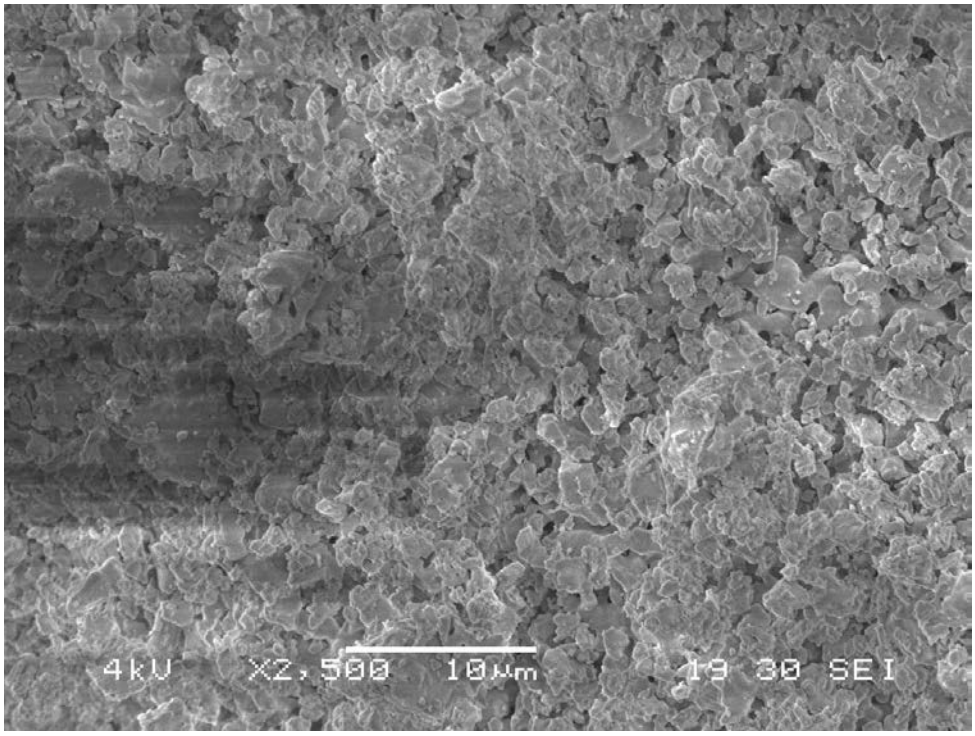

Figure 24: P-78.2 at 2500x and 4kV

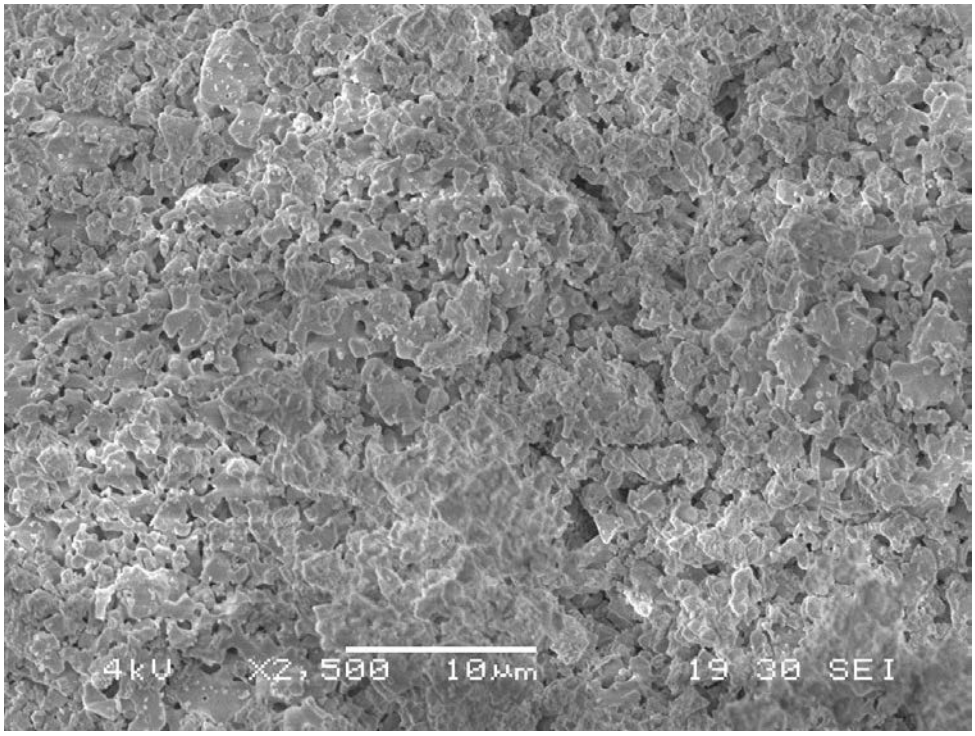

Figure 25: P-165.5 at 2500x and 4kV

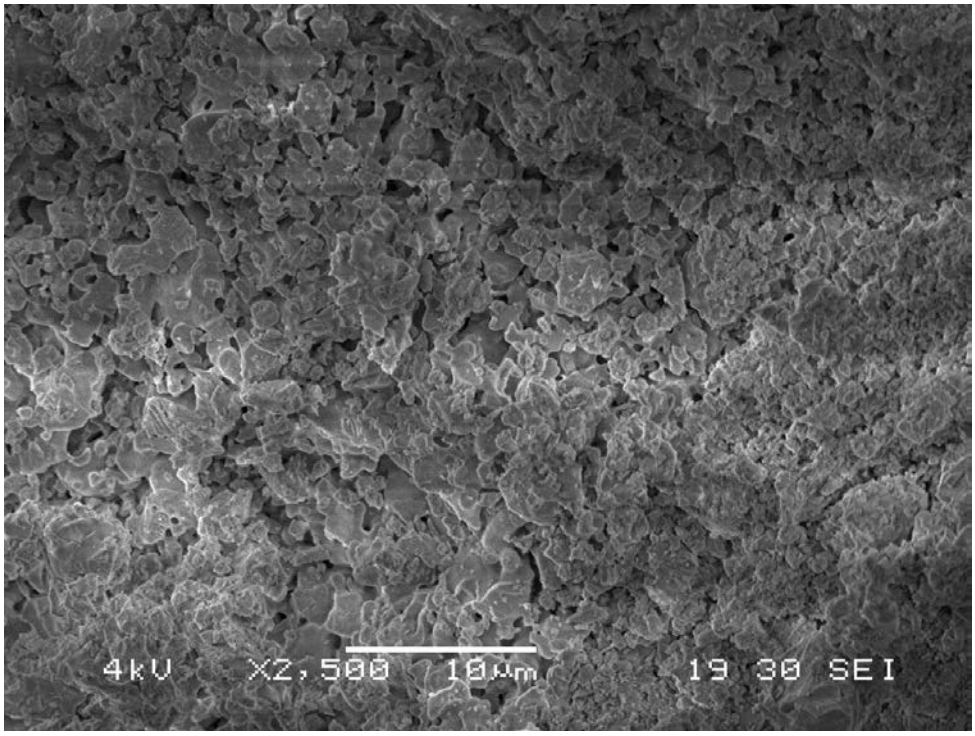

Figure 26: P-331 at 2500x and 4kV

3.2 Corrosion Analysis Before and After Phosphate Doping

Corrosion analysis results for silicate and phosphate ions released over a 2 day period is shown in Figure 27. Figure 27, shows that the release of Si ions from samples P-0, P-39.1, and P-165.5 are comparable ($p > 0.05$). While a greater quantity of Si ion release was seen for both samples P-78.2 and P-331 in the following order P-78.2 < P-331 ($p < 0.001$). As expected a significant increase in the release of phosphate ions is observed as the P dopant increases ($p < 0.001$) from sample P-0 to P-331. Furthermore, for sample P-39.1 the release of Si ions was greater than the phosphate ions released ($p < 0.05$). While for the samples P-78.2, P-165.5, and P-331, it is clearly seen that there is a significant difference between the amount of silicate and phosphate ions released ($p < 0.001$).

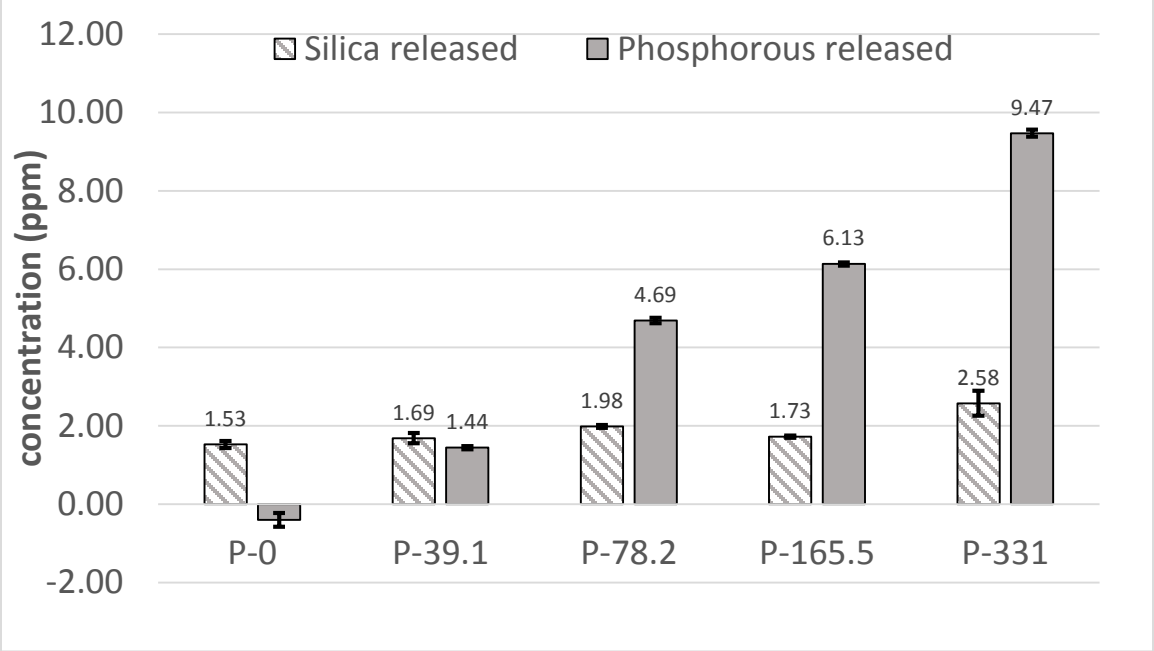

Figure 27: Si and P released from Cris samples after 2 day immersion in DI water

Figure 28, shows the % of phosphorous released from samples P-0, P-39.1, and P-78.2. ICP-OES analyses showed that the percent of released phosphate ions during immersion in DI water decreased as the phosphate content of doped Cris increased (P-39.1 released 92±.08% and P-331 released 71±.05%).

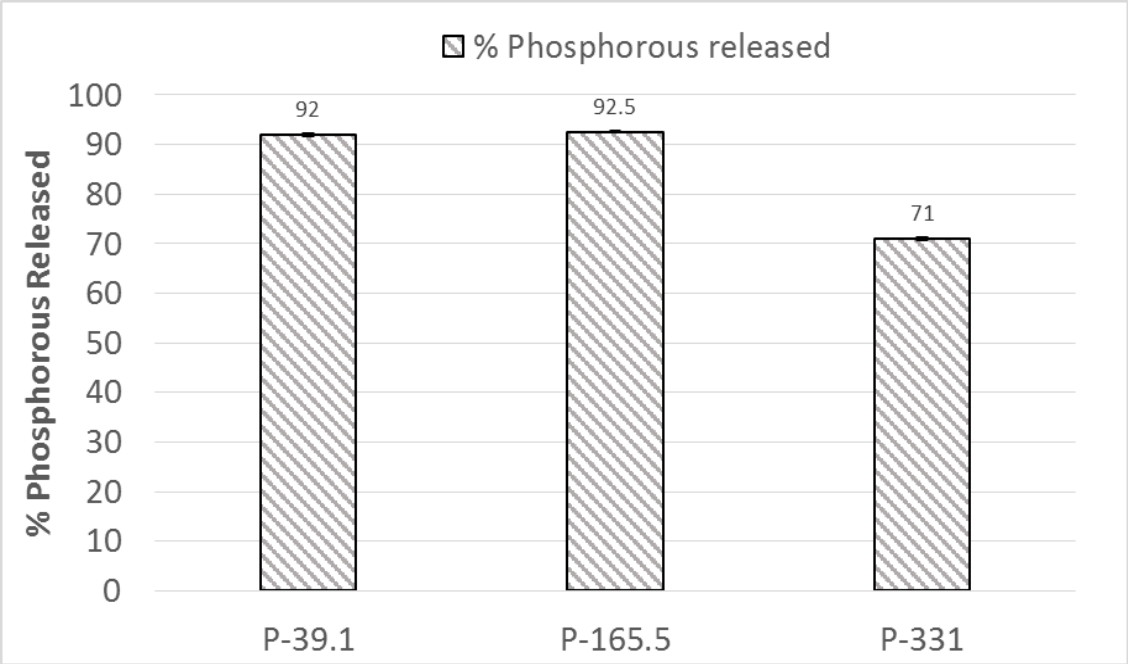

Figure 28: % phosphorous content released from samples P-0, P-39.1, and P-78.2

3.3 Surface Chemistry Analysis for Pre-Immersed Cris

Figure 29 (A-E), below shows a representative FTIR spectra of Cris samples doped with various concentrations of phosphate before and after immersion in DI water. There are no apparent changes in Figure 29A before and after immersion of the sample P-0. However, Figures 29 (B-E) after immersion in DI water, did show 4 main changes in the bands labeled (1), (2), (3), and (4) in the FTIR spectra due to the release of phosphate functional groups from the surface, which show the following: (1) an increase in area and intensity of the O-Si-O bending band around 488.3 cm^{-1}; (2) a disappearance of the v_4 PO_4/O-P-O bending band at 588 cm^{-1}; (3) an increase in the intensity and area of the Si-O-Si symmetric and asymmetric stretching bands located at 1017and 1119 cm^{-1}, and 1192 cm^{-1} , respectively; and (4) a decrease in intensity and area of the P=O stretching bands at 1331 cm^{-1}.

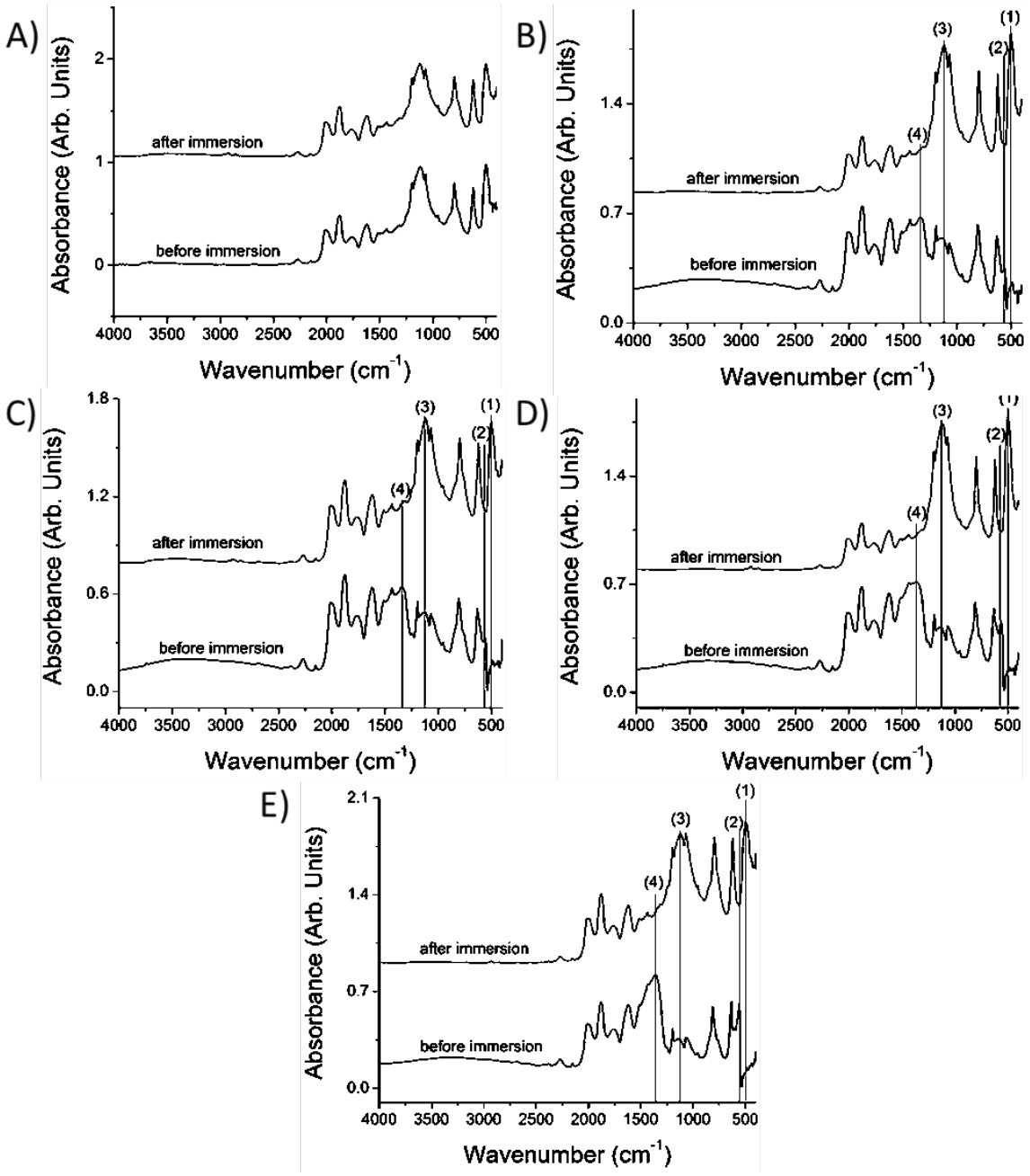

Figure 29: FTIR Spectra of Cris samples normalized to the highest peak intensity and base line corrected of A) P-0, B) P-39.1, C) P-78.2, D) P-165.5, and E) P-331 before and after immersion in DI water

Figure 30 (A-E) and 31 (A-E) are the Gaussian fitting of the FTIR spectra of Cris samples after immersion from 1230-470 cm^{-1} and 1560-1185 cm^{-1}, respectively.

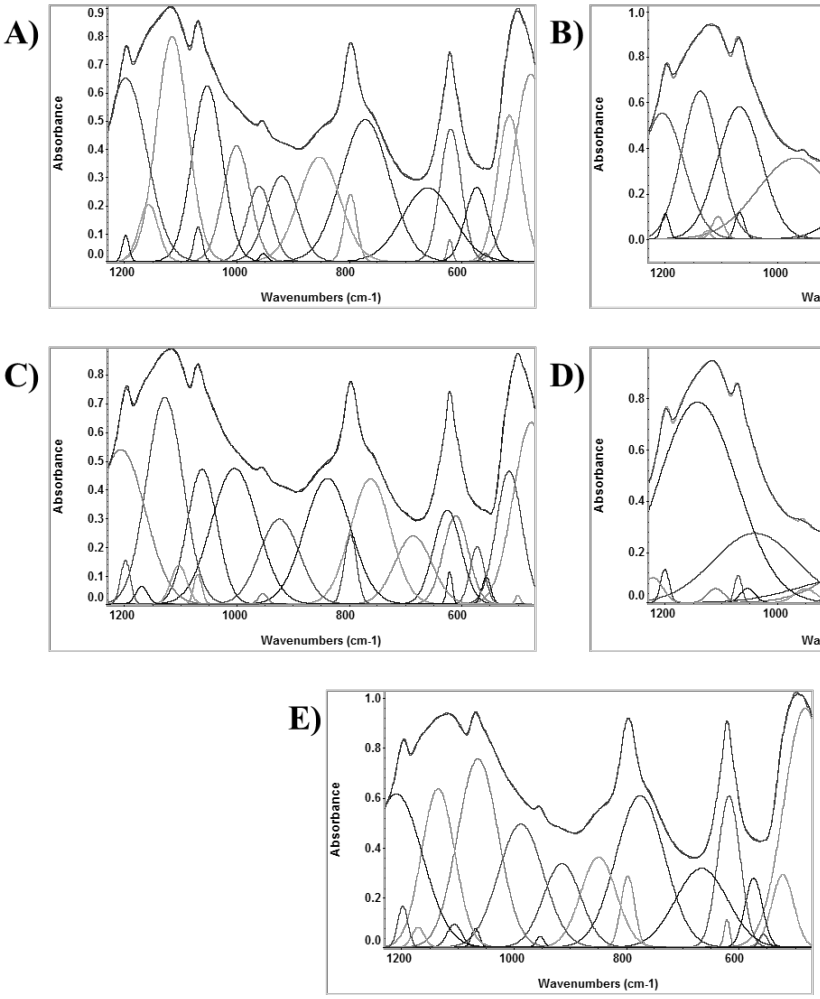

Figure 30: Gaussian peak fitting normalized to the highest peak intensity and base line corrected FTIR Spectra after Immersion of A) P-0, B) P-39.1, C) P-78.2, D) P-165.5, and E) P-331 from 1230-470 cm^{-1}

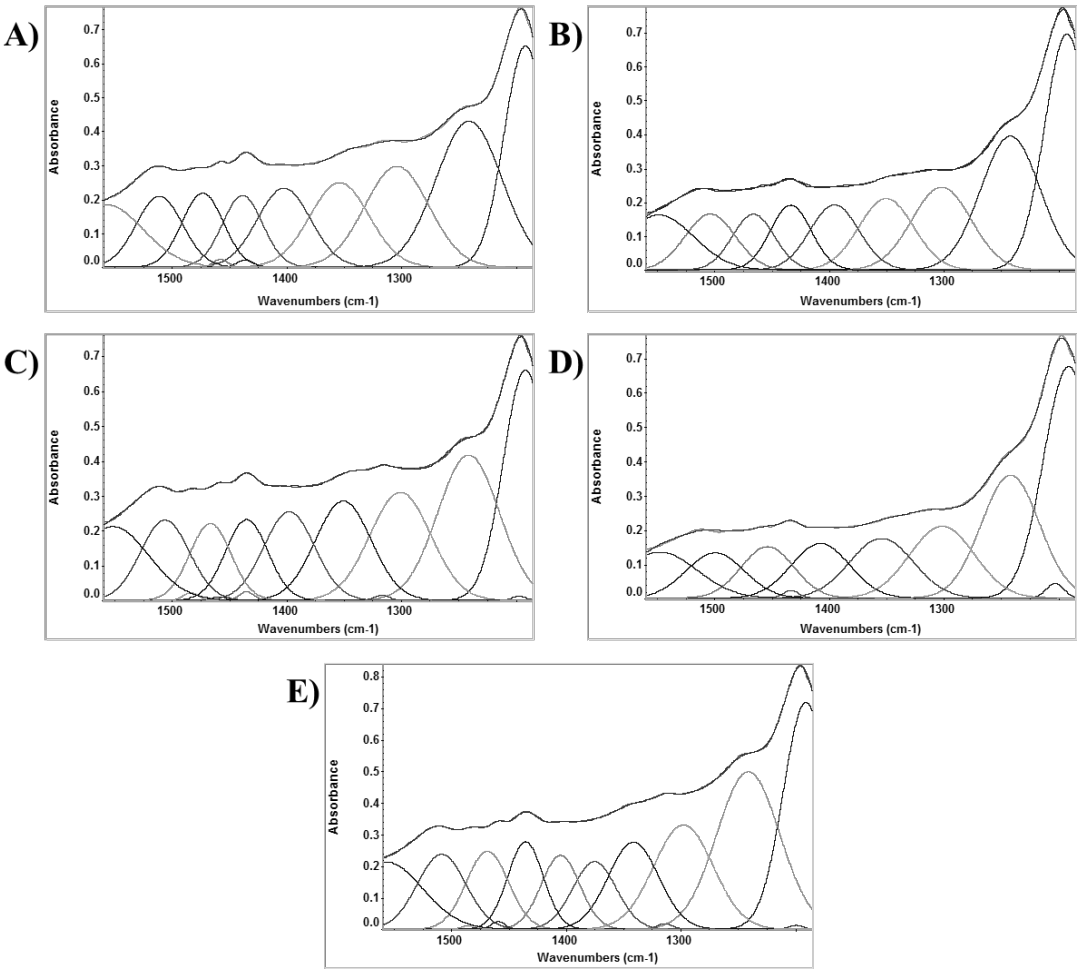

Figure 31: Gaussian peak fitting normalized to the highest peak intensity and base line corrected FTIR spectra after immersion of A) P-0, B) P-39.1, C) P-78.2, D) P-165.5, and E) P-331 from 1560-1185 cm^{-1}

The band assignments and areas before and after immersion, and before and after Gaussian fitting for samples P-0, P-39.1, P-78.2, P-165.5 and P-331 are documented in Tables 6, 7, 8, 9, and 10, respectively.

In Table 6, the silicate functional group band positions and areas in sample P-0 before and after immersion show little to no change in values before Gaussian fitting. Gaussian fitting though reveals that the surface of P-0 may have degraded due to the release of silicate functional groups which translates to the decrease in area of some

bands, and in some cases disappearance of whole bands. Gaussian fitting revealed the following changes in the functional groups after immersion: (1) a decrease in the area of the O-Si-O bending bands with symmetry *E*, 488.8 and 524.6 cm^{-1}; (2) disappearance of an O-Si-O bending band with symmetry A_2 at 680 cm^{-1}; (3) disappearance of a Si-O-Si symmetric stretching bands at 721.4 cm^{-1}; and (4) disappearance of O-H vibration bands at 1338.8 and 1486.9 cm^{-1}.

Table 6: Band position and area of functional groups found in non-immersed and pre-immersed P-0 samples before and after Gaussian fitting

		Wavenumbers (cm^{-1})			
		band position/area			
Functional Group	**Assignment**	**P-0 (no G-fit)**	**P-0-imm (no G-fit)**	**P-0 (G-fit)**	**P-0-imm (G-fit)**
O-Si-O bending	490, 500 [26-28]	498.4/23.6	499.5/22.8	488.8/64.3, 504.9/3.3, 524.6/4	476.8/48.9, 515.1/27.3, 557.8/0.4
O-Si-O bending	620 [26-28]	621.6/13.7	621.3/16.5	576.1/31.9, 621.5/1.1, 622.1/20.1, 651.3/5.1, 680.8/13	573.1/13.3, 619.5/21.8, 621.3/0.9, 660.3/29.5
Si-O-Si symmetric stretching	798[27], 797 [26, 28], 860-940 [35]	798/28.6	797.6/28.8	721.4/13.4, 761.8/20.4, 797.5/9.7, 829.2/49.1	771.7/54, 798/6.5, 853.4/33.8
Si-O-H stretching	~950 [32]	951.7/.4	955.7/0.5	910.3/21.9, 953.6/0.4, 969.5/29.3	920.57/20.8, 952.9/0.4, 960.3/14.3
Si-O-Si stretching	1025, 1050[32]	1072.3/2	1070.4/3.7	1040.2/46.6,1062.3/7.5, 1070.5/1.5	1000.6/24.3, 1053/41.5, 1069.1/2.1
Si-O-Si Asymmetric Stretching	1144, 1196, 1100 [28], 1120-1162 [32], 1160 [36]	1117.4/10.1, 1196.7/2.5	1119.8/10.4, 1196/2.4	1107.4/46.8, 1152.6/31.3, 1200.1/2.2 1207.5/58.6	1115.2/55.9, 1157.2/8.6, 1198.1/60.9
O-H vibrations	~1450 [34], ~1600 [33]	1434.9/0.5, 1458.3/0.07, 1482.6/0.03, 1509.8/0.9	1435.1/.5, 1457.7/0.07, 1497.4/0.03, 1511.9/1	1242.8/28.5, 1298.4/18.9, 1338.8/12.9, 1371.4/9.9, 1401.6/9, 1433/10.7, 1466.6/11.7, 1486.9/.4, 1509.3/11.7, 1557.9/16.5	1240.9/30.8, 1303.9/20.8, 1354/16.1, 1402.6/13.5, 1438.8/9.2, 1473.6/9.8, 1511.4/10.5, 1558.6/15

Table 7: Band position and area of functional groups found in non-immersed and pre-immersed P-39.1 samples before and after Gaussian fitting

		Wavenumbers (cm^{-1})			
		band position/area			
Functional Group	**Assignment**	**P-39.1 (no G-fit)**	**P-39.1-imm (no G-fit)**	**P-39.1 (G-fit)**	**P-39.1-imm (G-fit)**
O-Si-O bending	490, 500 [26-28]	488.1/5	488.3/32.9	487.9/15.8, 508/0.2, 524/2.4	473.2/25.11, 498.2/1.1, 509.8/43.5
HPO_4	551 [29-31]	none	none	552.2/3	none
$\nu_4 PO_4$/ O-P-O bending	567, 572, 602 [29-31]/ 577,597 [32]; 560 [33, 34]	557.6/3.5	none	562.7/1.1, 569.9/6.0 591.4/1.1	561.1/1.5
O-Si-O bending	620 [26-28]	629.8/11.8	621.5/14.6	618.6/28.8, 653.6/5.9	576.6/4.1, 619.3/16, 621.6/2.7, 662.1/55.2
P-O-P stretching	758.9 [32]; ~650, ~700 [33]	698.6/.02, 756.9/.5	none	633.6/2.5, 704.6/10.8	none
Si-O-Si symmetric stretching	798[27], 797 [26, 28], 860-940 [35]	807.6/7.1	797.6/26.1	761.6/22.7, 803.9/16.9, 844/23.9	760.1/1.3, 796.5/8.8, 807.6/52
Si-O-H stretching	~950 [32]	956.2/.4	956.2/.3	909.6/15.9, 952.4/0.8, 975.6/19.6	954.4/0.2, 968.2/60.2
Si-O-Si stretching	1025, 1050[32]	1069.8/3.1	1070.7/4.4	1044.9/30.6, 1052.2/0.5, 1068.8/1.2	1067.9/2.4, 1068.1/56.6
Si-O-Si Asymmetric Stretching	1144, 1196, 1100 [28], 1120-1162 [32], 1160 [36]	1143.9/3.4, 1193.7/2.3	1118/10.9, 1196.6/2.5	1122.0/40.3, 1162.3/.2, 1194.8/1.6, 1203.7/48.4	1106.1/2.6, 1125.7/.5, 1137.6/52.9, 1205.4/52.9
P=O stretching	1230-1300, 1390 [33]	1248.3/0.3, 1343.9/10.1	1311.6/0.5	1245.6/.3, 1347.8/.2, 1381/.1	none
P-O-H bending	1406 [32]	none	none	1409.8/.2, 1458.8/0.5	none
O-H vibrations	~1450 [34], ~1600 [33]	1434.7/0.6, 1456.9/0.1, 1480/0.03, 1510.6/1.4	1435.3/.4, 1456.9/0.05, 1480/.02, 1511.5/0.7	1242.3/23.1, 1301.5/30.8, 1338.8/23, 1372.2/19.6, 1403.8/18.6, 1435.6/19.9, 1469.8/20.6, 1485.7/0.1, 1509.8/23.9, 1561.6/32.6	1241.8/25.5, 1302/15.8, 1350.3/12.5, 1395.6/10.3, 1433.8/8.5, 1466.4/7.5, 1504.1/9, 1549.2/12.4

Table 8: Band position and area of functional groups found in non-immersed and pre-immersed P-78.2 samples before and after Gaussian fitting

Functional Group	Assignment	Wavenumbers (cm^{-1}) band position/area			
		P-78.2 (no G-fit)	P-78.2-imm (no G-fit)	P-78.2 (G-fit)	P-78.2-imm (G-fit)
O-Si-O bending	490, 500 [26-28]	486.6/3.8	500/21.7	484.3/9, 511.4/1.5, 523.9/0.8	475.8/50.9, 500/0.3 515.6/26.4
HPO_4	551 [29-31]	none	none	550.8/1.5	none
ν_4 PO_4/O-P-O bending	567, 572, 602 [29-31]/ 577,597 [32]; 560 [33, 34]	560.1/4.0	none	558.6/3.5, 571.5/3.3, 588.2/5.5	556.3/1.8
O-Si-O bending	620 [26-28]	631.4/10.4	621.3/17.3	627.4/28.8	572.5/6.3, 610.6/17.2, 621.6/1.3, 625.5/19.9
P-O-P stretching	758.9 [32]; ~650, ~700 [33]	757.4/0.5	none	633.7/0.6, 691.5/6.4	686.2/19.4
Si-O-Si symmetric stretching	798[27], 797 [26, 28], 860-940 [35]	808.1/8.7	798/30	763.2/31.7, 804.9/10.7, 844.5/21.6	762.2/38.8, 797.9/6.6, 838.7/44.8
Si-O-H stretching	~950 [32]	955.9/0.6	956.6/0.3	909.4/14.2, 953.5/0.6, 983.7/25.7	924.4/26.2, 953.7/0.7
Si-O-Si stretching	1025, 1050[32]	1068.7/4.1	1070.5/3.4	1061.2/34.9, 1069.2/0.8	1004.3/48.4, 1061.9/31, 1069.7/1.9
Si-O-Si Asymmetric Stretching	1144, 1196, 1100 [28], 1120-1162 [32], 1160 [36]	1123.2/3.4, 1193.8/2.4	1117.5/9.8, 1195.9/2.6	1104.2/2.2, 1168.7/3.1, 1195.1/3 1207.7/35.6	1103.3/4.8, 1128.4/58.2, 1169.6/1.6, 1198.4/3.3, 1206.6/58.4
P=O stretching	1230-1300, 1390 [33]	1245.3/0.4, 1342.1/16.3	1243.9/0.3, 1314.6/1	1246.9/.1, 1348.9/.2, 1378.8/.06	1317/0.2
P-O-H bending	1406 [32]	none	none	1406.4/.2, 1458.7/0.3	1459.3/0.1, 1483.7/0.3
O-H vibrations	~1450 [34], ~1600 [33]	1434.8/0.6, 1456.9/0.08, 1481.3/0.01, 1509.8/1.3	1435.1/0.5, 1450.9/0.06, 1482.7/0.02, 1511.8/1.1	1243.9/18.3, 1302/28.5, 1340.4/22.3, 1373.4/18.2, 1403.6/17.1, 1434.5/19, 1467/18.8, 1485.9/0.3, 1506.4/21.8, 1554.2/29.8	1241.3/28, 1300.8/20.6, 1350.7/17.3, 1397.9/14.1, 1435.2/10.7, 1466.9/9.8, 1506.5/12.2, 1552.3/16.7

Table 9: Band position and area of functional groups found in non-immersed and pre-immersed P-165.5 samples before and after Gaussian fitting

		Wavenumbers (cm^{-1})			
		band position/area			
Functional Group	**Assignment**	**P-165.5 (no G-fit)**	**P-165.5-imm (no G-fit)**	**P-165.5 (G-fit)**	**P-165.5-imm (G-fit)**
O-Si-O bending	490, 500 [26-28]	484.8/2.8	499.7/40.8	484.6/8.2, 509.2/0.7, 522.8/1	487.1/61, 505.8/5.8, 525.9/7.7
HPO_4	551 [29-31]	none	none	551.6/2.2	none
$\nu_4 PO_4$/ O-P-O bending	567, 572, 602 [29-31]/ 577,597 [32]; 560 [33, 34]	564.1/7.5	none	560.1/4.1, 572.6/7.3, 595/7.1	558.2/5.7
O-Si-O bending	620 [26-28]	631.8/8.5	621.7/13.4	631.5/28.9	615.5/25.1, 621.8/5.2
P-O-P stretching	758.9 [32]; ~650, ~700 [33]	690.4/0.01, 754.5/0.4	none	634.5/2.2, 693.2/6.4	none
P-O-P bending	800-870, ~780 [33]	none	none	810.8/0.4	868.7/22.7
Si-O-Si symmetric stretching	798[27], 797 [26, 28], 860-940 [35]	809.2/6.4	797.9/24.6	760.3/29.6, 805.4/13.3, 845.1/18.3	767/1.1, 779.3/65.3, 797.2/9.9
Si-O-H stretching	~950 [32]	956.1/0.3	956.8/0.2	905.7/14.6, 952.7/0.6, 982.2/21.5	913.3/0.4, 950.6/2.7
Si-O-Si stretching	1025, 1050[32]	1066.6/5.4	1072.6/2.8	1054.7/27.9, 1067.7/1	1040.4/50.5, 1053.6/1.8, 1070.2/1.7
Si-O-Si Asymmetric Stretching	1144, 1196, 1100 [28], 1120-1162 [32], 1160 [36]	1143/3.1, 1193.8/2.4	1117.2/11.3, 1197.2/2.6	1107.8/2.5, 1133.5/22.9, 1195.1/2, 1201.8/35.9	1110.3/2, 1142.4/137.4, 1200.7/2.5, 1221.9/4.2
P=O stretching	1230-1300, 1390 [33]	1245.6/0.2, 1355.9/15.9	1310.3/0.3	1237.5/10.6, 1320/60.2, 1392/46.2	none
P-O-H bending	1406 [32]	none	none	1447.1/31.9, 1458.6/0.1, 1496.2/27.5, 1520.9/2	1407.8/10.2, 1454/8.6
O-H vibrations	~1450 [34], ~1600 [33]	1433.8/0.4, 1459/0.7, 1483.6/0.03, 1510.9/0.8	1434.7/0.3, 1457/0.05, 1480.3/0.02, 1511.3/0.6	1246.1//0.4, 1435.5/0.3, 1520.9/2, 1559.2/39.1	1241.9/22.8, 1301.5/14.9, 1354.5/12.1, 1433.5/0.3, 1499.8/8.4, 1548.3/11

Table 10: Band position and area of functional groups found in non-immersed and pre-immersed P-331 samples before and after Gaussian fitting

		Wavenumbers (cm^{-1})			
		band position/area			
Functional Group	**Assignment**	**P-331 (no G-fit)**	**P-331-imm (no G-fit)**	**P-331 (G-fit)**	**P-331-imm (G-fit)**
O-Si-O bending	490, 500 [26-28]	484.6/2	497.7/30.2	476.1/7.5, 507.6/1.6, 522.2/0.6	481.6/91.6, 521.9/14.1
HPO_4	551 [29-31]	none	none	555.3/5.8	none
$\nu_4 PO_4$/ O-P-O bending	567, 572, 602 [29-31]/ 577,597 [32]; 560 [33, 34]	559.5/10.5	none	569.4/12, 594.1/8.5, 611.3/0.9	556.3/1
O-Si-O bending	620 [26-28]	633.4/5.4	621.1/17.7	635.2/25.4	573.5/10.7, 617.5/29.9, 621.3/1.4
P-O-P stretching	758.9 [32]; ~650, ~700 [33]	759.6/0.3	none	635.2/4.5, 695.3/0.6	666.4/36.6
P-O-P bending	800-870, ~780 [33]	none	none	812.6/2, 748/33.3	797.6/8.7
Si-O-Si symmetric stretching	798[27], 797 [26, 28], 860-940 [35]	810.7/5.6	796.3/35	760.4/.1 801.3/2, 830.2/33.4	775.3/65.8, 849.7/28.6,
Si-O-H stretching	~950 [32]	955.9/0.3	956.8/0.4	910.2/0.2, 955.6/0.3, 947.8/25.6	914.6/28, 953.4/0.7, 987.8/49.2
Si-O-Si stretching	1025, 1050[32]	1065.8/4.5	1069.3/5.5	1053.7/34.9, 1066.5/0.9	1064.3/68.2, 1068.7/1.3
Si-O-Si Asymmetric Stretching	1144, 1196, 1100 [28], 1120-1162 [32], 1160 [36]	1149/2.2, 1193.6/2	1120/7.4, 1195.8/2.4	1109/1.5, 1138.8/16.1, 1194.7/1.5	1106.1/3, 1135.2/46.6, 1170.7/2.2, 1198.1/3.7, 1209.6/71.4
P=O stretching	1230-1300, 1390 [33]	1249.4/0.2, 1358.8/22.4	1246.6/0.5, 1311.1/0.7	1316.2/35.4, 1360.9/37.9	1314/0.2
P-O-H bending	1406 [32]	none	none	1405.9/34.3, 1441.9/20.6, 1458.1/0.3, 1475.4/20.8, 1513/22.8	1405.1/9.8, 1459.7/.3, 1484.1/0.2
O-H vibrations	~1450 [34], ~1600 [33]	1432.1/0.4, 1458.3/0.06, 1480/0.01, 1511.2/0.8	1434.7/0.5, 1457/0.08, 1480.1/0.03, 1511.1/1	1245.3/20.3, 1245.3/0.2, 1436.8/0.4, 1565/33.1	1241/34.2, 1297.7/21.4, 1341.3/15.1, 1375.4/15.1, 1435.6/10.7, 1468.9/11.3, 1509/12.5, 1557.1/16.7

The main changes in Tables 7-10 of the silicate and phosphate functional groups due to the release of surface phosphate functional groups after immersion are illustrated in Figures 32-34. Figure 32, shows the increase in area that occurred to the O-Si-O bending bands after immersion in water for all doped samples. An increase in the area of the O-Si-O bending band around 490 cm^{-1} occurred (Figure 32A). Gaussian fitting revealed that the increase in the area of the O-Si-O bending band around 490 cm^{-1} was due to the increase of two O-Si-O bending bands around 480 and 520 cm^{-1} (Figures 32B and 32C). Additionally, there was an increase in the area of the O-Si-O bending band located around 620 cm^{-1} for all samples (Figure 32D). Gaussian fitting revealed that the increase in area of the O-Si-O bending band around 620 cm^{-1} was due to the appearance of new O-Si-O bending bands after immersion as shown in Tables 7-10.

In conjunction with the increase in the area of the O-Si-O bending bands after immersion (Figure 32), there was also a significant decrease in area of the O-P-O bending band at 557 cm^{-1} as shown in Tables 7-10. Gaussian fitting revealed that the decrease in area of the O-P-O bending band was due to the disappearance of O-P-O bending bands in all doped samples as shown in Tables 7-10. Furthermore, Gaussian fitting in Tables 7-10 revealed that after immersion bands belonging to P-O-P stretching and bending disappeared for all phosphate doped samples.

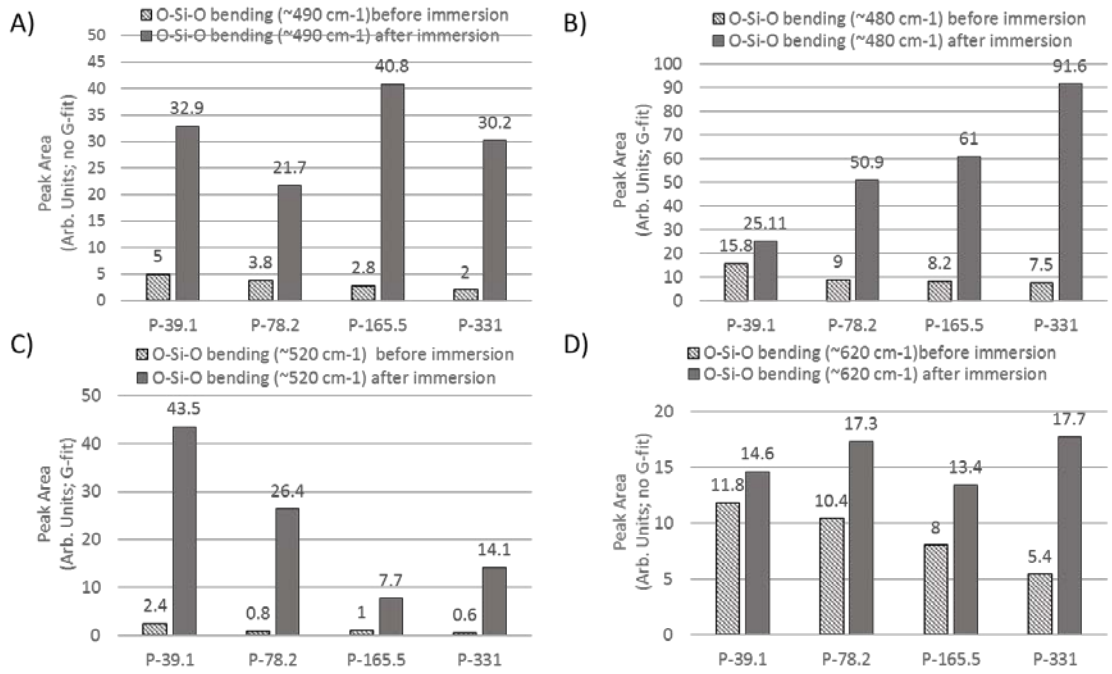

Figure 32: O-Si-O bending band area before and after immersion for A) O-Si-O bending band ~490 cm^{-1} (no G-fit), B) O-Si-O bending band ~480 cm-1 (G-fit), C) O-Si-O bending band ~520 cm-1 (G-fit), and D) O-Si-O bending band ~620 cm^{-1} (no G-fit)

Figure 33, shows the increase in area of the Si-O-Si symmetric stretching band at 797 cm^{-1} after immersion. Gaussian fitting confirmed this by showing an increase in the Si-O-Si symmetric stretching bands around 761.6, 803.9, and 844 cm^{-1} in Tables 7-10.

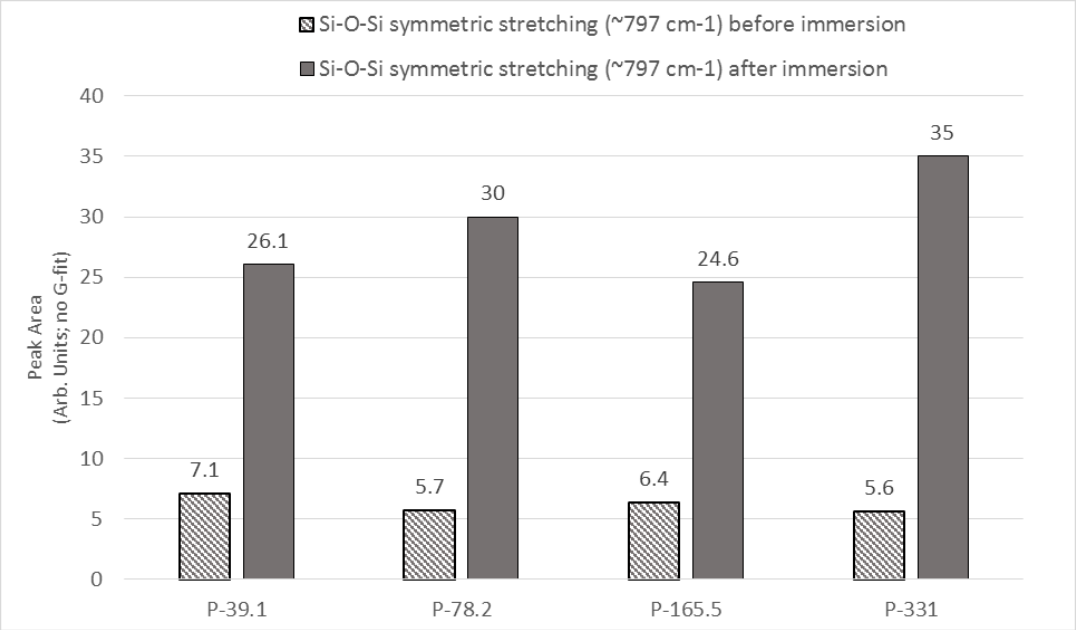

Figure 33: Si-O-Si symmetric stretching band area increasing after immersion (no G-fit)

Figure 34, shows the band area before and after immersion for Si-O-Si asymmetric stretching bands located at 1144 and 1193 cm^{-1}. There is an increase in area for the Si-O-Si asymmetric stretching bands located at 1144 and 1193 cm^{-1} after immersion. Gaussian fitting revealed that the increase in area for Si-O-Si asymmetric stretching bands was due to the appearance of new or increase of bands around 1100-1200 cm^{-1} corresponding to Si-O-Si asymmetric stretching bands as shown in Tables 7-10.

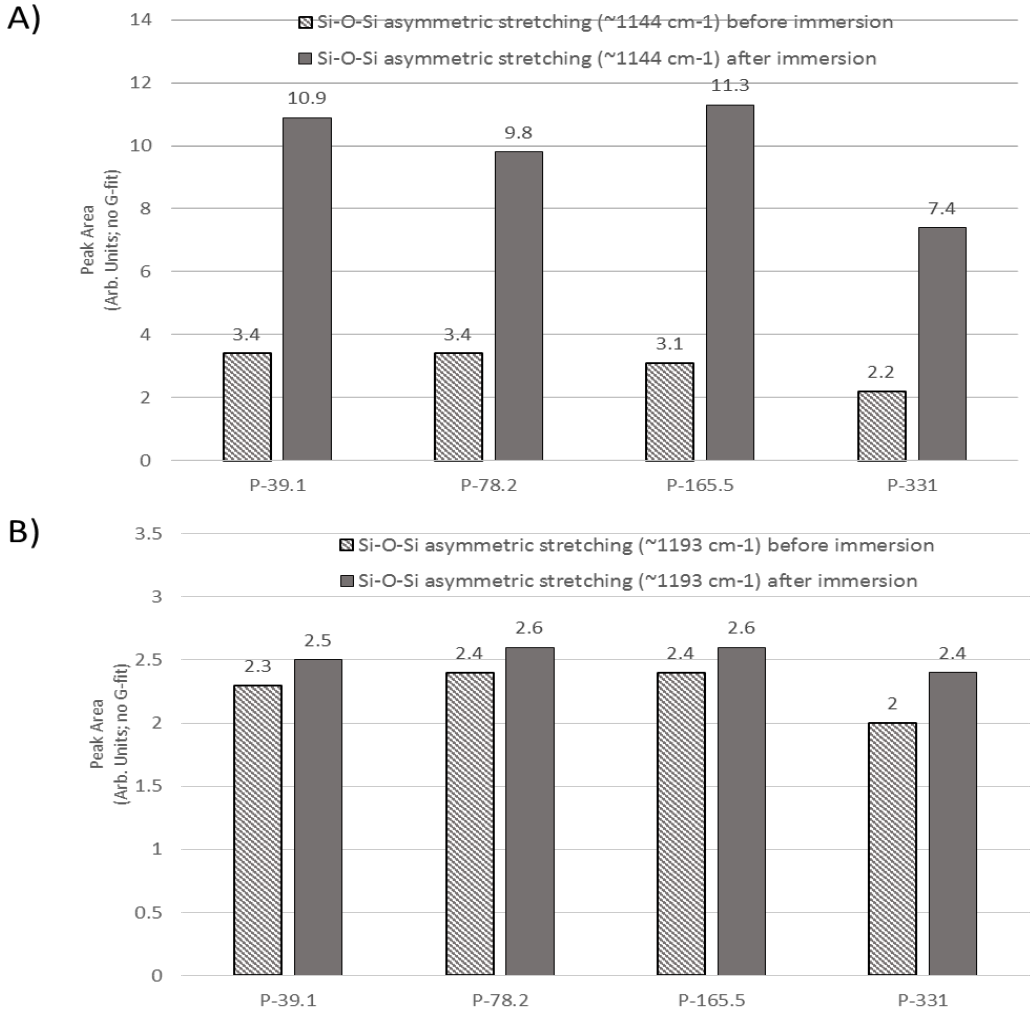

Figure 34: Si-O-Si asymmetric stretching band areas located at 1144 and 1193 cm^{-1} increasing after immersion (no G-fit)

Other changes were also noted in Tables 7-10, in addition to the ones illustrated in Figures 32-34 for doped samples releasing surface phosphate functional groups after immersion. Table 7, for sample P-39.1 showed the following changes after immersion: (1) Gaussian fitting showed a disappearance of a Si-O-H stretching band at 909.6 cm^{-1} accompanied by an increase in band area for Si-O-H stretching at 968.2 cm^{-1}; (2) an increase in area of the Si-O-Si stretching band located at 1069.8 cm^{-1} which Gaussian fitting showed occurred due to the disappearance of a Si-O-Si stretching band at 1044.9 cm^{-1} accompanied by an increase in band area for Si-O-Si stretching at 1068.1 cm^{-1}; (3) Gaussian fitting showed the disappearance of all P=O stretching and P-O-H bending bands; and (4) Gaussian fitting showed a disappearance of the O-H vibration bands 1338.8 and 1485.7 cm^{-1}.

Table 8, for sample P-78.2 shows the following changes after immersion: (1) Gaussian fitting showed a disappearance of the Si-O-H stretching band at 909.4 cm^{-1}; (2) Gaussian fitting showed the appearance of the Si-O-Si stretching band at 1004.3 cm^{-1}; (3) a decrease in the area of the P=O stretching band at 1342.1 cm^{-1} which according to Gaussian fitting is due the disappearance of the P=O stretching bands 1246.9 and 1378.8 cm^{-1}; and (4) Gaussian fitting shows the disappearance of the O-H vibration bands 1373.4 cm^{-1}.

Table 9, for sample P-165.5 shows the following changes after immersion: (1) Gaussian fitting shows a disappearance of the Si-O-H stretching band at 982.2 cm^{-1}; (2) Gaussian fitting shows the appearance of a Si-O-Si stretching band at 1040.4 cm^{-1}; (3) a complete disappearance of the P=O stretching bands after immersion; (4) disappearance of the P-O-H vibration bands which Gaussian fitting revealed as the disappearance of

bands at 1496.2 and 1520 cm^{-1}; and (5) Gaussian fitting showed the appearance of the O-H vibration bands 1301.5 and 1354.5 cm^{-1}.

Table 10, for sample P-331 shows the following changes after immersion: (1) increase in the area of the Si-O-H and Si-O-Si stretching bands; (2) Gaussian fitting showed the decrease in area and disappearance of P=O stretching bands at 1316.2 and 1360 cm^{-1}, respectively; (3) Gaussian fitting revealed the disappearance of the P-O-H vibration band at 1441.9 and 1513 cm^{-1}, and decrease in area of the bands at 1405.1, 1459.7, and 1484.1 cm^{-1}; and (4) Gaussian fitting showed the appearance of the O-H vibration bands 1297.7, 1341.3, 1375.4, 1435.6, 1468.9, 1509, and 1557.1 cm^{-1}.

The release of the phosphate functional groups from the surface of Cris after immersion exposed silicate functional groups present on the surface of Cris. For this reason there was a decrease in area and disappearance of phosphate functional groups and an increase in area and appearance of bands belonging to silicate functional groups after immersion in water.

3.4 Drug Adsorption of Cris Particles

Figure 35, shows the amount of Vanc adsorbed in mg onto 200 mg of non-immersed and pre-immersed Cris samples. Cris sample P-0 adsorbed the same amount of drug regardless of immersion. Non-immersed Cris samples P-0 and P-39.1 adsorbed a comparable amount of drug. While there was a statistically significant lower amount of drug adsorbed onto P-78.2 than adsorbed onto P-39.1 ($p < 0.001$), statistical analysis showed comparable amount of drug adsorbed onto P-78.2, P-165.5, and P-331. Releasing the phosphate from the material surface after immersion resulted in a significant increase in drug adsorption. Higher Vanc adsorption was noticed for all pre-immersed Cris samples compared to their corresponding non-immersed samples. Moreover, for pre-immersed samples there was a statistically significant increase in the amount of drug adsorbed in the order of P-0 < P-39.1 < P-78.2 ($p < 0.05$). However, a statistically significant decrease in the amount of the adsorbed drug in the order P-78.2 > P-165.5 > P-331 ($p < 0.001$) was observed.

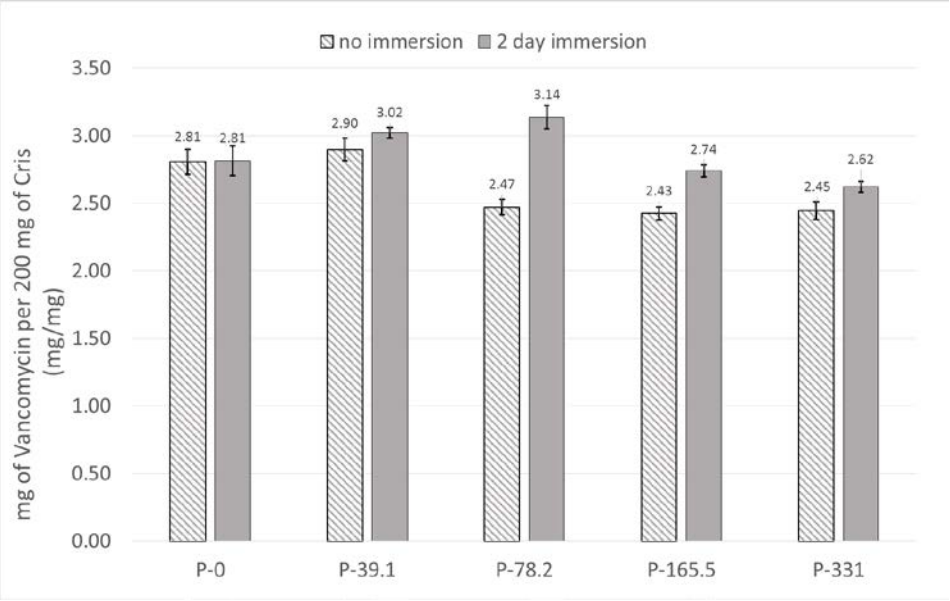

Figure 35: Amount of Vanc adsorbed onto non-immersed and pre-immersed Cris samples

Figure 36, indicates that a decrease in Vanc adsorption is due to an increase in the presence of P_2O_5.

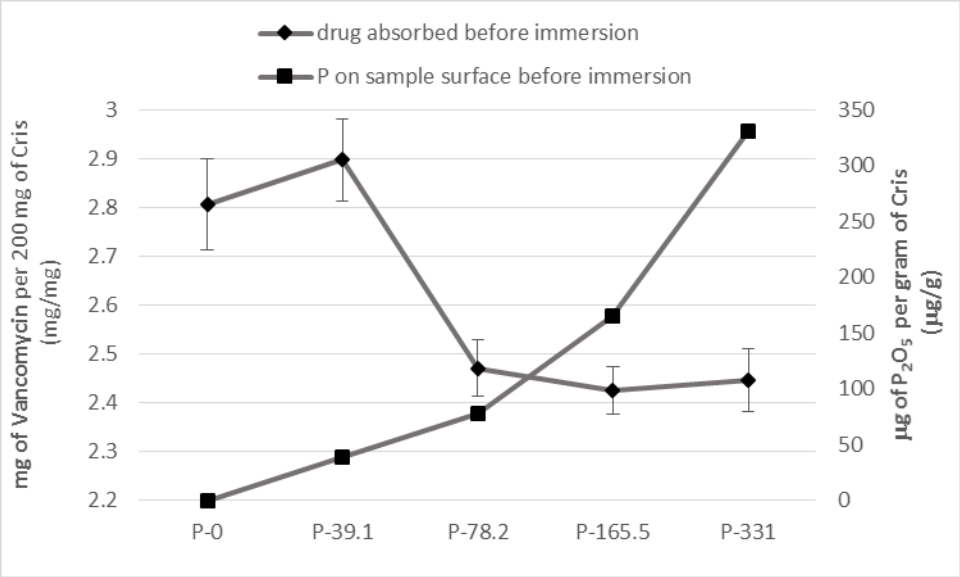

Figure 36: Vanc adsorption decreasing as P_2O_5 per gram of Cris increases on non-immersed samples

3.5 Surface Chemistry Analysis After Drug Adsorption

3.5.1 Surface Chemistry Analysis After Drug Adsorption for Non-Immersed Cris

Figure 37 (A-E), below shows a representative FTIR spectra of each non-immersed Cris sample with and without Vanc loading. Figure 37A, shows the following changes in sample P-0 after drug loading: (1) decrease in the area and intensity of the O-Si-O bending band with symmetry *E* near 500 cm^{-1}; (2) increase in the area of the O-Si-O bending band with symmetry A_2 at 621.6 cm^{-1}; (3) increase in area of the Si-O-Si symmetric stretching band at 798 cm^{-1}; (4) decrease in the area and intensity of the Si-O-Si stretching and Si-O-Si asymmetric stretching bands near 1050 and 1150 cm^{-1}, respectively; and (5) appearance of a*ν* C-C-O/ CO_2^- symmetric stretching bands corresponding to Vanc at 1246.6 and 1315.6 cm^{-1}. Figure 37B, shows the following changes in sample P-39.1 after drug loading: (1) decrease in the area and intensity of the O-Si-O bending band with symmetry *E* near 500 cm^{-1}; (2) increase in area of the Si-O-Si symmetric stretching band at 798 cm^{-1}; and (3) decrease in the area and intensity of the Si-O-Si stretching and Si-O-Si asymmetric stretching bands near 1050 and 1150 cm^{-1}, respectively. Figure 37C, shows the following changes in sample P-78.2 after drug loading: (1) increase in the area and intensity of the O-Si-O bending band with symmetry *E* near 500 cm^{-1}; (2) decrease in the area and intensity of the O-P-O bending at 560.1 cm^{-1}; (3) increase in the area and intensity of the Si-O-Si stretching and Si-O-Si asymmetric stretching bands near 1050 and 1150 cm^{-1}, respectively; and (4) decrease in the area of the P=O stretching bands near 1300 cm^{-1}. Figure 37D shows the following changes in sample P-165.5 after drug loading: (1) increase in the area and intensity of the O-Si-O bending band with symmetry *E* near 500 cm^{-1}; (2) decrease in the area and

intensity of the Si-O-Si stretching and Si-O-Si asymmetric stretching bands near 1050 and 1150 cm^{-1}, respectively; and (3) increase in the area and intensity of the P=O stretching bands near 1300 cm^{-1}. Figure 37E shows the following changes in sample P-331 after drug loading: (1) increase in the area and intensity of the O-Si-O bending band with symmetry *E* near 500 cm^{-1}; (2) decrease in the area of the O-P-O bending at 559.5 cm^{-1}; (3) increase in the area and intensity of the Si-O-Si stretching and Si-O-Si asymmetric stretching bands near 1050 and 1150 cm^{-1}, respectively; and (4) decrease in the area of the P=O stretching bands near 1300 cm^{-1}.

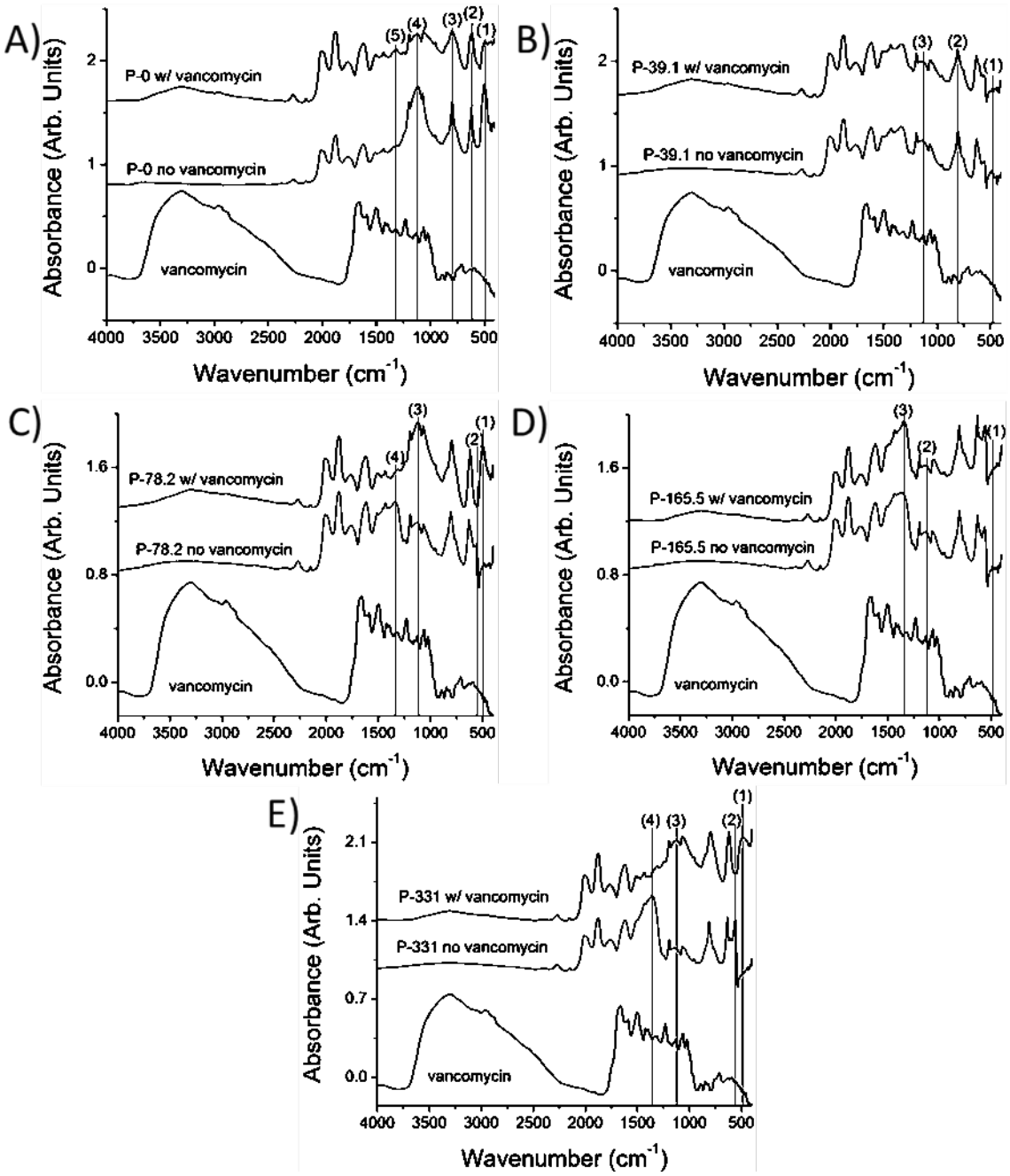

Figure 37: FTIR spectra of non-immersed Cris samples normalized to the highest peak intensity and base line corrected of A) P-0, B) P-39.1, C) P-78.2, D) P-165.5, and E) P-331 without and with vancomycin loading

Figure 38 (A-E) and 39 (A-E) shows the Gaussian fitting of the FTIR spectra for non-immersed Cris samples with Vanc loading from 1230-470 cm^{-1} and 1560-1185 cm^{-1}, respectively.

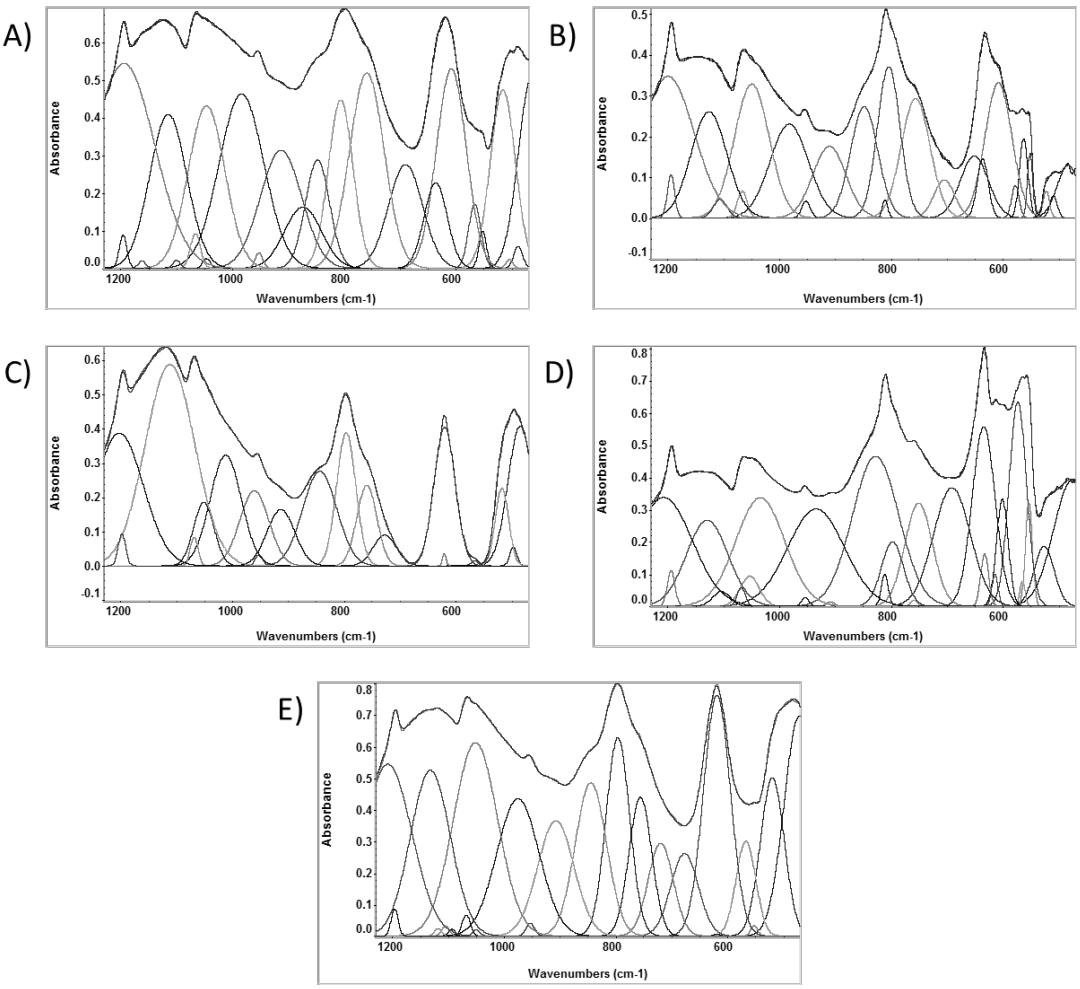

Figure 38: Gaussian peak fitting normalized to the highest peak intensity and base line corrected FTIR spectra of non-immersed and Vancomycin loaded Cris samples A) P-0, B) P-39.1, C) P-78.2, D) P-165.5, and E) P-331 from 1230cm^{-1} to 470 cm^{-1}

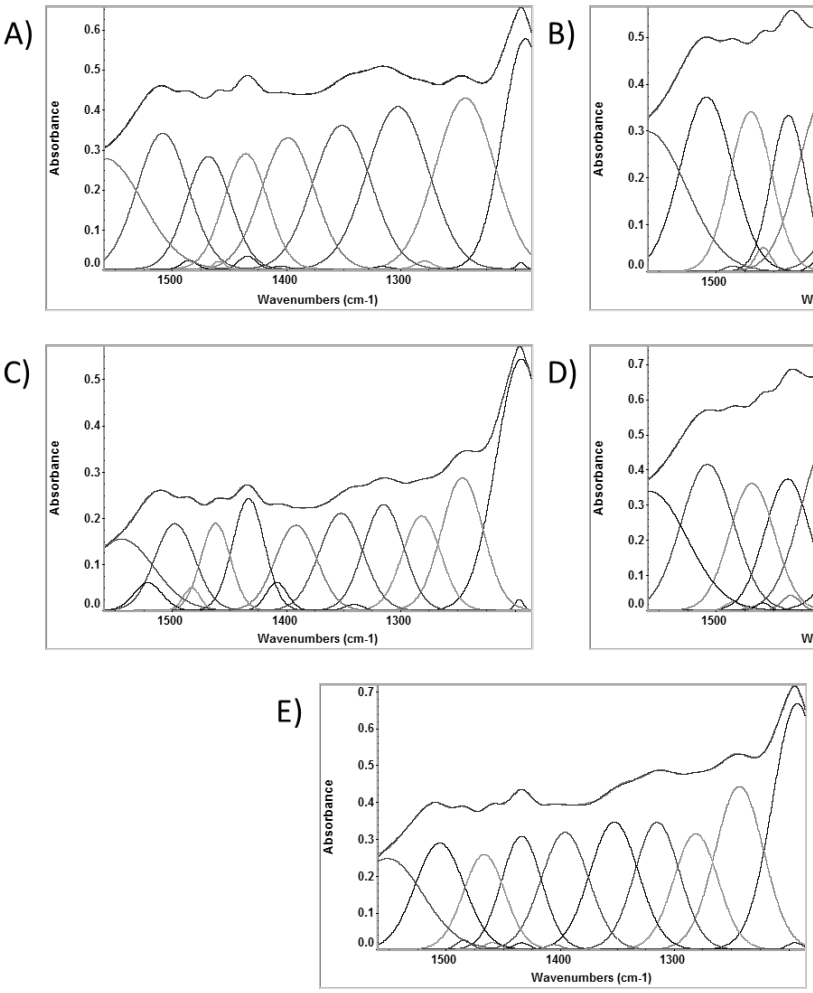

Figure 39: Gaussian peak fitting normalized to the highest peak intensity and base line corrected FTIR Spectra of non-immersed and Vancomycin loaded Cris samples A) P-0, B) P-39.1, C) P-78.2, D) P-165.5, and E) P-331 from 1560cm^{-1} to 1185 cm^{-1}

Figure 40A and 40B shows the Gaussian fit of FTIR spectra for Vanc at 1230-470 cm^{-1} and 1560-1185 cm^{-1}, respectively.

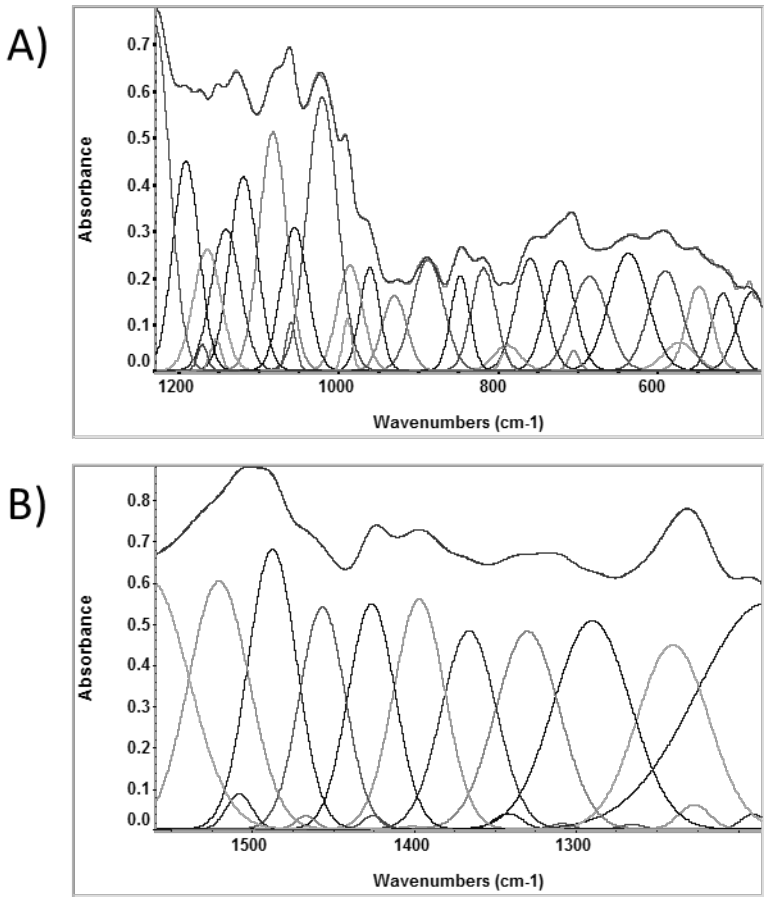

Figure 40: Gaussian peak fitting normalized to the highest peak intensity and base line corrected FTIR spectra of Vancomycin from A) 1230-470 cm^{-1} and B) 1560-1185 cm^{-1}

The band assignments and areas before and after Gaussian fitting of non-immersed Cris samples with and without Vanc loading are documented below in Table 11-15.

Table 11: Band position and area of functional groups found in non-immersed P-0 samples with and without Vanc loading and before and after Gaussian fitting

		Wavenumbers (cm^{-1})			
		band position/area			
Functional Group	**Assignment**	**P-0 (no G-fit)**	**P-0-Vanc (no G-fit)**	**P-0 (G-fit)**	**P-0-Vanc (G-fit)**
O-Si-O bending	490, 500 [26-28]	498.4/23.6	489.1/5.4	488.8/64.3, 504.9/3.3, 524.6/4	468.6/32.9, 489.8/2.1, 504/1.2, 520/19.3
O-Si-O bending	620 [26-28]	621.6/13.7	618.1/20.1	576.1/31.9, 621.5/1.1, 622.1/20.1, 651.3/5.1, 680.8/13	550.9/2.1, 565.2/6.3, 605.7/30.6, 635.7/16.4, 691.2/20.7
Si-O-Si symmetric stretching	798[27], 797 [26, 28], 860-940 [35]	798/28.6	797.7/27.1	721.4/13.4, 761.8/20.4, 797.5/9.7, 829.2/49.1	758/38.1, 803.7/23.7, 846.1/20.5,
N-H rocking mode	~810 [32]	none	none	none	860.8/7.5
Si-O-H stretching	~950 [32]	951.7/.4	955.5/0.5	910.3/21.9, 953.6/0.4, 969.5/29.3	909.1/31.4, 952.9/0.9, 982.5/46
Si-O-Si stretching	1025, 1050[32]	1072.3/2	1064.9/6.1	1040.2/46.6, 1062.3/7.5, 1070.5/1.5	1052.6/0.2, 1058.6/52.9, 1069.6/1.5
Si-O-Si Asymmetric Stretching	1144, 1196, 1100 [28], 1120-1162 [32], 1160 [36]	1117.4/10.1, 1196.7/2.5	1120.7/4.4, 1194.3/1.8	1107.4/46.8, 1152.6/31.3, 1200.1/2.2 1207.5/58.6	1096.9/1.3, 1151.2/2.8, 1194.81/65, 1194.82/1
a*v* C-C-O/ CO_2^- symmetric stretch	1230 [37]/ 1396 [22]	none	1246.6/0.4, 1315.6/3.3	none	1122.4/18.8, 1168.2/1, 1279/0.4, 1316/0.1,
N-H vibrations / NH_2	1436.7, 1486.4 [32]/ 1445, 1460, 1472 [22]	none	none	none	1398.8/19.1, 1459.2/0.2
O-H vibrations	~1450 [34], ~1600 [33]	1434.9/0.5, 1458.3/0.07, 1482.6/0.03, 1509.8/0.9	1434.4/0.7, 1458.2/0.1, 1485.4/0.09, 1509.7/1.5	1242.8/28.5, 1298.4/18.9, 1338.8/12.9, 1371.4/9.9, 1401.6/9, 1433/10.7, 1466.6/11.7, 1486.9/.4, 1509.3/11.7, 1557.9/16.5	1243.1/27.8, 1302.2/27.4, 1351.4/22.9, 1405.2/0.1, 1434.4/0.6, 1435.8/13.7, 1468.5/13.6 1485.4/0.3, 1508.6/19, 1559.4/22.9

Drug binding was associated to the following changes to the FTIR spectra of sample P-0 as confirmed by Gaussian fitting in Table 11: (1) increase in the bands located at 621.6, 951.7, and 1072.3 cm^{-1} corresponding to O-Si-O bending with symmetry *E,* Si-O-H stretching, and Si-O-Si stretching, respectively; (2) increase in area of the O-H vibration bands at 1434.9, 1458.3, 1482.6, and 1509.8 cm^{-1}; (3) a decrease in the area of the bands at 498.4, 798, and 1117.4 and 1196 cm^{-1} corresponding to O-Si-O bending with symmetry A_2, Si-O-Si symmetric stretching (band at 721.4 cm^{-1} disappeared after drug loading according to Gaussian fitting in Table 11), and Si-O-Si asymmetric stretching; and (4) the appearance of a*v* C-C-O/ CO_2^- symmetric stretching bands corresponding to Vanc at 1246.6 and 1315.6 cm^{-1}.

Additionally, Gaussian fitting reveals other bands belonging to Vanc which are associated to drug binding onto sample P-0. The N-H rocking mode bands appear at 860.8 cm^{-1}. The a*v* C-C-O/ CO_2^- symmetric stretching bands appear at 1122.4, 1168, 1279, and 1316 cm^{-1}. The N-H vibrations / NH_2 bands that appear at 1398.8 and 1459.2 cm^{-1}.

Table 12: Band position and area of functional groups found in non-immersed P-39.1 samples with and without Vanc loading and before and after Gaussian fitting

		Wavenumbers (cm^{-1})			
		band position/area			
Functional Group	**Assignment**	**P-39.1 (no G-fit)**	**P-39.1-Vanc (no G-fit)**	**P-39.1 (G-fit)**	**P-39.1-Vanc (G-fit)**
O-Si-O bending	490, 500 [26-28]	488.1/5	484.8/2.3	487.9/15.8, 508/0.2, 524/2.4	483.1/6.4, 509.4/0.9, 522.4/0.9
HPO_4	551 [29-31]	none	none	552.2/3	551.4/1.8
ν_4 PO_4/O-P-O bending	567, 572, 602 [29-31]/ 577,597 [32]; 560 [33, 34]	557.6/3.5	565.4/2.5	562.7/1.1, 569.9/6.0 591.4/1.1	562.8/3.6, 577.8/1.3
O-Si-O bending	620 [26-28]	629.8/11.8	632/10.2	618.6/28.8, 653.6/5.9	608/19.9, 651.3/9.5
P-O-P stretching	758.9 [32]; ~650, ~700 [33]	698.6/.02, 756.9/.5	758.2/.4	633.6/2.5, 704.6/10.8	636.2/3.5, 705/4.2
Si-O-Si symmetric stretching	798[27], 797 [26, 28], 860-940 [35]	807.6/7.1	809.4/6.1	761.6/22.7, 803.9/16.9, 844/23.9	756.4/18.8, 804.6/18.7, 848.6/16.5
N-H rocking mode	~810 [32]	none	none	none	811.1/0.5
Si-O-H stretching	~950 [32]	956.2/.4	955.9/0.3	909.6/15.9, 952.4/0.8, 975.6/19.6	910.9/12.9, 952.8/0.7, 982.8/19.7
Si-O-Si stretching	1025, 1050[32]	1069.8/3.1	1065.8/6.3	1044.9/30.6, 1052.2/0.5, 1068.8/1.2	1049.8/25.4, 1067.1/1.4
Si-O-Si Asymmetric Stretching	1144, 1196, 1100 [28], 1120-1162 [32], 1160 [36]	1143.9/3.4, 1193.7/2.3	1150.1/2.6, 1193.5/2.1	1122.0/40.3, 1162.3/.2, 1194.8/1.6, 1203.7/48.4	1106.6/1.3, 1126.6/20.8, 1194.6/1.6, 1199.9/40.4
aν C-C-O/ CO_2^- symmetric stretch	1230 [37]/ 1396 [22]	none	none	none	1242.3/22.6, 1311.5/32.7
P=O stretching	1230-1300, 1390 [33]	1248.3/0.3, 1343.9/10.1	1250/0.3, 1341.2/8.9	1245.6/.3, 1347.8/.2, 1381/.1	1245.3/0.3, 1348.3/0.1,
P-O-H bending	1406 [32]	none	none	1409.8/.2, 1458.8/0.5	1404.4/21.9, 1408.2/0.5
O-H vibrations	~1450 [34], ~1600 [33]	1434.7/0.6, 1456.9/0.1, 1480/0.03, 1510.6/1.4	1434.4/0.7, 1457.4/0.07, 1486.3/0.08, 1508.4/1.4	1242.3/23.1, 1301.5/30.8, 1338.8/23, 1372.2/19.6, 1403.8/18.6, 1435.6/19.9, 1469.8/20.6, 1485.7/0.1, 1509.8/23.9, 1561.6/32.6	1360.3/23.9, 1436.9/12.5, 1459/0.8, 1469.8/15.6, 1485.7/0.1, 1508.7/21.1 , 1560.3/24.9

Drug binding was associated to the following changes in the FTIR spectra of sample P-39.1 as confirmed by Gaussian fitting in Table 12: (1) decrease in area of the bands at 488.1, 557.6, 629.8, 807.6, 956.2, 1069.8, 1248.3, and 1343.9 cm^{-1} corresponding to O-Si-O bending with symmetry A_2, O-P-O bending (Gaussian fitting showed the disappearance of the band at 591.4 cm^{-1}), O-Si-O bending with symmetry *E*, Si-O-Si symmetric stretching, Si-O-H stretching, Si-O-Si stretching (Gaussian fitting showed the disappearance of the band at 1052.2 cm^{-1}), and P=O stretching (Gaussian fitting showed the disappearance of the band at1381 cm^{-1}); (2) disappearance of the band at 698.6 cm^{-1} and decrease in area of the band at 756.9 cm^{-1} both corresponding to P-O-P stretching; (3) decrease in the area of both bands at 1143.9 and 1193.7 cm^{-1} corresponding to Si-O-Si asymmetric stretching; and (4) a decrease of the P=O stretching band 1343.9 cm^{-1}.

Additionally, Gaussian fitting in Table 12, reveals other changes in bands corresponding to phosphate, silicate, or Vanc functional groups which are associated to drug binding onto sample P-39.1. There is an increase in the area of the P-O-H bending band at 1409.8 cm^{-1}. Disappearance of O-H vibration bands at 1242.3, 1301.5, 1338.8, and 1403.8 cm^{-1}. Appearance of N-H rocking mode bands at 811.1 cm^{-1}, and a*ν* C-C-O/ CO_2^- symmetric stretching bands at 1242.3 and 11311.5 cm^{-1} corresponding to Vanc.

Table 13: Band position and area of functional groups found in non-immersed P-78.2 samples with and without Vanc loading and before and after Gaussian fitting

		Wavenumbers (cm^{-1})			
		band position/area			
Functional Group	**Assignment**	**P-78.2 (no G-fit)**	**P-78.2-Vanc (no G-fit)**	**P-78.2 (G-fit)**	**P-78.2-Vanc (G-fit)**
O-Si-O bending	490, 500 [26-28]	486.6/3.8	496/15.9	484.3/9, 511.4/1.5, 523.9/0.8	484.6/22.5, 497/0.8, 517.4/6.7
HPO_4	551 [29-31]	none	none	550.8/1.5	none
***v*$_4$ PO_4/ O-P-O bending**	567, 572, 602 [29-31]/ 577,597 [32]; 560 [33, 34]	560.1/4.0	none	558.6/3.5, 571.5/3.3, 588.2/5.5	566.6/0.2, 577.4/0.02,
O-Si-O bending	620 [26-28]	631.4/10.4	620.7/18.9	627.4/28.8	620.1/19
P-O-P stretching	758.9 [32]; ~650, ~700 [33]	757.4/0.5	none	633.7/0.6, 691.5/6.4	727.5/4.6
Si-O-Si symmetric stretching	798[27], 797 [26, 28], 860-940 [35]	808.1/8.7	797.4/6.2	763.2/31.7, 804.9/10.7, 844.5/21.6	759.5/10.5, 796.5/16.6, 843.9/21
Si-O-H stretching	~950 [32]	955.9/0.6	956.6/0.3	909.4/14.2,953.5/0.6 , 983.7/25.7	913.5/10.1, 952.8/0.5, 961.1/14.2
Si-O-Si stretching	1025, 1050[32]	1068.7/4.1	1069.7/3.8	1061.2/34.9, 1069.2/0.8	1051.5/8.4, 1068.9/1.4
Si-O-Si Asymmetric Stretching	1144, 1196, 1100 [28], 1120-1162 [32], 1160 [36]	1123.2/3.4, 1193.8/2.4	1117.7/6.7, 1195.4/2.8	1104.2/2.2, 1168.7/3.1, 1195.1/3 1207.7/35.6	1012.4/22.5, 1112.1/65.1, 1198.3/1.5, 1203/41.7
a*v* C-C-O/ CO_2^- symmetric stretch	1230 [37]/ 1396 [22]	none	1313.8/.2	none	1281.4/8.5, 1314.9/9.9
P=O stretching	1230-1300, 1390 [33]	1245.3/0.4, 1342.1/16.3	1241.3/0.3, 1341.6/0.2	1246.9/.1, 1348.9/.2, 1378.8/.06	1245.8/13.1, 1352.1/9.9
P-O-H bending	1406 [32]	none	none	1406.4/.2, 1458.7/0.3	1408.6/1.3
N-H vibrations / NH_2	1436.7, 1486.4 [32]/ 1445, 1460, 1472 [22]	none	none	none	1391.7/8.3
O-H vibrations	~1450 [34], ~1600 [33]	1434.8/0.6, 1456.9/0.08, 1481.3/0.01, 1509.8/1.3	1434.9/0.6, 1458.7/0.08, 1488.8/0.06, 1510.6/1.3	1243.9/18.3, 1302/28.5, 1340.4/22.3, 1373.4/18.2, 1403.6/17.1, 1434.5/19, 1467/18.8, 1485.9/0.3, 1506.4/21.8, 1554.2/29.8	1340.8/0.2, 1433.3/8.3, 1462.2/6, 1483.2/0.8, 1498.1/8.1, 1521.5/1.8, 1544.9/10.9

Drug binding was associated to the following changes in the FTIR spectra of sample P-78.2 as confirmed by Gaussian fitting in Table 13: (1) increase in the area of the band at 486.6 cm^{-1}, corresponding to O-Si-O bending with symmetry A_2; (2) increase in the area of the bands at 1123.2 and 1193.8 cm^{-1}, corresponding to Si-O-Si asymmetric stretching; (3) decrease in the area of bands at 808.1, 955.9, and 1068.7 cm^{-1} corresponding to Si-O-Si symmetric stretching, Si-O-H stretching, and Si-O-Si stretching; and (4) Disappearance of the bands at 560.1 and 757.4 cm^{-1}, corresponding to O-P-O bending (Gaussian fitting showed the disappearance of a band at 558.6 cm^{-1}) and P-O-P stretching bands (Gaussian fitting showed the disappearance of the band at 633.7 cm^{-1}), respectively.

Gaussian fitting in Table 13, reveals other changes or appearance of bands corresponding to phosphate, silicate, or Vanc functional groups which are associated to drug binding onto sample P-78.2. P=O stretching bands around 1378.8 cm^{-1} disappeared. After drug loading O-H vibration bands at 1243.9, 1302, 1373.4, 1403.6, and 1458.7 cm^{-1} disappeared. Appearance of aν C-C-O/ CO_2^- symmetric stretching bands appear at 1281.4 and 1314.9 cm^{-1}, and N-H vibrations / NH_2 bands appear at 1391.7 cm^{-1} corresponding to Vanc.

Table 14: Band position and area of functional groups found in non-immersed P-165.5 samples with and without Vanc loading and before and after Gaussian fitting

		Wavenumbers (cm^{-1})			
		band position/area			
Functional Group	**Assignment**	**P-165.5 (no G-fit)**	**P-165.5-Vanc (no G-fit)**	**P-165.5 (G-fit)**	**P-165.5-Vanc (G-fit)**
O-Si-O bending	490, 500 [26-28]	484.8/2.8	483.7/1.4	484.6/8.2, 509.2/0.7, 522.8/1	476.2/32.4, 526.2/8.3
HPO_4	551 [29-31]	none	none	551.6/2.2	553.5/4.8
***v*$_4$ PO_4/ O-P-O bending**	567, 572, 602 [29-31]/ 577,597 [32]; 560 [33, 34]	564.1/7.5	557.1/8.5	560.1/4.1, 572.6/7.3, 595/7.1	573.3/24.9, 601/8.6, 614.2/1.3
O-Si-O bending	620 [26-28]	631.8/8.5	633.1/8.2	631.5/28.9	632.7/2.7
P-O-P stretching	758.9 [32]; ~650, ~700 [33]	690.4/0.01, 754.5/0.4	756.8/0.5	634.5/2.2, 693.2/6.4	634.5/28.6, 691.3/30.4
P-O-P bending	800-870, ~780 [33]	none	none	810.8/0.4	811.6/1.5
Si-O-Si symmetric stretching	798[27], 797 [26, 28], 860-940 [35]	809.2/6.4	810/11.7	760.3/29.6, 805.4/13.3, 845.1/18.3	750.9/19.7, 797.8/9.8, 828/48.3
Si-O-H stretching	~950 [32]	956.1/0.3	955.8/0.3	905.7/14.6, 952.7/0.6, 982.2/21.5	909.1/0.2, 934.7/38.3 , 954.2/0.4
Si-O-Si stretching	1025, 1050[32]	1066.6/5.4	1062.3/5.7	1054.7/27.9, 1067.7/1	1053.5/3.9, 1068.7/1
Si-O-Si Asymmetric Stretching	1144, 1196, 1100 [28], 1120-1162 [32], 1160 [36]	1143/3.1, 1193.8/2.4	1143.7/2.06, 1193.3/2.1	1107.8/2.5, 1133.5/22.9, 1195.1/2, 1201.8/35.9	1104.3/1.7, 1129.7/24.7, 1194.5/1.8, 1207.6/43.1
a*v* C-C-O/ CO_2^- symmetric stretch	1230 [37]/ 1396 [22]	none	none	none	1034.7/36.8
P=O stretching	1230-1300, 1390 [33]	1245.6/0.2, 1355.9/15.9	1245.2/0.2, 1345.7/10.1	1237.5/10.6, 1320/60.2, 1392/46.2	1245.5/0.1, 1311.3/38.2
P-O-H bending	1406 [32]	none	none	1447.1/31.9, 1458.6/0.1, 1496.2/27.5, 1520.9/2	1402.4/28.2
N-H vibrations / NH_2	1436.7, 1486.4 [32]/ 1445, 1460, 1472 [22]	none	none	none	1468.9/17.7, 1485.1/0.4, 1507.9/23.8,
O-H vibrations	~1450 [34], ~1600 [33]	1433.8/0.4, 1459/0.7, 1483.6/0.03, 1510.9/0.8	1433.4/0.7, 1459.6/0.1, 1482.7/0.08, 1507.1/1.2	1246.1//0.4, 1435.5/0.3, 1520.9/2, 1559.2/39.1	1243.3/22.9, 1357.3/33.6, 1434.8/0.8, 1437.6/18.4, 1459.3/0.2, 1558.4/27.6

Drug binding was associated to the following changes in the FTIR spectra of sample P-165.5 as confirmed by Gaussian fitting in Table 14: (1) increase in the area of the bands at 564.1 and 809.2 cm^{-1}, corresponding to O-P-O bending and Si-O-Si symmetric stretching; and (2) decrease in the area of the bands at 484.8 and 631.8 cm^{-1}, and 1355 cm^{-1}, corresponding to O-Si-O bending (Gaussian fitting showed the disappearance of the band at 509.2 cm^{-1}) and P=O stretching (Gaussian fitting showed the disappearance of the band at 1381cm^{-1}).

Gaussian fitting in Table 14, reveals other changes and bands corresponding to phosphate, silicate, or Vanc functional groups which are associated to drug binding onto sample P-165.5. Both P-O-P stretching and P-O-P bending bands show an increase in area (Table 14). Si-O-Si stretching band at 1053.5 cm^{-1} shows a sharp decrease in area. Si-O-Si asymmetric stretching bands at 1129.7 and 1207.6 cm^{-1} show an increase in area. P-O-H bending only had one band present at 1402.4 cm^{-1}after drug loading. After drug loading P-165.5 had an appearance of an extra O-H vibration band at 1520.9 cm^{-1}. The appearance of aν C-C-O/ CO_2^- symmetric stretching bands appear at 1034.7 cm^{-1}, and N-H vibrations / NH_2 bands appear at 1468.9, 1485.1, and 1507.9 cm^{-1} corresponding to Vanc.

Table 15: Band position and area of functional groups found in non-immersed P-331 samples with and without Vanc loading and before and after Gaussian fitting

		Wavenumbers (cm^{-1})			
		band position/area			
Functional Group	**Assignment**	**P-331 (no G-fit)**	**P-331-Vanc (no G-fit)**	**P-331 (G-fit)**	**P-331-Vanc (G-fit)**
O-Si-O bending	490, 500 [26-28]	484.6/2	486.1/14.2	476.1/7.5, 507.6/1.6, 522.2/0.6	471.9/46.8, 519.8/26.7
HPO_4	551 [29-31]	none	none	555.3/5.8	552.5/0.5
***v*$_4$ PO_4/ O-P-O bending**	567, 572, 602 [29-31]/ 577,597 [32]; 560 [33, 34]	559.5/10.5	none	569.4/12, 594.1/8.5, 611.3/0.9	567.3/13.2
O-Si-O bending	620 [26-28]	633.4/5.4	619.5/18.6	635.2/25.4	619.1/46
P-O-P stretching	758.9 [32]; ~650, ~700 [33]	759.6/0.3	none	695.3/0.6	677.1/16.2, 719.9/16.5
P-O-P bending	800-870, ~780 [33]	none	849.1/0.3	812.6/2, 748/33.3	none
Si-O-Si symmetric stretching	798[27], 797 [26, 28], 860-940 [35]	810.7/5.6	797/14.4	760.4/.1 801.3/2, 830.2/33.4	756.3/22.3, 796.6/33.2, 844.8/33.9
Si-O-H stretching	~950 [32]	955.9/0.3	957/0.4	910.2/0.2, 955.6/0.3, 947.8/25.6	907.7/29.7, 953.4/0.7, 975.6/41.3
Si-O-Si stretching	1025, 1050[32]	1065.8/4.5	1065.8/6.1	1053.7/34.9, 1066.5/0.9	1051.5/60.9, 1068.2/1.2
Si-O-Si Asymmetric Stretching	1144, 1196, 1100 [28], 1120-1162 [32], 1160 [36]	1149/2.2, 1193.6/2	1120.6/3.6, 1194.5/2.0	1109/1.5, 1138.8/16.1, 1194.7/1.5	1105.3/0.5, 1132.5/46.9, 1196.5/1.3, 1208.8/58.7
a*v* C-C-O/ CO_2^- symmetric stretch	1230 [37]/ 1396 [22]	none	1311.6/0.3	none	1094.1/0.3, 1118.7/0.3, 1281.1/15.2
P=O stretching	1230-1300, 1390 [33]	1249.4/0.2, 1358.8/22.4	1245/0.5, 1341.6/0.2	1316.2/35.4, 1360.9/37.9	1315/16.9, 1352.7/18.3, 1395.8/16.4
P-O-H bending	1406 [32]	none	none	1405.9/34.3, 1441.9/20.6, 1458.1/0.3, 1475.4/20.8, 1513/22.8	1405.6/0.1
N-H vibrations/ NH_2	1436.7, 1486.4 [32]/ 1445, 1460, 1472 [22]	none	none	none	1466.8/11.6, 1484.7/0.3
O-H vibrations	~1450 [34], ~1600 [33]	1432.1/0.4, 1458.3/0.06, 1480/0.01, 1511.2/0.8	1434.5/0.7, 1458.2/0.08, 1485.4/0.09, 1509.7/1.3	1245.3/20.3, 1245.3/0.2, 1436.8/0.4, 1565/33.1	1242.8/23.4, 1434/13.4, 1459.5/0.2, 1505.8/15.4, 1551.7/19.2

Drug binding was associated to the following changes to in the FTIR spectra of sample P-331 as confirmed by Gaussian fitting in Table 15: (1) the increase in the area of the bands at 484.6, 633.4, 810.7, 955.9, and 1065.8, cm^{-1}, corresponding to O-Si-O bending with symmetry A_2 (Gaussian fitting showed the increase in area of bands at 471.9 and 519.8 cm^{-1}), O-Si-O bending with symmetry *E* (Gaussian fitting showed the increase in area of band at 619.1 cm^{-1}), Si-O-Si symmetric stretching (Gaussian fitting showed the increase in area of bands at 756.3 and 796.6 cm^{-1}) , Si-O-H (Gaussian fitting showed the increase in area of bands at 907.7, 953.4, and 975.6 cm^{-1}) stretching, and Si-O-Si stretching (Gaussian fitting showed the increase in area of bands at 1051.5 and 1068.2 cm^{-1}); (2) Si-O-Si asymmetric stretching band at 1149 increases; (3) P=O stretching bands at 1249.4 and 1358.8 cm^{-1} decrease in area; and (4) disappearance of O-P-O bending band at 559.5 cm^{-1} (Gaussian fitting showed the disappearance of the band at 594.1 and 611.3 cm^{-1}).

Gaussian fitting in Table 15, reveals other changes to phosphate and Vanc functional group bands which are associated to drug binding onto sample P-331. P-O-P bending bands at 748 and 812.6 cm^{-1} disappeared. P-O-H bending bands 1441.9, 1475.4, and 1513 cm^{-1} bands disappeared after drug loading. The appearance of a*ν* C-C-O/ CO_2^- symmetric stretching bands appear at 1094.1, 1118.7, and 1281.1 cm^{-1}, and N-H vibrations / NH_2 bands appear at 1466.8 and 1484.7 cm^{-1} which correspond to Vanc.

3.5.2 Surface Chemistry Analysis After Drug Adsorption for Pre-Immersed Cris

Figure 41 (A-E), below shows a representative FTIR spectra of each pre-immersed Cris sample with and without Vanc loading. All of the samples displayed in Figure 41 (A-E) shows the following changes after drug loading: (1) decrease in the area and intensity of the O-Si-O bending band with symmetry *E* near 500 cm^{-1}; (2) decrease in the area and intensity of the O-Si-O bending with symmetry A_2 near 620 cm^{-1}; (3) decrease in the intensity and area of the Si-O-Si symmetric stretching band near 727 cm^{-1}; and (4) decrease in the area and intensity of the Si-O-Si stretching and Si-O-Si asymmetric stretching bands near 1050 and 1150 cm^{-1}, respectively. In addition only sample P-165.5 (Figure 41D) shows an increase in area and intensity of the band marked (5) that belongs to P=O stretching bands near 1300 cm^{-1}.

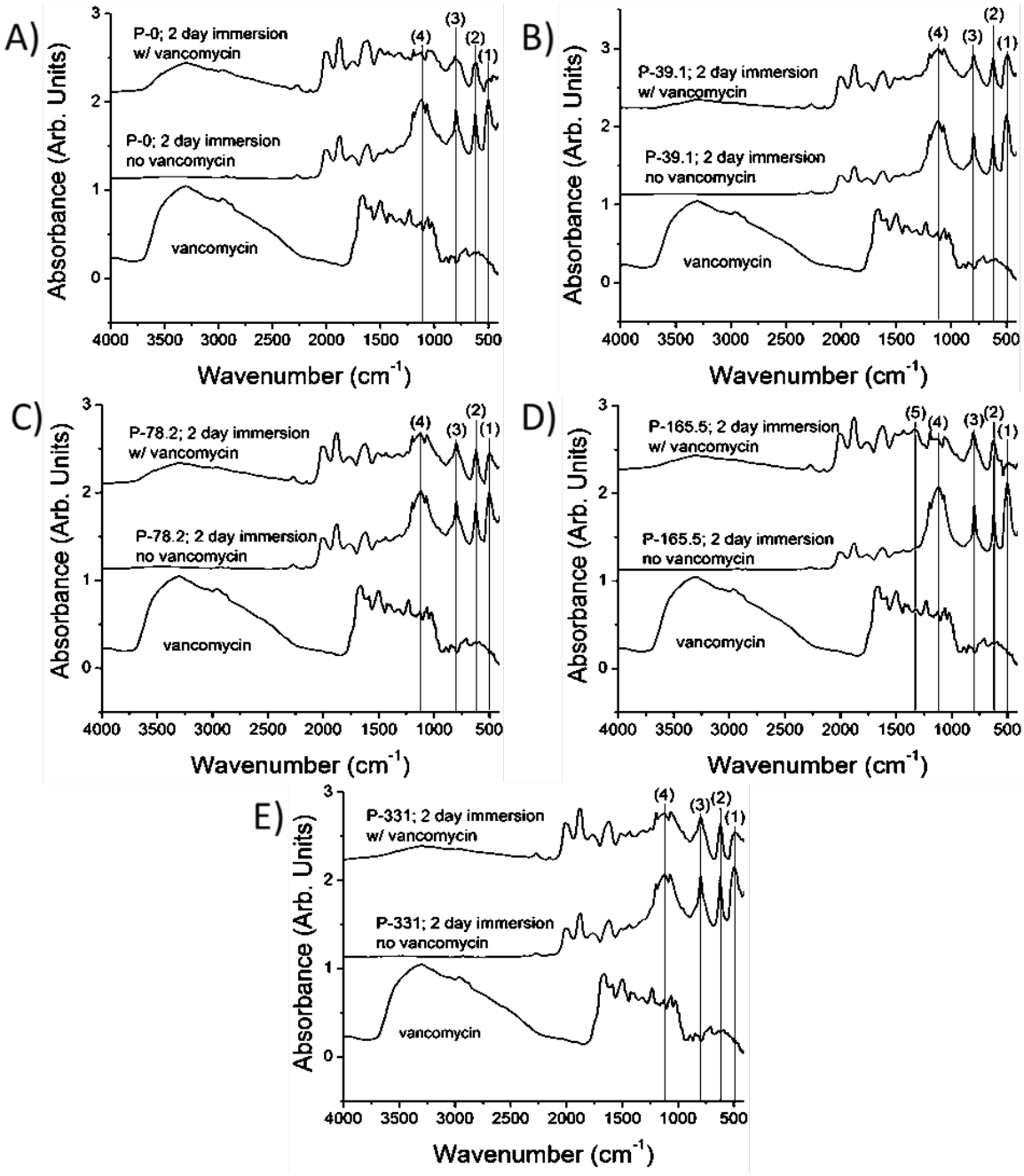

Figure 41: FTIR spectra of pre-immersed Cris samples normalized to the highest peak intensity and base line corrected of A) P-0, B) P-39.1, C) P-78.2, D) P-165.5, and E) P-331 after immersion without and with Vancomycin loading

Figure 42 (A-E) and 43 (A-E) shows the Gaussian fitting of the FTIR spectra with pre-immersed and vancomycin loaded Cris samples from 1230-470 cm^{-1} and 1560-1185 cm^{-1}, respectively.

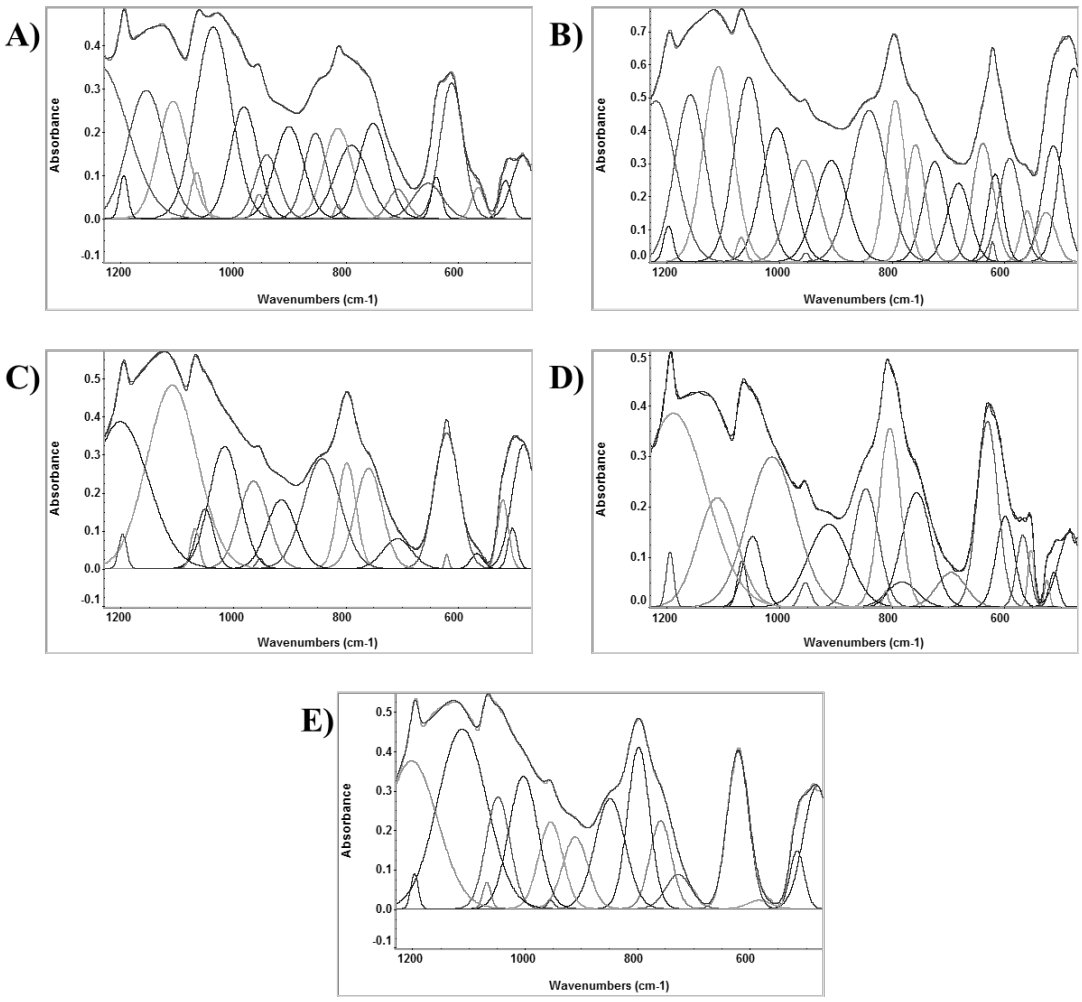

Figure 42: Gaussian peak fitting normalized to the highest peak intensity and base line corrected FTIR spectra of pre-immersed and Vancomycin loaded Cris samples A) P-0, B) P-39.1, C) P-78.2, D) P-165.5, and E) P-331 from 1230cm^{-1} to 470 cm^{-1}

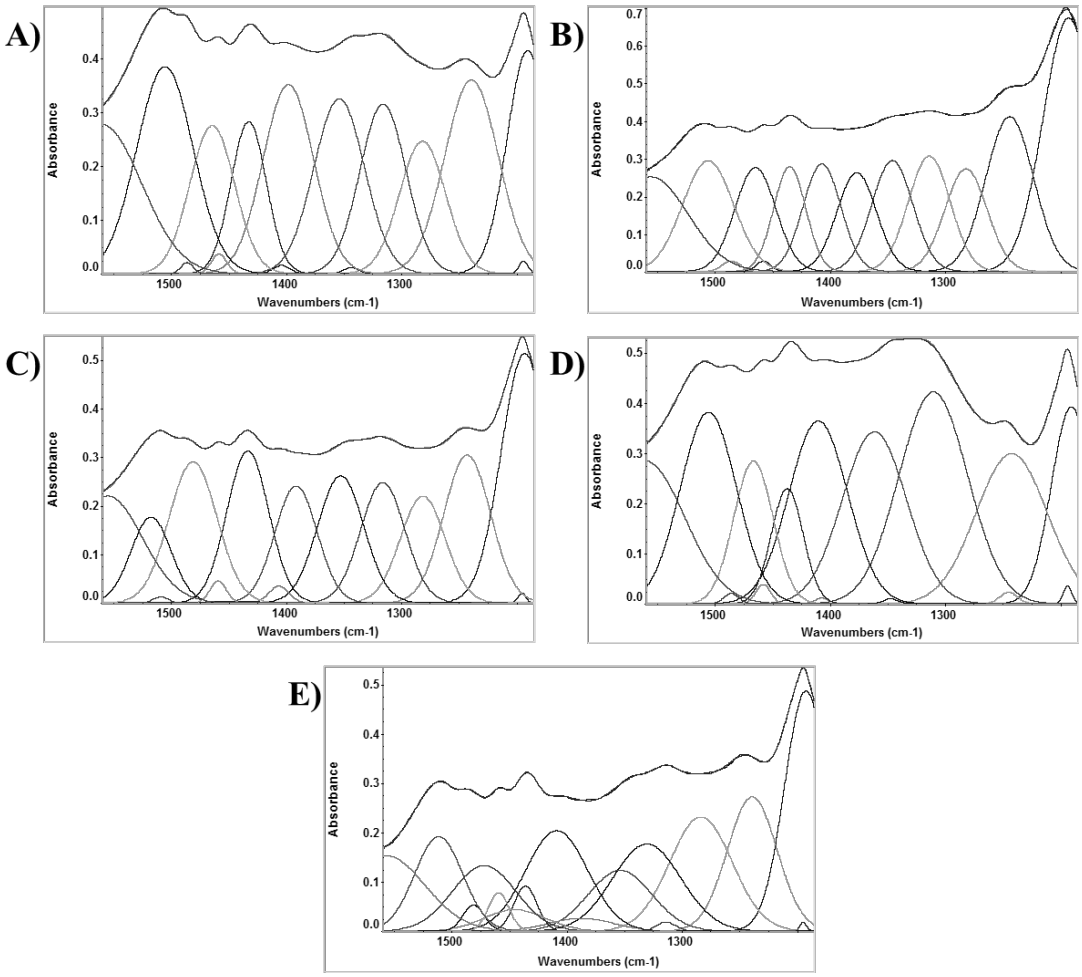

Figure 43: Gaussian peak fitting normalized to the highest peak intensity and base line corrected FTIR spectra of pre-immersed and Vancomycin loaded Cris samples A) P-0, B) P-39.1, C) P-78.2, D) P-165.5, and E) P-331 from 1560cm^{-1} to 1185 cm^{-1}

Figure 44A and 44B shows the Gaussian fit of the FTIR spectra of Vanc at 1230-470 cm^{-1} and 1560-1185 cm^{-1}, respectively.

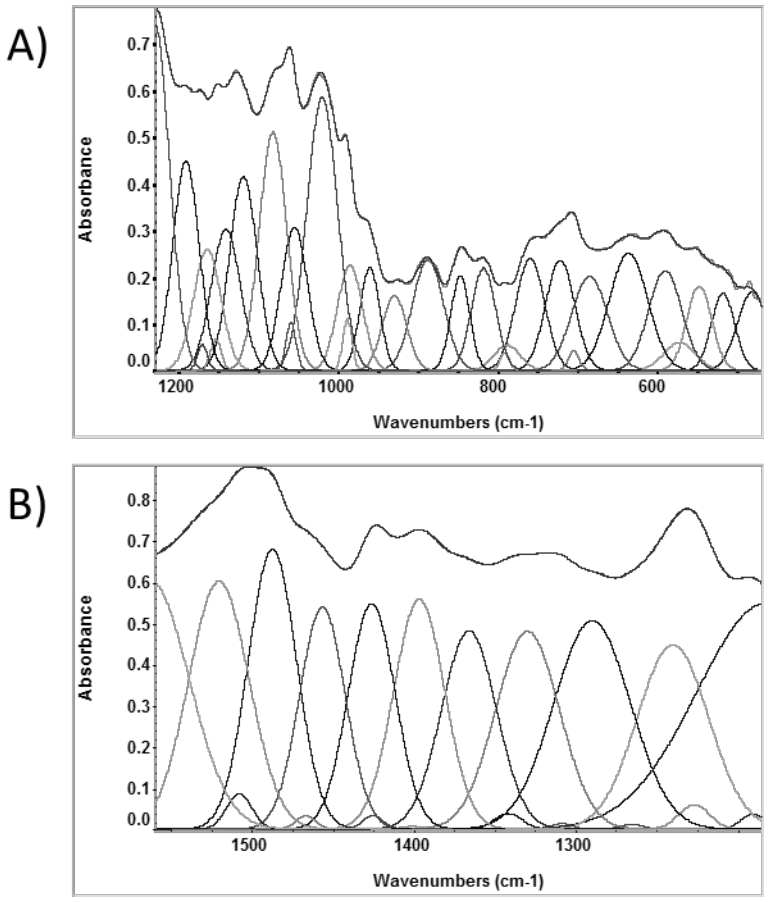

Figure 44: Gaussian peak fitting normalized to the highest peak intensity and base line corrected FTIR spectra of Vancomycin from A) 1230-470 cm^{-1} and B) 1560-1185 cm^{-1}

The band assignments and areas before and after Gaussian fitting of pre-immersed Cris samples without and with Vanc loading are documented below in Tables 16-20.

Table 16: Band position and area of functional groups found in pre-immersed P-0 samples with and without Vanc loading and before and after Gaussian fitting

		Wavenumbers (cm^{-1})			
		band position/area			
Functional Groups	**Assignment**	**P-0-imm (no G-fit)**	**P-0-imm-vanc (no G-fit)**	**P-0-imm (G-fit)**	**P-0-imm-Vanc (G-fit)**
O-Si-O bending	490, 500 [26-28]	499.5/22.8	486.5/3.2	476.8/48.9, 515.1/27.3, 557.8/0.4	484.7/7.2, 516/2.2
O-Si-O bending	620 [26-28]	621.3/16.5	611.5/18.8	573.1/13.3, 619.5/21.8, 621.3/0.9, 660.3/29.5	564.7/2, 611.8/15.6, 639/2.1, 653.8/5.1
Si-O-Si symmetric stretching	798[27], 797 [26, 28], 860-940 [35]	797.6/28.8	812.1/23.7	771.7/54, 798/6.5, 853.4/33.8	751.6/13.8, 789.8/12.2, 854/9.8
N-H rocking mode	~810 [32]	none	none	none	814.3/13
Si-O-H stretching	~950 [32]	955.7/0.5	956.6/0.4	920.57/20.8, 952.9/0.4, 960.3/14.3	901.2/13.6, 940.7/7.6, 954.3/1.1
Si-O-Si stretching	1025, 1050[32]	1070.4/3.7	1060.5/8.5	1000.6/24.3, 1053/41.5, 1069.1/2.1	981.5/15.8, 1036/35.1, 1065.6/2.7
Si-O-Si Asymmetric Stretching	1144, 1196, 1100 [28], 1120-1162 [32], 1160 [36]	1119.8/10.4, 1196/2.4	1128.1/3.2, 1193.7/1.5	1115.2/55.9, 1157.2/8.6, 1198.1/60.9	1107.7/17.8, 1155.3/24.3, 1195.5/1.8,
av C-C-O/ CO_2^- symmetric stretch	1230 [37]/ 1396 [22]	none	1245.2/0.6, 1318.3/2.7	none	1238.3/43.6, 1281.7/12.3, 1343.8/0.1, 1398.4/19.3
N-H vibrations / NH_2	1436.7, 1486.4 [32]/ 1445, 1460, 1472 [22]	none	none	none	1458.7/0.5, 1486.4/0.2
O-H vibrations	~1450 [34], ~1600 [33]	1435.1/.5, 1457.7/0.07, 1497.4/0.03, 1511.9/1	1431.2/0.7, 1459.9/0.1, 1488.1/0.2, 1507.2/1.4	1240.9/30.8, 1303.9/20.8, 1354/16.1, 1402.6/13.5, 1438.8/9.2, 1473.6/9.8, 1511.4/10.5, 1558.6/15	1239/21.1, 1316.1/15.8, 1354.2/17.9, 1404.4/0.2, 1432.9/10.8, 1464.6/13.4, 1505.8/23.6, 1560.4/23.8

Drug binding was associated to the following changes in the FTIR spectra of sample P-0 as confirmed by Gaussian fitting in Table 16: (1) decrease in the bands located at 499.5, 797.6, and 955.7 cm^{-1} corresponding to bands O-Si-O bending with symmetry A_2 (Gaussian fitting showed the disappearance of the band at 557.8 cm^{-1}), Si-O-Si symmetric stretching (Gaussian fitting showed the decrease of bands around 771.7 and 853.4 cm^{-1}), and Si-O-H stretching (Gaussian fitting showed the decrease of bands around 920.5 and 960.3 cm^{-1}); (2) decrease in area of the Si-O-Si asymmetric stretching bands, at 1119.8 and 1196 cm^{-1} (Gaussian fitting showed the decrease of bands around 1115.2 and 1198.1 cm^{-1}); and (3) an increase in the area of the bands at 1435.1, 1457.7, 1497.4, and 1511.9 cm^{-1} corresponding to O-H vibrations.

Additionally, Gaussian fitting in Table 16 reveals other changes and bands corresponding to silicate or Vanc functional groups which are associated to drug binding onto sample P-0. Si-O-Si stretching bands at 1000.6 and 1053 cm^{-1} decrease in area. O-Si-O bending bands with symmetry *E* at 573.1, 619.5, 660.3 cm^{-1} decrease in area. Appearance of N-H rocking mode bands appear at 814.3 cm^{-1}, aν C-C-O/ CO_2^- symmetric stretching bands appear at 1238.3, 1281.7, 1343.8, and 1398.4 cm^{-1}, and N-H vibrations / NH_2 bands appear at 1458.7 and 1486.4 cm^{-1} which correspond to Vanc.

Table 17: Band position and area of functional groups found in pre-immersed P-39.1 samples with and without Vanc loading and before and after Gaussian fitting

		Wavenumbers (cm^{-1})			
		band position/area			
Functional Groups	**Assignment**	**P-39.1-imm (no G-fit)**	**P-39.1-imm-Vanc (no G-fit)**	**P-39.1-imm (G-fit)**	**P-39.1-imm-Vanc (G-fit)**
O-Si-O bending	490, 500 [26-28]	488.3/32.9	494.9/20.5	473.2/25.11, 498.2/1.1, 509.8/43.5	476.6/32.2, 512.7/17.3, 525.6/6.2
***v*$_4$ PO_4/ O-P-O bending**	567, 572, 602 [29-31]/ 577,597 [32]; 560 [33, 34]	none	none	561.1/1.5	559.5/4.5
O-Si-O bending	620 [26-28]	621.5/14.6	620.8/14.4	576.6/4.1, 619.3/16, 621.6/2.7, 662.1/55.2	590.6/15.7, 616.5/9.3, 621.3/0.6, 638/16.8, 681.4/12.2
P-O-P stretching	758.9 [32]; ~650, ~700 [33]	none	none	none	758.1/15.2
Si-O-Si symmetric stretching	798[27], 797 [26, 28], 860-940 [35]	797.6/26.1	796.3/26.1	760.1/1.3, 796.5/8.8, 807.6/52	794.1/21.5, 840.7/36.5
Si-O-H stretching	~950 [32]	956.2/.3	956.2/0.3	954.4/0.2, 968.2/60.2	908.1/22.1 ,953.2/0.3, 957.5/20.8
Si-O-Si stretching	1025, 1050[32]	1070.7/4.4	1069.2/4.4	1067.9/2.4, 1068.1/56.6	1054.9/36.5, 1068.6/1.4
Si-O-Si Asymmetric Stretching	1144, 1196, 1100 [28], 1120-1162 [32], 1160 [36]	1118/10.9, 1196.6/2.5	1117.9/5.2, 1195.1/1.9	1106.1/2.6, 1125.7/.5, 1137.6/52.9, 1205.4/52.9	1109.4/39, 1159/35, 1198.1/2.2, 1220.1/42.3
a*v* C-C-O/ CO_2^- symmetric stretch	1230 [37]/ 1396 [22]	none	1249.3/1.9	none	1004.8/27.8, 1282/12.5
P=O stretching	1230-1300, 1390 [33]	1311.6/0.5	1313.4/1	none	none
P-O-H bending	1406 [32]	none	none	none	1407.4/11.7
N-H vibrations / NH_2	1436.7, 1486.4 [32]/ 1445, 1460, 1472 [22]	none	none	none	1458.3/0.4, 1486.3/0.5
O-H vibrations	~1450 [34], ~1600 [33]	1435.3/.4, 1456.9/0.05, 1480/.02, 1511.5/0.7	1434.8/0.6, 1457.6/0.07, 1487.7/0.08, 1509.6/1.2	1241.8/25.5, 1302/15.8, 1350.3/12.5, 1395.6/10.3, 1433.8/8.5, 1466.4/7.5, 1504.1/9, 1549.2/12.4	1244/21.4, 1313.9/14, 1346.1/13.1, 1377.1/11.3, 1435.4/9.7, 1465.2/12.3, 1506.4/16.3, 1556.4/20.5

Drug binding was associated to the following changes in the FTIR spectra of sample P-39.1 as confirmed by Gaussian fitting in Table 17: (1) decrease in the bands located at 488.3 and 621.5 corresponding to bands O-Si-O bending with symmetry A_2 (Gaussian fitting showed the decrease of the band around 509.8 cm^{-1}) and O-Si-O bending with symmetry *E* (Gaussian fitting showed the decrease of the bands around 619.3, 621.6, and 662.1 cm^{-1}); and (2) an increase in the area of the bands at 1435.3, 1456.9, 1480, and 1511.5 cm^{-1} corresponding to O-H vibrations (Gaussian fitting showed the increase of the bands around 1244, 1346.1, 1377.1, 1435.4, 1465.2, 1506.4, and 1556.4 cm^{-1}).

Additionally, Gaussian fitting in Table 17, reveals other changes and bands corresponding to phosphate, silicate, or Vanc functional groups which are associated to drug binding onto sample P-39.1. O-P-O bending bands at 561.1 cm-1 decreased. Disappearance of a band at 760.1 cm^{-1} band corresponding to Si-O-Si symmetric stretching. Appearance of the Si-O-H stretching bands at 908.1 cm^{-1}. Si-O-Si stretching band at 1068.1 cm^{-1} decreased. Increase in area of the Si-O-Si asymmetric stretching bands around 1106.1, 1159, and 1220.1 cm^{-1}. The absence of the P=O stretching bands. The appearance of a*ν* C-C-O/ CO_2^- symmetric stretching bands appeared at 1004.8 and 1282 cm^{-1} and N-H vibrations / NH_2 bands appear at 1458 and 1486.3 cm^{-1} corresponding to Vanc.

Table 18: Band position and area of functional groups found in pre-immersed P-78.2 samples with and without Vanc loading and before and after Gaussian fitting

		Wavenumbers (cm^{-1})			
		band position/area			
Functional Groups	**Assignment**	**P-78.2-imm (no G-fit)**	**P-78.2-imm-Vanc (no G-fit)**	**P-78.2-imm (G-fit)**	**P-78.2-imm-Vanc (G-fit)**
O-Si-O bending	490, 500 [26-28]	500/21.7	495/9.2	475.8/50.9, 500/0.3 515.6/26.4	483.6/16.5, 503.5/2.1, 520.7/4.3
v_4 PO_4/ O-P-O bending	567, 572, 602 [29-31]/ 577,597 [32]; 560 [33, 34]	none	none	556.3/1.8	none
O-Si-O bending	620 [26-28]	621.3/17.3	620.9/17.6	572.5/6.3, 610.6/17.2, 621.6/1.3, 625.5/19.9	566.9/1, 620.6/19.6, 620.7/0.3, 656/0.1
P-O-P stretching	758.9 [32]; ~650, ~700 [33]	none	none	686.2/19.4	708.5/4.9, 759.3/15.7
Si-O-Si symmetric stretching	798[27], 797 [26, 28], 860-940 [35]	798/30	798.3/26.7	762.2/38.8, 797.9/6.6, 838.7/44.8	798.4/11.3, 842.6/23.6
Si-O-H stretching	~950 [32]	956.6/0.3	956.8/0.3	924.4/26.2, 953.7/0.7	914.9/11.7, 952.4/0.4, 964.4/14.8
Si-O-Si stretching	1025, 1050[32]	1070.5/3.4	1068.1/5.5	1004.3/48.4, 1061.9/31, 1069.7/1.9	1015.9/21.8, 1050.4/6, 1068.6/2
Si-O-Si Asymmetric Stretching	1144, 1196, 1100 [28], 1120-1162 [32], 1160 [36]	1117.5/9.8, 1195.9/2.6	1121.7/5.6, 1194.8/1.7	1103.3/4.8, 1128.4/58.2, 1169.6/1.6, 1198.4/3.3, 1206.6/58.4	1109/53.7, 1197.4/1.5, 1201.6/48.5
P=O stretching	1230-1300, 1390 [33]	1243.9/0.3, 1314.6/1	1244.6/0.4, 1317.7/1.4	1317/0.2	1316.3/11.9
P-O-H bending	1406 [32]	none	none	1459.3/0.1, 1483.7/0.3	1406.8/0.7
N-H vibrations / NH_2	1436.7, 1486.4 [32]/ 1445, 1460, 1472 [22]	none	none	none	1447.2/0.2, 1517.9/7.67,
O-H vibrations	~1450 [34], ~1600 [33]	1435.1/0.5, 1450.9/0.06, 1482.7/0.02, 1511.8/1.1	1434.1/0.6, 1458.6/0.9, 1486.7/0.07, 1509.8/1.4	1241.3/28, 1300.8/20.6, 1350.7/17.3, 1397.9/14.1, 1435.2/10.7, 1466.9/9.8, 1506.5/12.2, 1552.3/16.7	1242.8/15.4, 1281.5/10.6, 1352.9/13, 1391.7/11, 1433.7/14.2, 1459.5/0.7, 1509.4/0.1, 1555.6/16.7

Drug binding was associated to the following changes in the FTIR spectra of sample P-78.2 as confirmed by Gaussian fitting in Table 18: (1) decrease in the bands located at 500 and 798 cm^{-1} corresponding to bands O-Si-O bending with symmetry A_2 (Gaussian fitting showed the decrease of the bands around 475.8 and 515.6 cm^{-1}) and Si-O-Si symmetric stretching (Gaussian fitting showed the disappearance and decrease of the bands around 762.2 and 838.7 cm^{-1}); (2) the decrease in area of the Si-O-Si asymmetric stretching bands, at 1117.5 and 1195.9 cm^{-1} (Gaussian fitting showed the disappearance bands around 1128.4 and 1169.6 cm^{-1}); and (3) P=O stretching bands at 1243.9 and 1314.6 cm^{-1} increasing in area (Gaussian fitting showed the increase of the band at 1317 cm^{-1}).

Additionally, Gaussian fitting in Table 18 reveals other changes and bands corresponding to phosphate, silicate, or Vanc functional groups which are associated to drug binding onto the pre-immersed sample of P-78.2. ν_4 PO_4/O-P-O bending band at 556.3 cm^{-1}, disappeared after drug loading. O-Si-O bending with symmetry E bands at 572.5, 621.6, and 625.5 cm^{-1} decreased in area. Si-O-H stretching band at 914.9 cm^{-1} appeared after drug loading. Si-O-Si stretching bands at 1004.3, 1061.9, and 1069.7 cm-1 decreased. Decrease in the area of the bands around 1242.8, 1281.5, 1352.9, 1391.7 and 1509.4 cm^{-1} corresponding to O-H vibrations. The presence of vancomycin in sample P-78.2, is noted by the appearance N-H vibrations / NH_2 bands which appear at 1447.2 and 1517.9 cm^{-1}.

Table 19: Band position and area of functional groups found in pre-immersed P-165.5 samples with and without Vanc loading and before and after Gaussian fitting

Functional Groups	Assignment	Wavenumbers (cm^{-1}) band position/ area			
		P-165.5-imm (no G-fit)	P-165.5-imm-Vanc (no G-fit)	P-165.5-imm (G-fit)	P-165.5-imm-Vanc (G-fit)
O-Si-O bending	490, 500 [26-28]	499.7/40.8	506.9/2.7	487.1/61, 505.8/5.8, 525.9/7.7	483.1/7.7, 512/1.4, 524.6/0.6
HPO_4	551 [29-31]	none	555.5/1.5	none	552.6/1.5
***v*$_4$ PO_4/O-P-O bending**	567, 572, 602 [29-31]/ 577,597 [32]; 560 [33, 34]	none	none	558.2/5.7	none
O-Si-O bending	620 [26-28]	621.7/13.4	629.5/13.2	615.5/25.1, 621.8/5.2	567.1/4, 598.6/7.2, 630.1/16.9, 694.6/4.3
P-O-P stretching	758.9 [32]; ~650, ~700 [33]	none	none	none	756.3/14.9
P-O-P bending	800-870, ~780 [33]	none	none	868.7/22.7	846.8/13.2
Si-O-Si symmetric stretching	798[27], 797 [26, 28], 860-940 [35]	797.9/24.6	808.1/30.2	767/1.1, 779.3/65.3, 797.2/9.9	782.3/3.2, 804/16.7
N-H rocking mode	~810 [32]	none	none	none	811.3/0.3
Si-O-H stretching	~950 [32]	956.8/0.2	956.2/0.4	913.3/0.4, 950.6/2.7	912.8/15, 954.2/1.1
Si-O-Si stretching	1025, 1050[32]	1072.6/2.8	1064.3/7.7	1040.4/50.5, 1053.6/1.8, 1070.2/1.7	1013.8/31.9, 1048.2/5.9, 1067.3/1.8
Si-O-Si Asymmetric Stretching	1144, 1196, 1100 [28], 1120-1162 [32], 1160 [36]	1117.2/11.3, 1197.2/2.6	1149/3, 1193.7/2.2	1110.3/2, 1142.4/137.4, 1200.7/2.5, 1221.9/4.2	1110.9/18.8, 1189.3/56.6, 1195.3/1.8
a*v* C-C-O/ CO_2^- symmetric stretch	1230 [37]/ 1396 [22]	none	none	none	1244.8/0.4, 1361.7/23.9
P=O stretching	1230-1300, 1390 [33]	1310.3/0.3	1249.7/0.4, 1326.9/7.4	none	none
P-O-H bending	1406 [32]	none	none	1407.8/10.2, 1454/8.6	1407.4/0.1, 1458.5/0.6
N-H vibrations/ NH_2	1436.7, 1486.4 [32]/ 1445, 1460, 1472 [22]	none	none	none	1410.5/23.3, 1467/12.1, 1486.2/0.3
O-H vibrations	~1450 [34], ~1600 [33]	1434.7/0.3, 1457/0.05, 1480.3/0.02, 1511.3/0.6	1434/0.7, 1457.7/0.1, 1487.2/0.1, 1509.1/1.5	1241.9/22.8, 1301.5/14.9, 1354.5/12.1, 1433.5/0.3, 1499.8/8.4, 1548.3/11	1242.3/23.2, 1310.4/31.6, 1347.6/0.1, 1437.6/7.9, 1506.1/23.3, 1560.8/24.2

Drug binding was associated to the following changes in the FTIR spectra of the pre-immersed sample of P-165.5 as confirmed by Gaussian fitting in Table 19: (1) decrease in the bands located at 499.7 cm^{-1} corresponding to bands O-Si-O bending with symmetry A_2 (Gaussian fitting showed the decrease of the bands around 487.1, 505.8, and 525.9 cm^{-1}); (2) increase in the Si-O-H stretching band at 956.8 cm^{-1} increases (Gaussian fitting showed the increase of the bands at 913.3 cm^{-1}); (3) decrease in area of the Si-O-Si asymmetric stretching bands, at 1117.2 and 1197.2 cm^{-1} (Gaussian fitting showed the disappearance of the bands at 1142.4 cm^{-1}); and (4) an increase in the area of the bands at 1434.7, 1457, 1480.3, and 1511.3 cm^{-1} corresponding to O-H vibrations (Gaussian fitting showed the increase in area of the bands around 1241.9, 1301.5, 1433.5, 1499.8, and 1548.3 cm^{-1}).

Additionally, Gaussian fitting in Table 19 reveals other changes and bands corresponding to phosphate, silicate, or Vanc functional groups which are associated to drug binding onto the pre-immersed sample of P-165.5. O-P-O bending band at 558.2 cm^{-1}, decreased in area. O-Si-O bending bands 567.1 and 694.6 cm^{-1} appeared. Decrease in P-O-P bending band 868.7 cm^{-1}. Si-O-Si stretching band at 1040.4 cm^{-1} area decreased. P=O stretching bands are not present. P-O-H bending bands at 1407.8 and 1454 cm^{-1} decreased in area. The appearance of N-H rocking mode bands at 811.3 cm^{-1}, aν C-C-O/ CO_2^- symmetric stretching band at 1244.8 and 1361.7 cm^{-1}, and N-H vibrations / NH_2 bands at 1410.5, 1467, and 1486.2 cm^{-1} corresponding to Vanc.

Table 20: Band position and area of functional groups found in pre-immersed P-331 samples with and without Vanc loading and before and after Gaussian fitting

		Wavenumbers (cm^{-1})			
		band position/area			
Functional Groups	**Assignment**	**P-331-imm (no G-fit)**	**P-331-imm-Vanc (no G-fit)**	**P-331-imm (G-fit)**	**P-331-imm-Vanc (G-fit)**
O-Si-O bending	490, 500 [26-28]	497.7/30.2	487.5/7.4	481.6/91.6, 521.9/14.1	480.9/18.4, 515.9/4.6
HPO_4	551 [29-31]	none	none	none	none
***v*$_4$ PO_4/O-P-O bending**	567, 572, 602 [29-31]/ 577,597 [32]; 560 [33, 34]	none	none	556.3/1	583.3/1
O-Si-O bending	620 [26-28]	621.1/17.7	620.1/18.5	573.5/10.7, 617.5/29.9, 621.3/1.4	621.1/18.9
P-O-P stretching	758.9 [32]; ~650, ~700 [33]	none	none	666.4/36.6	727.3/4.8, 758.7/10.7
P-O-P bending	800-870, ~780 [33]	none	none	797.6/8.7	798.1/20
Si-O-Si symmetric stretching	798[27], 797 [26, 28], 860-940 [35]	796.3/35	797.1/32.2	775.3/65.8, 849.7/28.6,	848.8/18.6
Si-O-H stretching	~950 [32]	956.8/0.4	956.8/0.4	914.6/28, 953.4/0.7, 987.8/49.2	910.8/10.1, 954.3/12.1
Si-O-Si stretching	1025, 1050[32]	1069.3/5.5	1066.7/6.7	1064.3/68.2, 1068.7/1.3	1003.1/21.6, 1048.3/15, 1068.2/1.1
Si-O-Si Asymmetric Stretching	1144, 1196, 1100 [28], 1120-1162 [32], 1160 [36]	1120/7.4, 1195.8/2.4	1125.2/4.2, 1194.6/1.8	1106.1/3, 1135.2/46.6, 1170.7/2.2, 1198.1/3.7, 1209.6/71.4	1111.8/49.8, 1196.9/1.4, 1202.1/43.2
a*v* C-C-O/ CO_2^- symmetric stretch	1230 [37]/ 1396 [22]	none	none	none	1354/8.5
P=O stretching	1230-1300, 1390 [33]	1246.6/0.5, 1311.1/0.7	1246.3/0.4, 1313.4/0.03	1314/0.2	1313.9/0.3
P-O-H bending	1406 [32]	none	none	1405.1/9.8, 1459.7/.3, 1484.1/0.2	1409.1/13.7
N-H vibrations/ NH_2	1436.7, 1486.4 [32]/ 1445, 1460, 1472 [22]	none	none	none	1445.7/2.8, 1459.7/1.7, 1481.5/1.1
O-H vibrations	~1450 [34], ~1600 [33]	1434.7/0.5, 1457/0.08, 1480.1/0.03, 1511.1/1	1434.8/0.7, 1458.3/0.1, 1488.7/0.07, 1510.4/1.5	1241/34.2, 1297.7/21.4, 1341.3/15.1, 1375.4/15.1, 1435.6/10.7, 1468.9/11.3, 1509/12.5, 1557.1/16.7	1238.9/14.7, 1283.6/15.7, 1330.7/13.1, 1387.7/1.7, 1436.3/2.2, 1472.3/9.1, 1511.9/9.9, 1558.3/13.2

Drug binding was associated to the following changes in the FTIR spectra of the pre-immersed sample of P-331 as confirmed by Gaussian fitting in Table 20: (1) decrease in the bands located at 497.7, 621.1, 796.3 cm^{-1} corresponding to bands O-Si-O bending with symmetry A_2 (Gaussian fitting showed the decrease of the bands around 481.6 and 521.9 cm^{-1}), O-Si-O bending with symmetry *E* (Gaussian fitting showed the disappearance of the bands around 573.5 and 617.5 cm^{-1}), and Si-O-Si symmetric stretching (Gaussian fitting showed the disappearance and decrease in area of the bands at 775.3 and 849.7 cm^{-1}, respectively); and (2) P=O stretching bands at 1246.6 and 1311.1 cm^{-1} decrease in area.

Additionally, Gaussian fitting in Table 20 reveals other changes and bands corresponding to phosphate, silicate, or Vanc functional groups which are associated to drug binding onto sample P-331. Decrease in P-O-P stretching band area. Increase in P-O-P bending band area at 797.8 cm^{-1}. Decrease in band area and disappearance of Si-O-H stretching bands at 914.6 and 987.8 cm^{-1}, respectively. Si-O-Si stretching band at 1064.3 cm^{-1} decreased in area. Si-O-Si asymmetric stretching bands 1135.2 and 1170.7 cm^{-1} disappeared. P-O-H bending bands at 1459.7 and 1484.1 cm-1 disappeared. Decrease in the area of all bands corresponding to O-H vibrations. The appearance of a*v* C-C-O/ CO_2^- symmetric stretching bands appear at 1354 cm^{-1}, and N-H vibrations / NH_2 bands appear at 1445.7, 1459.7, and 1481.5 cm^{-1} corresponding to Vanc.

3.5.3 Comparison between Drug Adsorption and Surface Chemistry Analysis

Figures 45 (A-B), 46 (A-B), 47 (A-B), and 48 (A-B), shows a comparison between the amount of drug absorbed and the area under the O-Si-O (~498 cm^{-1}) bending and v_4 PO_4/O-P-O (557 cm^{-1}) bending, O-Si-O (~620 cm^{-1}) bending and v_4 PO_4/O-P-O (557 cm^{-1}) bending, O-Si-O (~498 cm^{-1}) bending and P=O (1343.9 cm^{-1}) bending, and O-Si-O (~620 cm^{-1}) bending and P=O (1343.9 cm^{-1}) bending bands for non-immersed and pre-immersed samples, respectively. Figure 45A, 46A, 47A, and 48A, shows that for the non-immersed samples the amount of drug adsorbed decreases as the area of the phosphate functional group bands increase and the silicate functional group band decreases. After immersion, the release of phosphate content from the surface of the samples is noticed by the significant decrease in area of the phosphate functional group bands and increase in area of the silicate functional group bands which contributes to a higher adsorption of Vanc for all samples (Figures 45B, 46B, 47B, and 48B).

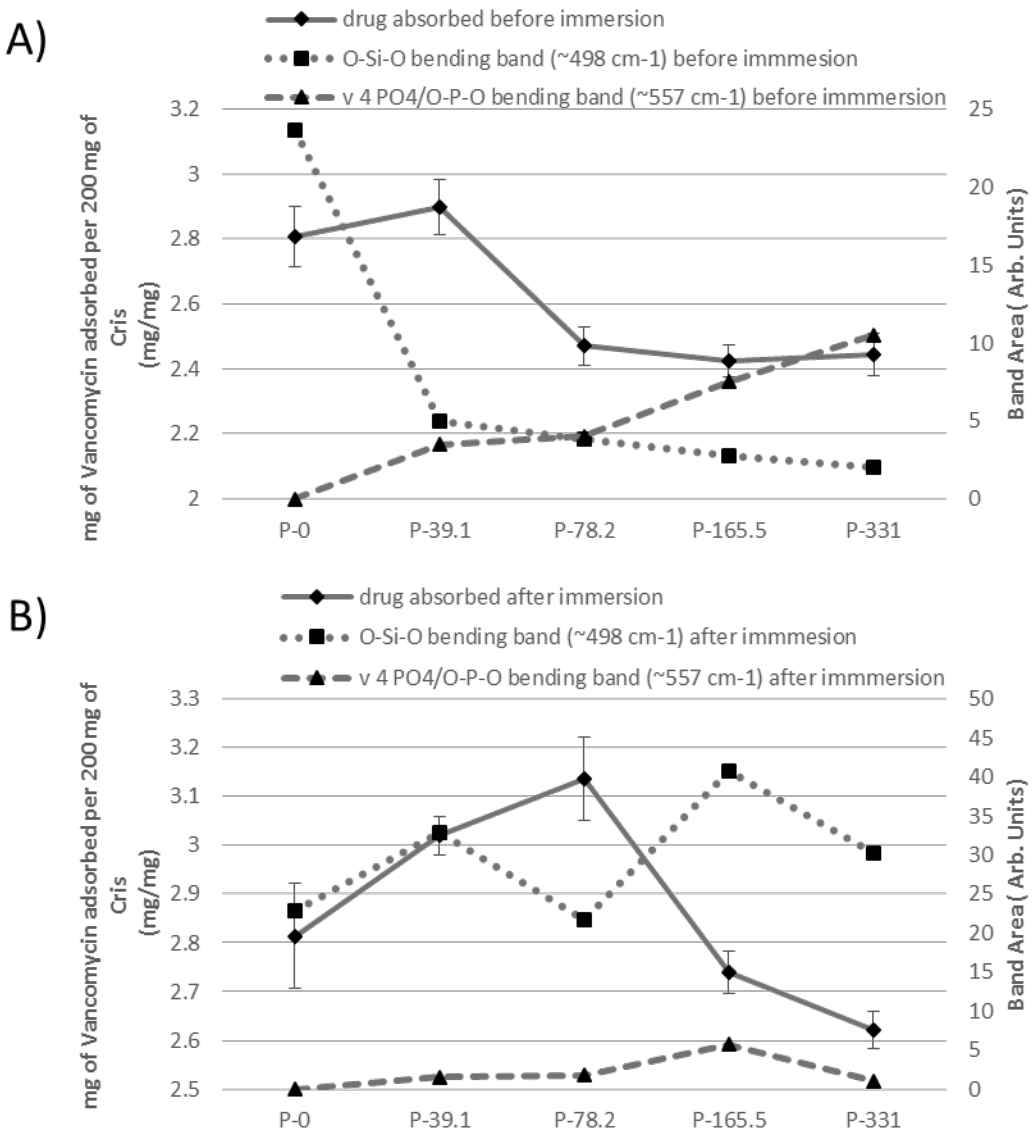

Figure 45: Amount of Vanc adsorbed vs. the area under the O-Si-O bending (~498 cm^{-1}) and v $_4$ PO_4/O-P-O (557 cm^{-1}) bending bands on ceramic samples P-O, P-39.1, P-78.2, P-165.5, and P-331 A) before and B) after immersion

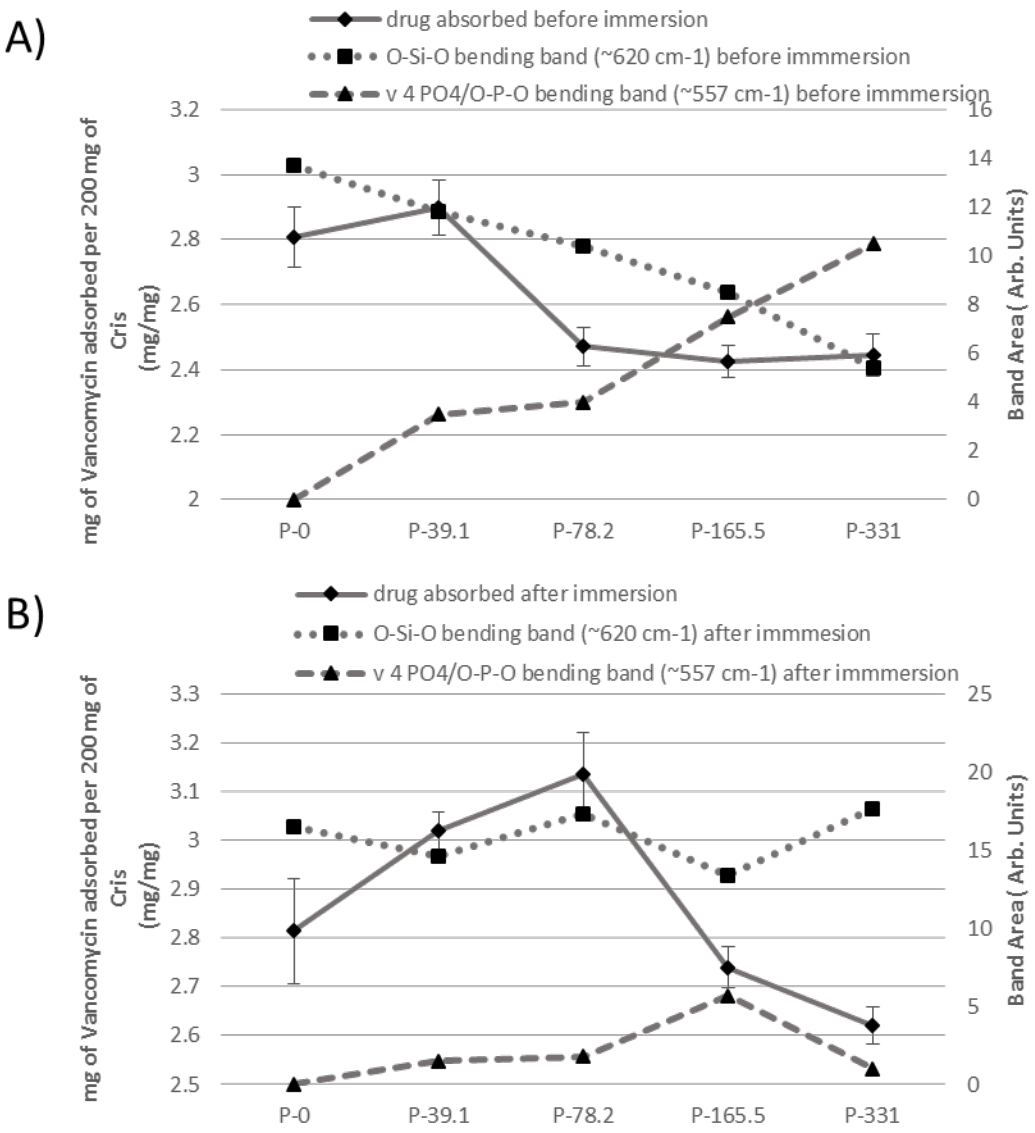

Figure 46: Amount of Vanc adsorbed vs. the area under the O-Si-O bending (~620 cm-1) and v 4 PO4/O-P-O (557 cm-1) bending bands on ceramic samples P-O, P-39.1, P-78.2, P-165.5, and P-331 A) before and B) after immersion

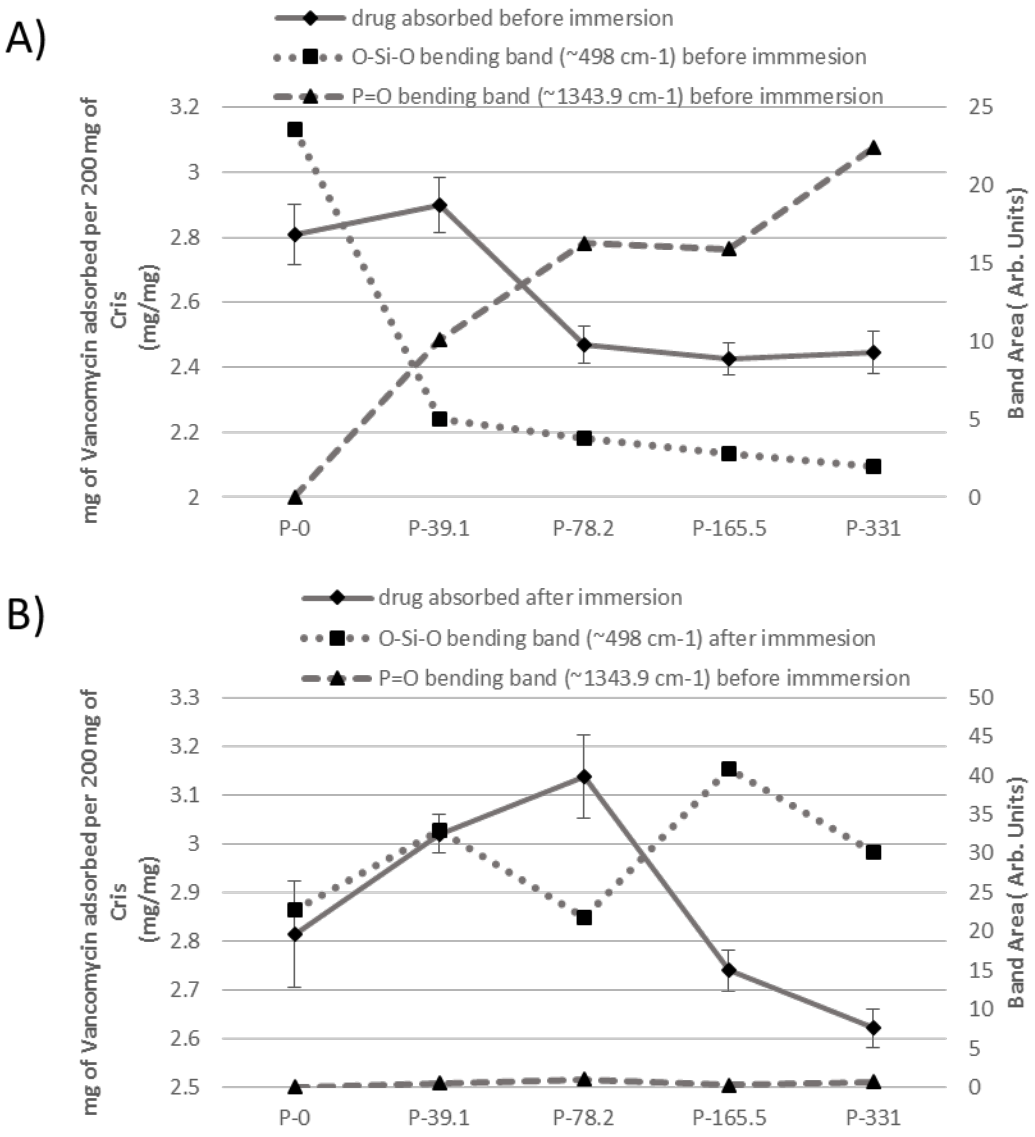

Figure 47: Amount of Vanc adsorbed vs. the area under the O-Si-O bending (~498 cm^{-1}) and P=O (1343.9 cm^{-1}) bending bands on ceramic samples P-O, P-39.1, P-78.2, P-165.5, and P-331 A) before and B) after immersion

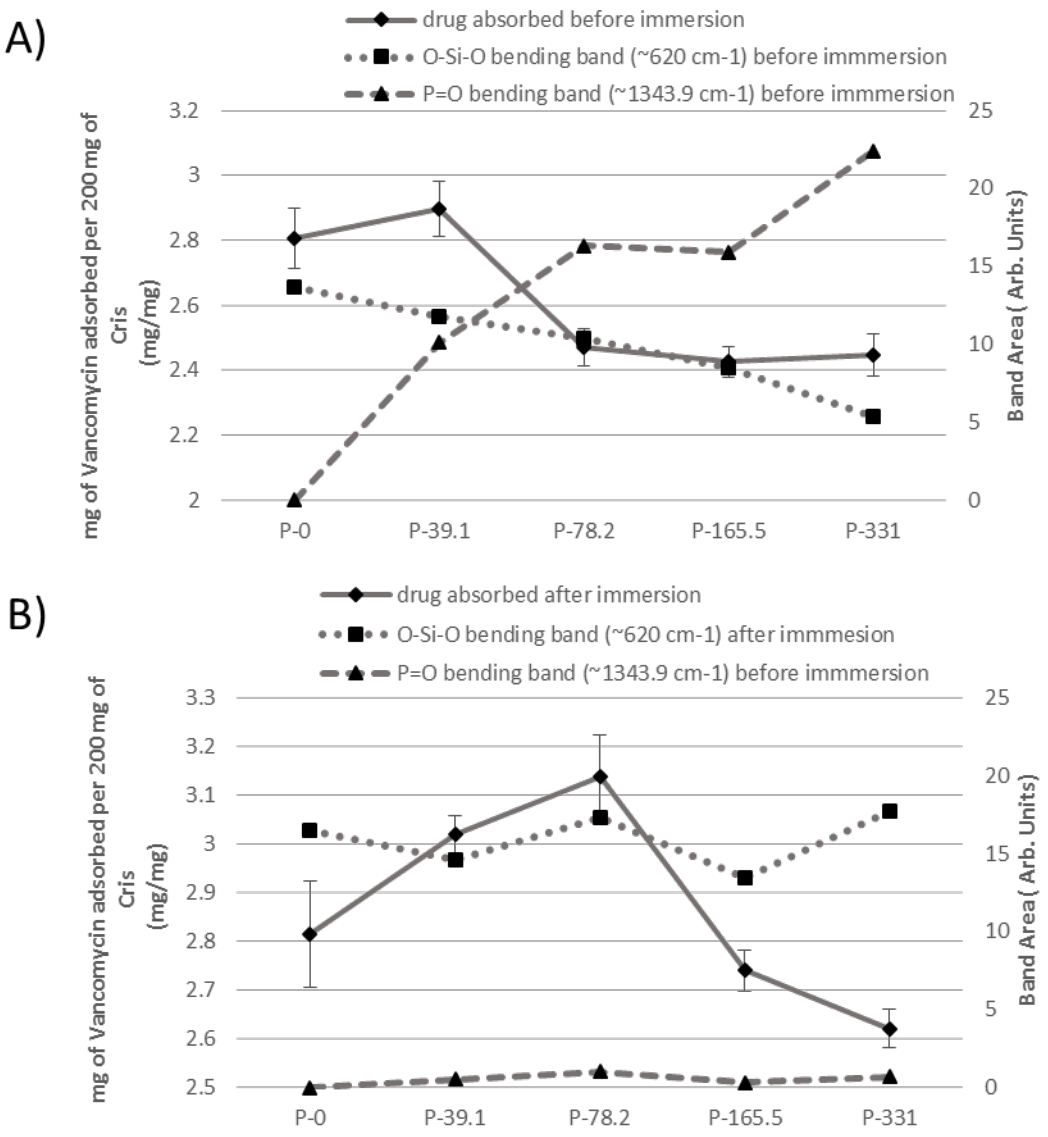

Figure 48: Amount of Vanc adsorbed vs. the area under the O-Si-O bending (~620 cm-1) and P=O (1343.9 cm-1) bending bands on ceramic samples P-O, P-39.1, P-78.2, P-165.5, and P-331 A) before and B) after immersion

3.6 Drug Release Kinetics of Cris

3.6.1 Vancomycin Release Kinetics of Non-Immersed Cris

Figure 49, shows the cumulative drug release profile over a 96 hour period of non-immersed Cris samples P-0, P-39.1, P-78.2, P-165.5 and P-331. The drug release kinetics demonstrated a statistically significant decrease ($p < 0.05$) in the total cumulative release of Vanc from non-immersed Cris sample P-0 (1.521±.026 mg) to P-331 (1.276±.016 mg). The total amount of drug release from non-immersed Cris samples P-0, P-39.1, P-78.2, P-165.5, and P-331 is 1.521±.026 mg, 1.372±.021 mg, 1.266±.013 mg, 1.347±.0 mg, and 1.276±.016 mg, respectively. Additionally samples P-78.2 and P-165.5 stopped releasing a detectable amount of Vanc at 48 hrs. While samples P-0, P-39.1, and P-331 stopped releasing detectable amount of Vanc at 96 hours. Furthermore, during the first four hours of burst release the percentage of drug released from the total amount of drug loaded for samples P-0 was 41 % and for P-331 was 26 % indicating the effect of phosphate content on decreasing the drug release rate. After the 4 hours of Vanc release the amount of Vanc available for release on samples P-0 and P-331 was .898 mg and .945 mg, respectively.

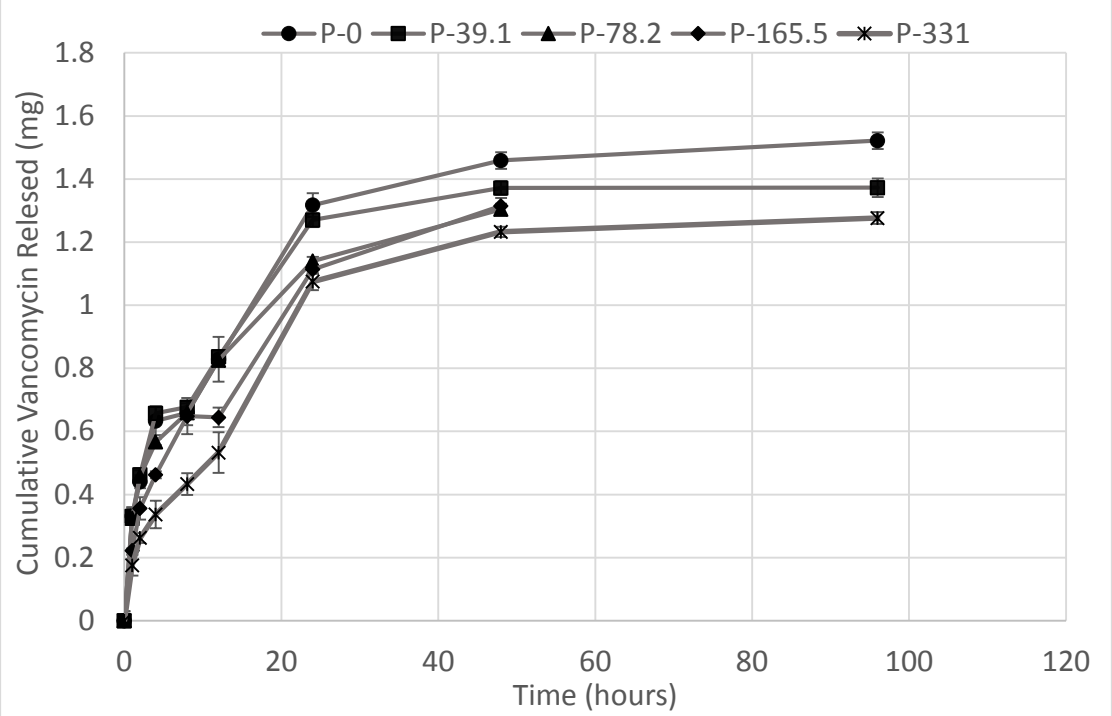

Figure 49: Cumulative drug release within 96 hour period of non-immersed samples

Figure 50, shows the release of Vanc during the first 24 hours for non-immersed Cris samples. The results show the Vanc release decreases significantly from the non-immersed samples of P-0 to P-331 up to 24 hours ($p < 0.001$).

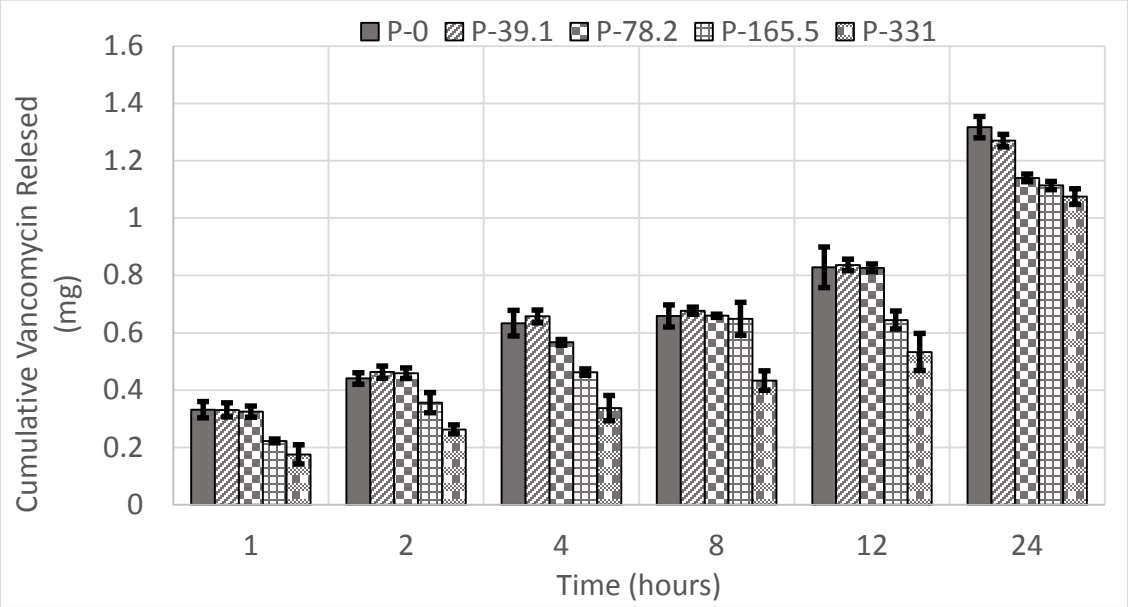

Figure 50: Vanc release during 24 hours for samples P-0, P-39.1, P-78.2, P-165.5, and P-331

Figure 51, shows the % of Vanc released over a 48 hour period for non-immersed samples P-0, P-39.1, P-78.2, P-165.5, and P-331. The total % of drug released from non-immersed samples P-0, P-39.1, P-78.2, P-165.5, and P-331 is 37.66±.89 mg, 31.55±.96 mg, 34.8±.6 mg, 37.54±1.02 mg, and 33.46±.77 mg, respectively. The drug release kinetics demonstrated a statistically significant decrease ($p < 0.05$) in the percent of Vanc released from non-immersed Cris samples P-0 (37.66±.89 %) to P-331 (33.46±.77 %) of Vanc.

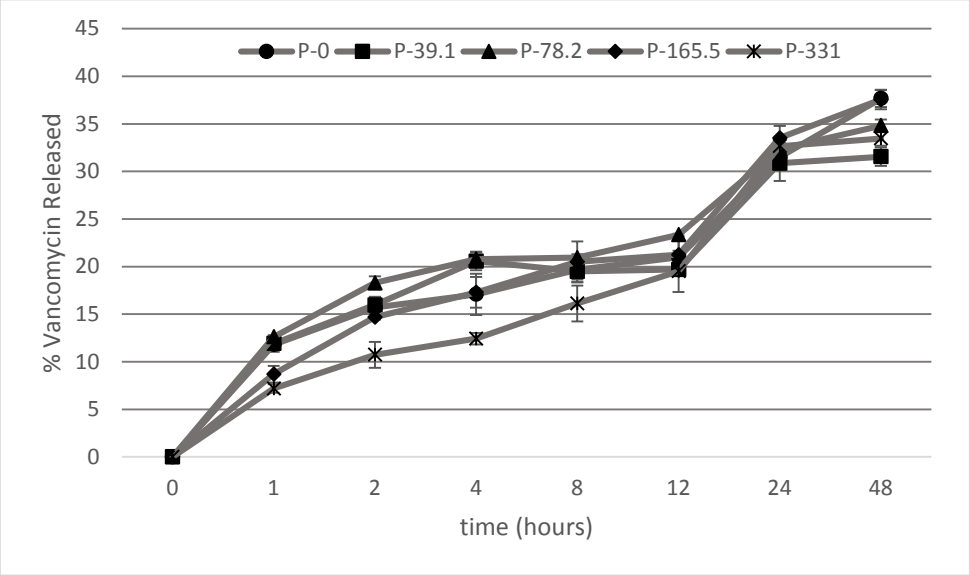

Figure 51: % of Vanc released over 48 hours for non-immersed samples P-0, P-39.1, P-78.2, P-165.5, and P-331

Figure 52, shows the rate of drug release of non-immersed Cris samples over 96 hours. Drug release for P-0, P-39.1, and P-331 drug release after 96 hours is undetectable. Drug release for P-78.2 and P-165.5 at 48 hours is undetectable. During the first 4 hours of drug release there is a decrease ($p < 0.05$) in the release rate of drug from non-immersed samples P-0 (31.9±3.1 mg of Vanc/h/mL) to P-331 (19.7±2.9 mg of Vanc/h/mL). From 8 to 96 hours there is no difference in the rate of drug release between the samples ($p < 0.05$).

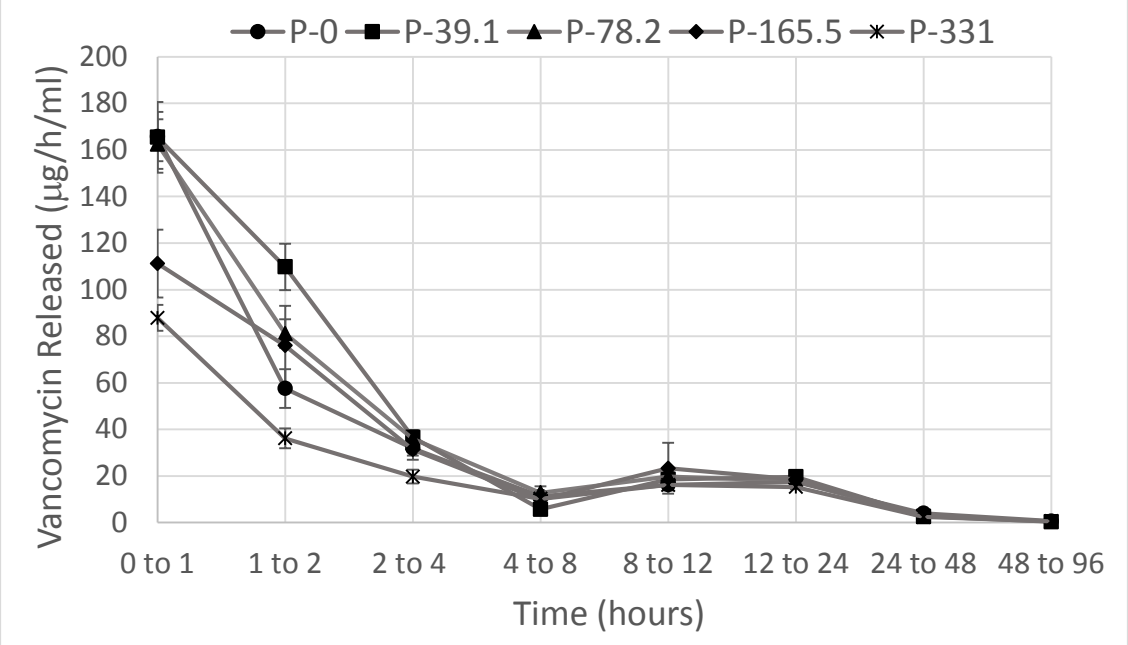

Figure 52: Rate of drug release over 96 hour period for non-immersed Cris samples

Figure 53, shows the rate of drug release over the first 4 hours for non-immersed Cris samples. Table 21, shows the deceleration of drug release over the first 4 hours and R-squared value for the linear line fit used to calculate the deceleration of drug release for non-immersed Cris samples. The deceleration of drug release from sample P-0 to P-331 during the first 4 hours decreased from -66.92 to -34.07 μg of Vanc/mL /hr^2, for control non-immersed Cris.

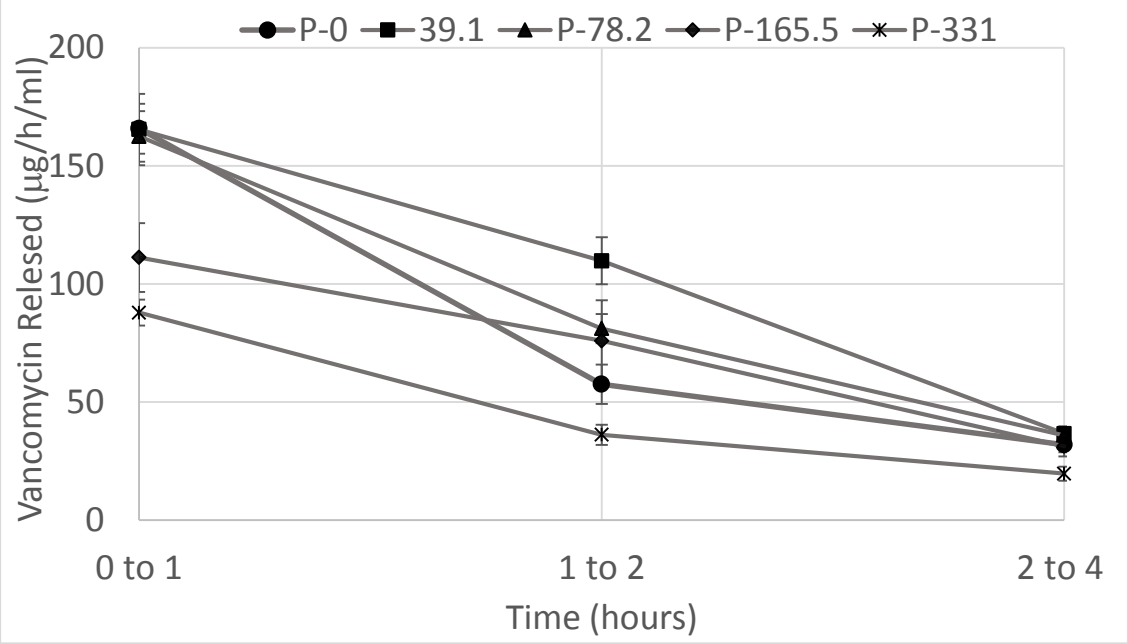

Figure 53: Rate of drug release over the first 4 hours for non-immersed Cris samples

Table 21: Deceleration of drug release over the first 4 hours and R-squared value for the linear line fit used to calculate the deceleration of the drug release rate for non-immersed Cris samples

sample	Deceleration of drug release (μg/ml/h^2)	R^2
P-0	-66.928	0.8875
P-39.1	-64.388	0.9938
P-78.2	-63.281	0.9735
P-165.5	-39.963	0.9954
P-331	-34.076	0.9179

Figure 54, shows the rate of drug release over the first 8 hours for non-immersed Cris samples. Table 22, shows the deceleration of drug release over the first 8 hours and R-squared value for the linear line fit used to calculate the deceleration of drug release for non-immersed Cris samples. The deceleration of drug release from sample P-0 to P-331 during the first 8 hours decreased from -48.91 to -24.96 μg of Vanc/mL /hr^2, for control non-immersed Cris.

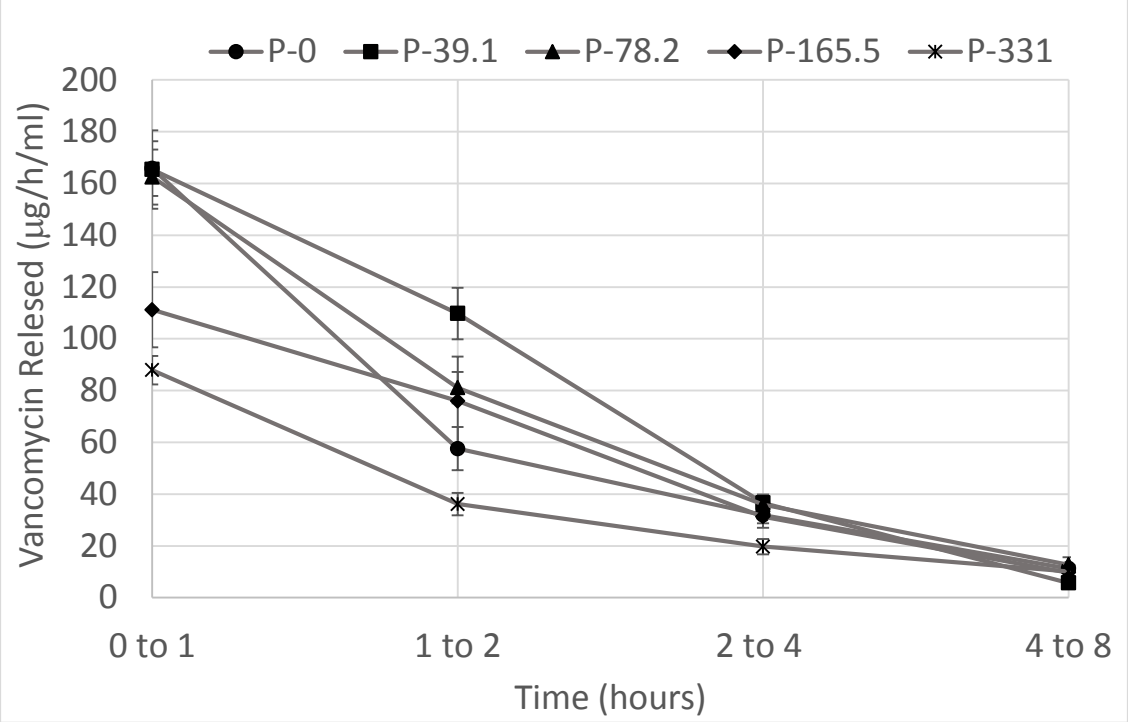

Figure 54: Rate of drug released over the first 8 hours for non-immersed samples of Cris

Table 22: Deceleration of drug release over the first 8 hours and R-squared value for the linear line fit used to calculate the deceleration of the drug release rate for non-immersed Cris samples

sample	Deceleration of drug release (μg/ml/h^2)	R^2
P-0	-48.91	0.8436
P-39.1	-55.219	0.9787
P-78.2	-49.438	0.9345
P-165.5	-34.939	0.9841
P-331	-24.963	0.8654

3.6.2 Vancomycin Release Kinetics of Pre-Immersed Cris

Figure 55, shows the cumulative drug release profile over a 96 hour period for pre-immersed Cris samples. The drug release kinetics demonstrated a statistically significant increase ($p < 0.05$) in the total cumulative release of Vanc from pre-immersed Cris samples P-0 (1.505±.014 mg) to P-331 (1.581±.057 mg). The total amount of drug release from pre-immersed samples P-0, P-39.1, P-78.2, P-165.5, and P-331 is 1.505±.014 mg, 1.387±.027 mg, 1.393±.045 mg, 1.525±.046 mg, and 1.581±.057 mg, respectively. Additionally samples P-78.2, P-165.5, and P-331 stopped releasing a detectable amount of Vanc at 48 hrs. While samples P-0 and P-39.1 stopped releasing detectable amount of Vanc at 96 hours. Furthermore, during the first four hours of burst release the percentage of drug released from the total amount of drug loaded for samples P-0 was 42 % and for P-331 was 30 % indicating the effect of phosphate content on decreasing the drug release rate. After the 4 hours of Vanc release the amount of Vanc available for release from samples P-0 and P-331 was .873 mg and 1.106 mg, respectively.

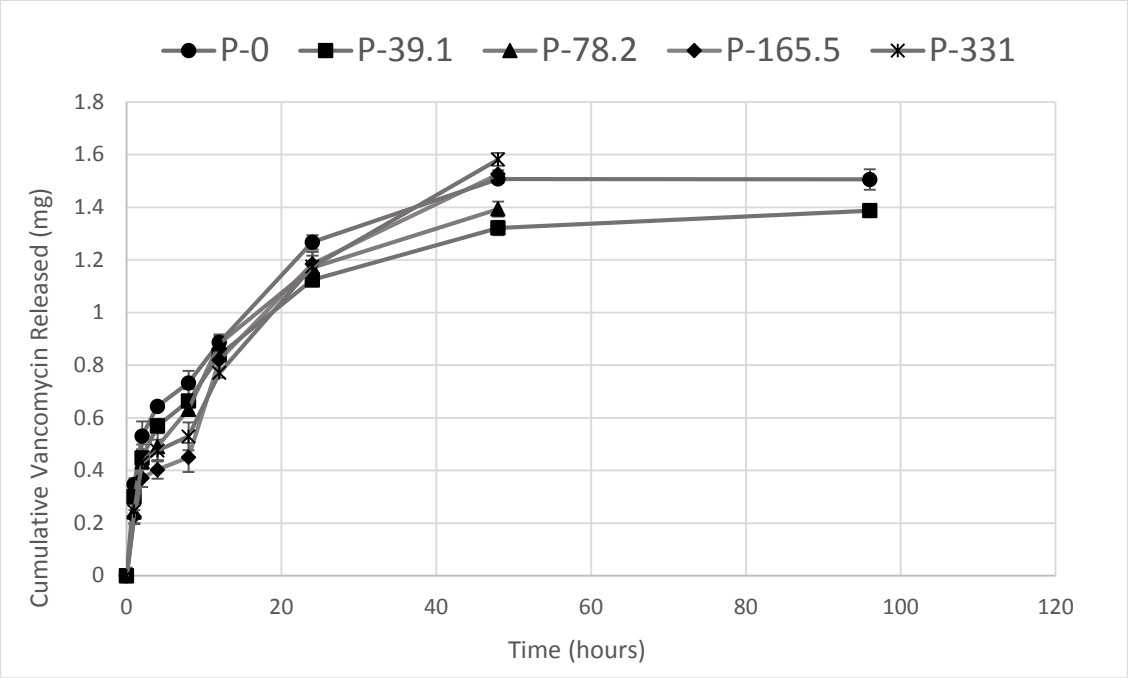

Figure 55: Cumulative drug release within 96 hour period of pre-immersed samples

Figure 56, shows the release of Vanc during the first 24 hours for pre-immersed Cris samples. The release of drug for samples P-39.1, P-78.2, P-165.5, and P-331 was comparable and greater than that of the non-immersed samples for the first 24 hours, but still the burst release of P-0 for the first 24 hours was greater than all other samples ($p < 0.05$).

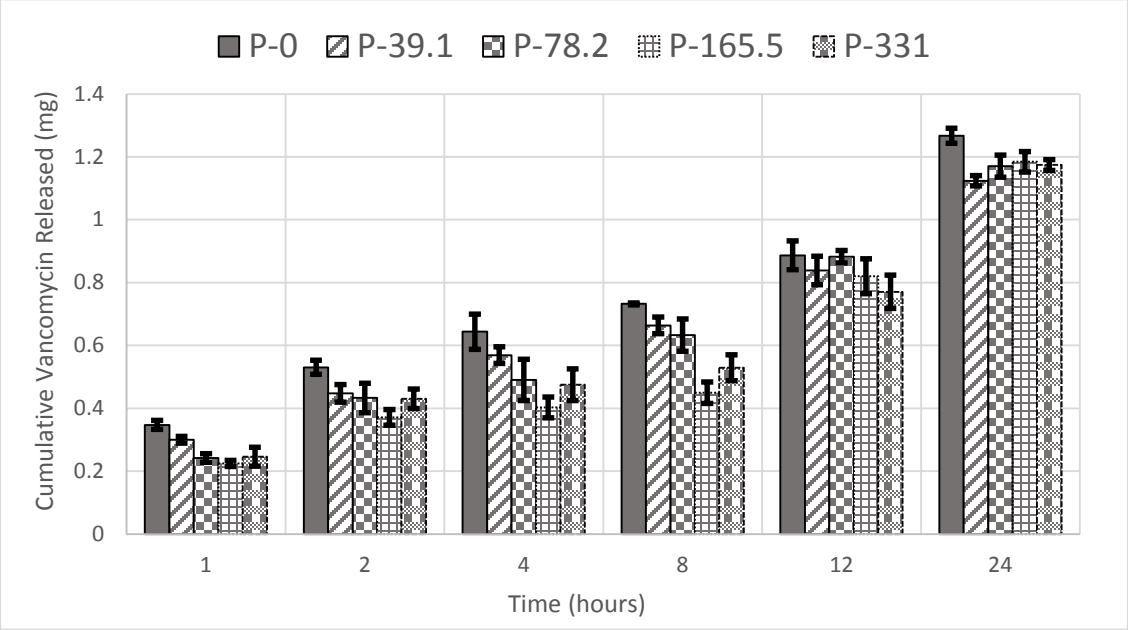

Figure 56: Vanc release during 24 hours for pre-immersed Cris samples

Figure 57, shows % of Vanc released over a 48 hour period for pre-immersed samples P-0, P-39.1, P-78.2, P-165.5, and P-331. The total % of drug released from non-immersed samples P-0, P-39.1, P-78.2, P-165.5, and P-331 is 33.59±1.35 mg, 29.79±0.82 mg, 30.19±1.4 mg, 38.52±0.1 mg, and 42.27±1.51 mg, respectively. The drug release kinetics demonstrated a statistically significant increase ($p < 0.05$) in the percent of Vanc released from pre-immersed Cris samples P-0 (33.59±1.35 %) to P-331 (42.27±1.51 %) of Vanc.

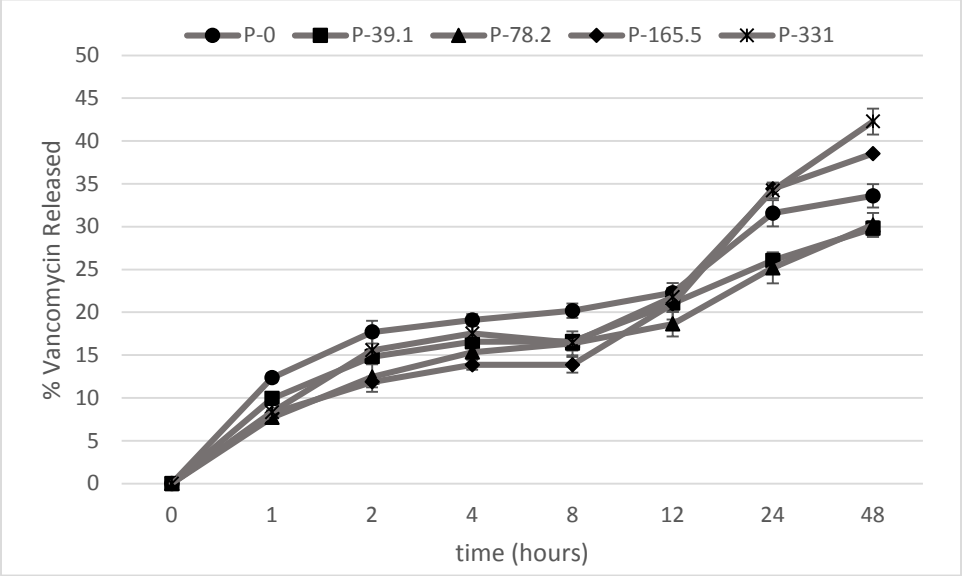

Figure 57: % of Vanc released over 48 hours for pre-immersed samples P-0, P-39.1, P-78.2, P-165.5, and P-331

Figure 58, shows the rate of drug release of pre-immersed Cris samples over 96 hours. The pre-immersed samples show a decrease ($p < 0.05$) in the rate of release in the first hour of drug release from samples P-0 (173.5±7.2 mg of Vanc/h/mL) to P-331 (123±14.9 mg of Vanc/h/mL). From 2 to 96 hours there is no difference in the rate of drug release between the samples ($p < 0.05$).

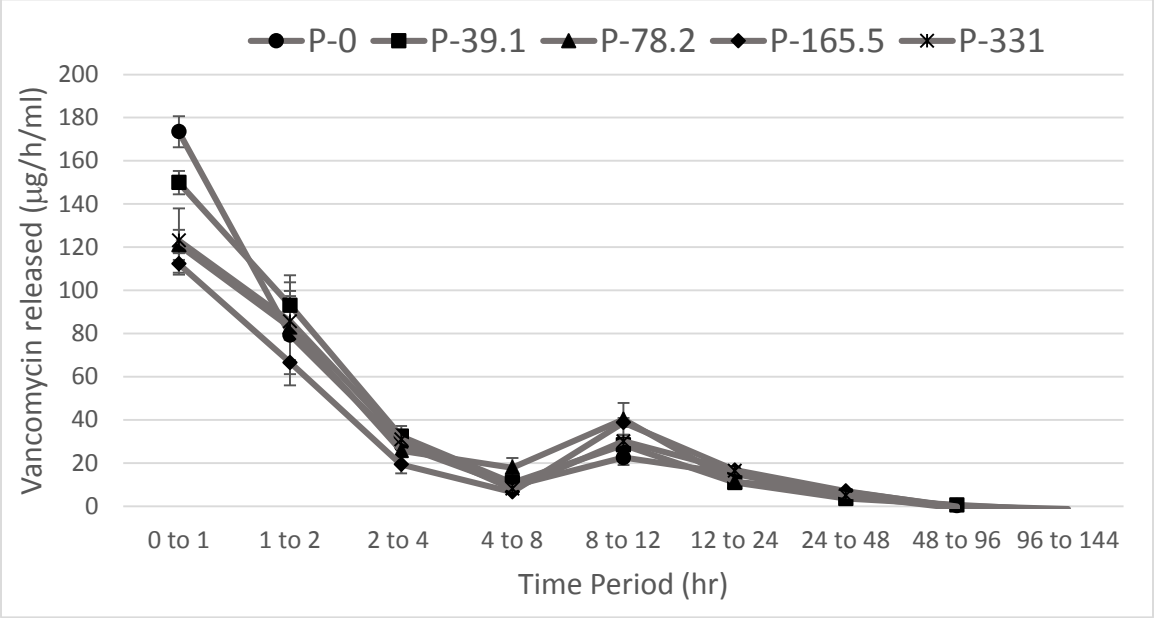

Figure 58: Rate of drug released over 96 hour period for pre-immersed samples

Figure 59, shows the rate of drug release over the first 4 hours for pre-immersed Cris samples. Table 23, shows the deceleration of drug release over the first 4 hours and R-squared value for the linear line fit used to calculate the deceleration of drug release for pre-immersed Cris samples. The deceleration of drug release from samples P-0 to P-331 during the first 4 hours decreased from -72.60 to -46.04 μg of Vanc/mL /hr^2, for pre-immersed Cris.

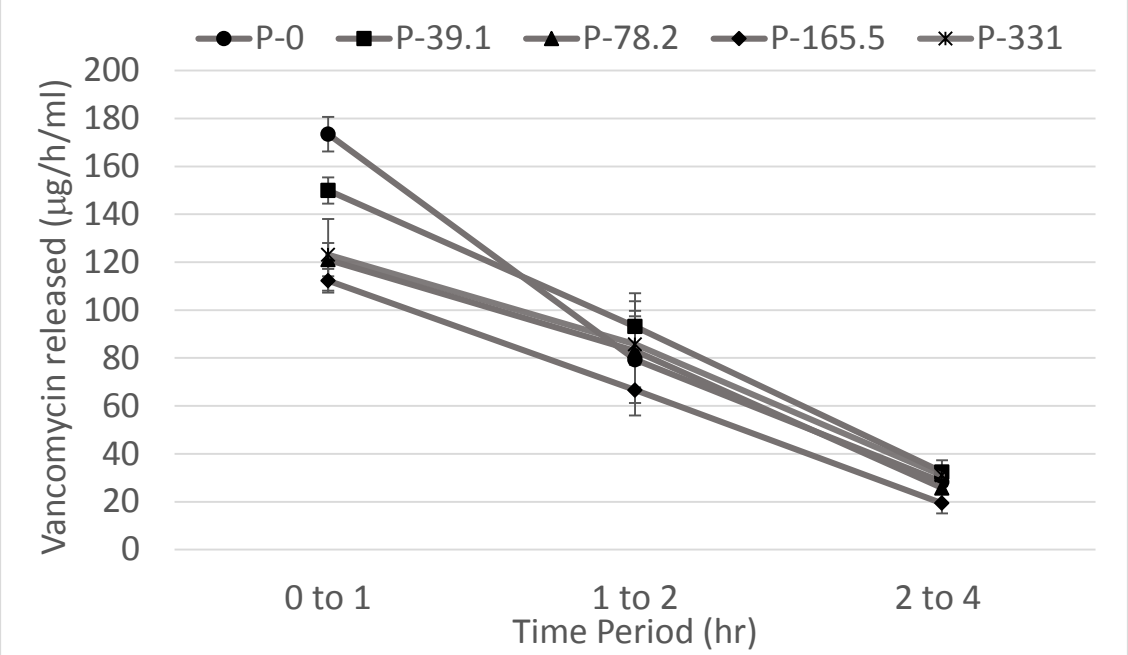

Figure 59: Rate of drug release over the first 4 hours for pre-immersed Cris samples

Table 23: Deceleration of drug release over the first 4 hours and R-squared value for the linear line fit used to calculate the deceleration of the drug release for pre-immersed cris samples

sample	Deceleration of drug release (μg/ml/h^2)	R-squared
P-0	-72.608	0.9714
P-39.1	-58.767	0.9996
P-78.2	-47.677	0.9868
P-165.5	-46.453	0.9999
P-331	-46.049	0.9883

Figure 60, shows the rate of drug release over the first 8 hours for pre-immersed Cris samples. Table 24, shows the deceleration of drug release over the first 8 hours and R-squared value for the linear line fit used to calculate the deceleration of drug release for pre-immersed Cris samples. The deceleration of drug release from samples P-0 to P-331 during the first 8 hours decreased from -54.331 to -39.978 μg of Vanc/mL /hr^2, for pre-immersed Cris.

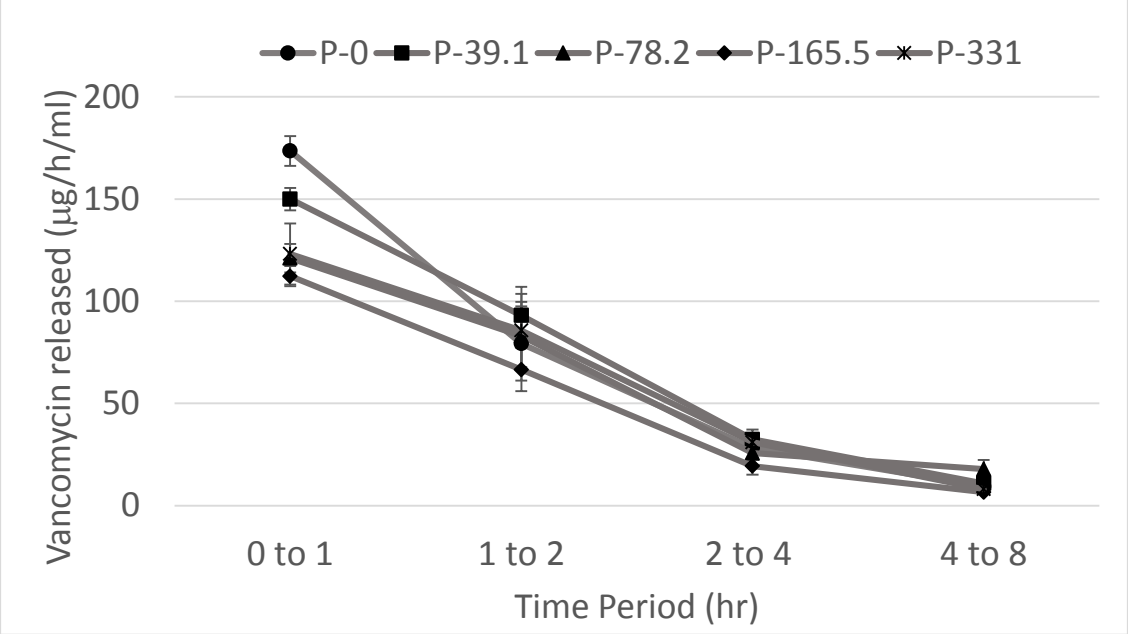

Figure 60: Rate of drug release over the first 8 hours for pre-immersed Cris samples

Table 24: Deceleration of drug release over the first 8 hours and R-squared value for the linear line fit used to calculate the deceleration of the drug release for pre-immersed Cris samples

sample	Deceleration of drug release (μg/ml/h^2)	R-squared
P-0	-54.331	0.912
P-39.1	-47.774	0.9657
P-78.2	-36.686	0.9356
P-165.5	-36.411	0.9517
P-331	-39.978	0.9788

CHAPTER 4: DISCUSSION

The results from this study show that increasing the phosphate content in a silicate based bioceramic decreases drug adsorption, and the rate and amount of drug released. It was shown that a higher availability of silicate functional groups was responsible for higher drug adsorption while a higher content of phosphate functional groups caused a decrease in drug adsorption. This study shows that drug adsorption and release (burst and sustained release) can be modified by the change in concentration of phosphate and silicate functional groups on bioceramics surface.

4.1 Modification of Silicate Structure via Phosphate Doping

XRD and FTIR confirmed phosphate silicate substitution in the silicate structure. XRD demonstrated an increase in the unit cell volume as the P_2O_5 concentration increased from sample P-0 (170.5373 $Å^3$) to P-331 (170.6466 $Å^3$). The increase in unit cell volume of Cris doped samples is due to the smaller ionic radii of silicate (Si^{+}4;0.4 Å) in comparison to phosphate (P^{-3}; 2.12 Å) [24]. Furthermore, FTIR showed that the v_4 PO4/O-P-O bending band around 557.6 cm^{-1} and P=O stretching band around 1343.9 cm^{-1} increased in area for samples P-39.1 and P-331 from 3.5 to 10.5 and from 10.1 to 22.4, respectively. Additionally, Gaussian fitting revealed a greater presence of P-O-P stretching, P-O-P bending, and P-O-H stretching bands as P_2O_5 content increased. In conjunction with the increase of the v_4 PO4/O-P-O bending band and P=O stretching band, a decrease in area of the O-Si-O bending bands around 488.1 and 629.8 cm^{-1} was noticed for samples P-39.1 to P-331 from 5 to 2 and from 11.8 to 5.4, respectively. Gaussian fitting revealed a decrease in area of the O-Si-O bending, Si-O-Si symmetric stretching, Si-O-Si stretching, Si-O-Si asymmetric stretching, and O-H vibrations bands as P_2O_5 content increased. The FTIR results suggest that the phosphate functional groups have bonded to silicate functional groups and formed Si-O-P bonds after thermal treatment (Figure 61).

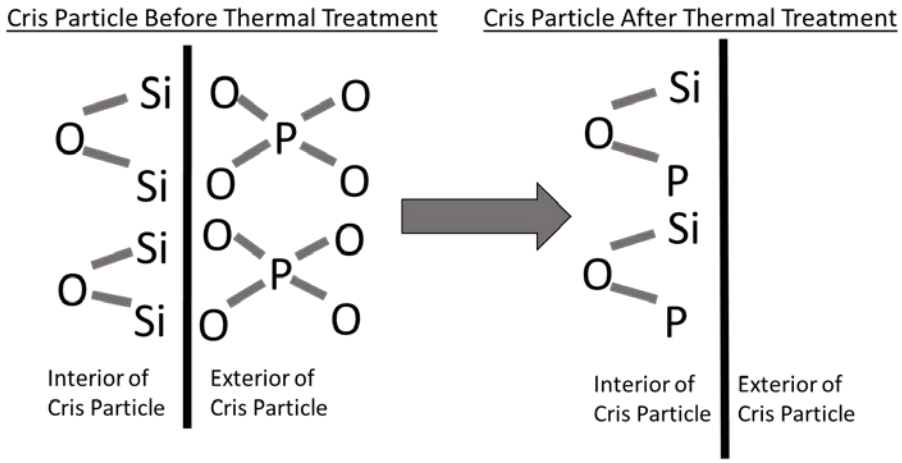

Figure 61: Cris before (P_20_5 on surface of particle) and after (P_20_5 bonding to silicate functional groups to form Si-O-P bonds) thermal treatment

As the availability of silicate functional groups on the surface of Cris decreased due to the creation of Si-O-P bonds, the formation of polymeric P-O-P bonds occurred on the surface of Cris thus explaining the increase in area of phosphate functional group bands and decrease in silicate functional group bands as P_2O_5 content increased (Figure 62).

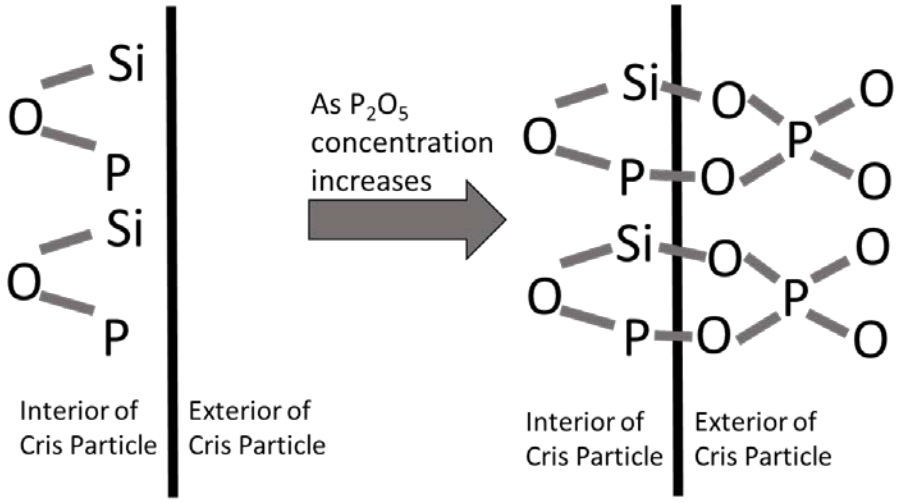

Figure 62: Doped Cris forming P-O-P polymeric chains as P_20_5 concentration increases

It is assumed that the concentration of phosphate functional groups would decrease from the surface to the center of the Cris particles. This assumption is made due to the higher presence (in area) of phosphate functional groups in FTIR spectra before and after immersion as phosphate content increases in doped Cris samples (Figure 63).

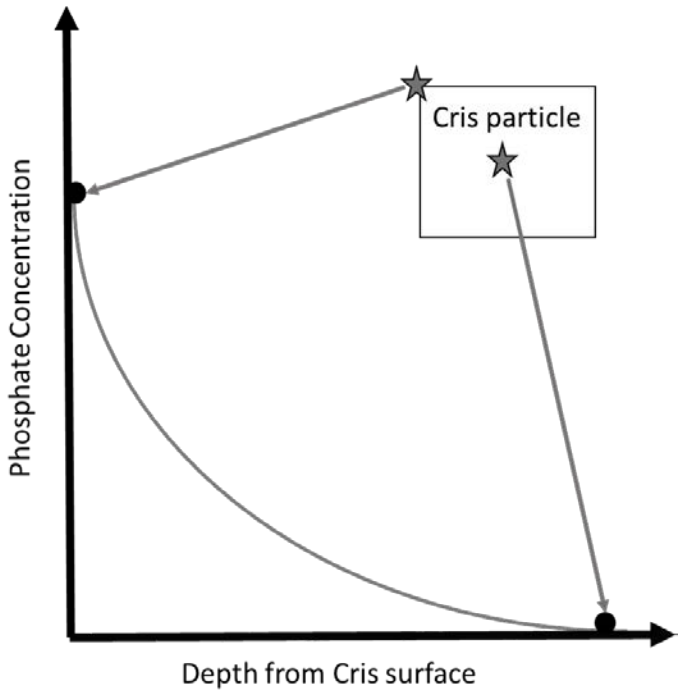

Figure 63: Phosphate concentration decreasing towards the center of Cris particle

4.2 Corrosion Analysis of Non-Doped and Doped Cris

ICP-OES analyses showed that the percent of released phosphate ions during immersion in DI water decreased as the phosphate content of doped Cris increased (P-39.1 released 92±.08% and P-331 released 71±.05%). Which is due to the greater % ionic character of Si-O (51.3%) compared to P-O (38.73%). The higher % ionic character of Si-O bonds makes them easier to ionize and detach from the material surface and vice versa for P-O bonds. In other words it will be harder to remove a polymerized P-O-P bond in comparison to a Si-O-P bond. Furthermore, FTIR proved this assumption by showing an increase in the area of the O-Si-O bending bands around 488.1 and 629.8 cm^{-1} after immersion for sample P-331 from 2 to 30.2 and from 5.4 to 17.7, respectively. In fact an increase in the O-Si-O bending band area around 488.1 and 629.8 cm^{-1} can be seen for all other doped samples. Additionally, a significant increase in the Si-O-Si symmetric and Si-O-Si asymmetric band areas is noticed after immersion for all doped samples. In conjunction with the increase in area of the silicate functional group bands, a decrease in area for all phosphate functional bands is observed for all doped samples. These results from the FTIR analysis showed that the phosphate ions released from the material activated the surface and exposed the silicate functional groups for pre-immersed samples of Cris (Figure 64).

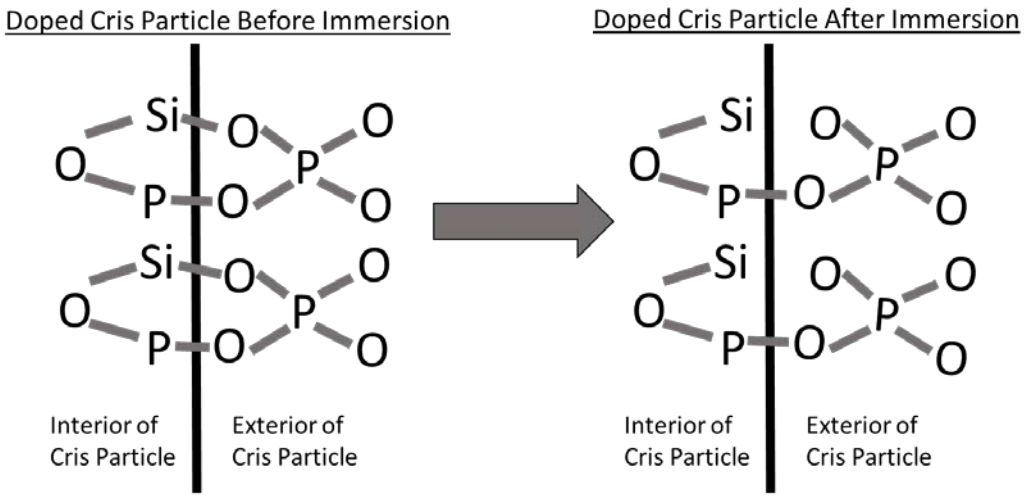

Figure 64: Cris before immersion showing formation of polymeric P-O-P chains on surface due to increase in P_20_5 content and after immersion showing the exposure of surface silicate functional groups

4.3 Role of Phosphate and Silicate Functional Groups on Drug Adsorption

4.3.1 Role of Phosphate and Silicate Functional Groups on Drug Adsorption for Non-Immersed Cris Samples

HPLC and FTIR analyses showed that ceramics that had higher content of O-Si-O bending bands facilitated Vanc adsorption. On the other hand surfaces with a higher content of v_4 PO_4/O-P-O bending and P=O stretching bands did not enhance Vanc adsorption. This is apparent as the Vanc adsorbed for samples P-0 to P-331 decreases from 2.81±.09 to 2.45±.06 mg, respectively ($p < 0.001$). FTIR with Gaussian fitting shows that the drug adsorption (signaled by a significant decrease in band area or disappearance) of the silicate functional groups decreases as the phosphate content increases. This can clearly be seen in the O-Si-O bending band at 498 cm^{-1} of sample P-0 where a decrease in band area occurs from 23.6 to 5.4 after drug immersion due to drug adsorption, but for sample P-331 there is an increase in the O-Si-O bending band area from 2 to 14.2 after drug immersion. This same result is noted in other bands of silicate functional groups of doped samples. This increase in area of the O-Si-O bending band of P-331, and other silicate functional bands in doped samples may be due to the release of surface phosphate functional groups. This assumption is based on the Gaussian fitting results of the FTIR data for sample P-331 (contains the most P_2O_5) which shows the disappearance of O-P-O bending (594.1 and 611.3 cm^{-1}), P-O-P bending (812.6 and 748 cm^{-1}), and P-O-H stretching bands (1441.9, 1458.1, 1475.4, and 1513 cm^{-1}) which may be due to either phosphate release from the surface exposing the silica functional groups or drug adsorption. Comparison between the drug binding may also be affected by the positive charge of silicate ions (SiO_2^{+4}) in comparison to the phosphate ion (PO_4^{-3}). Since

most of the functional groups on Vanc have a negative charge it is possible that the increase in phosphate content repelled the drug molecule while the silicate has a greater tendency to attract the Vanc molecule. A similar result was found by Xia et. al. where the increase in silicate content of their samples (58S and 77S) increased the adsorption of amino (NH_2^{-1}) and hydroxyl (OH^{-1}) gentamicin functional groups [15].

4.3.2 Role of Phosphate and Silicate Functional Groups on Drug Adsorption for Pre-Immersed Cris Samples

As concluded in section 4.2, FTIR analysis showed that the phosphate ions released from the material activated the surface and exposed the silicate functional groups for pre-immersed samples of Cris. The activation of the exposed silicate functional groups is apparent in the results of the Gaussain fitting of FTIR due to the decrease of all silicate functional group bands (O-Si-O bending, Si-O-Si symmetric stretching, Si-O-H stretching, Si-O-Si stretching, and Si-O-Si asymmetric stretching) in each sample after drug loading indicating adsorption of Vanc onto the silicate functional groups. The increase in drug adsorption is noticed for all pre-immersed doped samples P-39.1, P-78.2, P-165.5, and P-331 which adsorbed 4% (3.02 ± 0.03 mg), 22% (3.14 ± 0.08 mg), 12% (2.74 ± 0.04 mg), and 7% (2.62 ± 0.03 mg) more drug than the non-immersed samples, respectively. The small increase in drug adsorption for samples P-165.5 and P-33.1 may be due to the high % of P_2O_5 still left on the surface of the samples which the Gaussian fitting of FTIR confirms by the large presence of phosphate functional group bands still present after immersion. Once again these results are in agreement with those that Xia et. al. obtained [15]. Similarly, it was found in El-Ghannam's results that the amount of fetal bovine serum adsorbed onto SCPC samples C1S3, C1S1 and C3S1 decreased as the mole % of phosphate content increased (5.0%, 11.5%, and 20.5%, respectively) and vice versa for mole % of silicate content (63.7%, 49.0%, and 29.2%, respectively) [17].

4.4 Role of Phosphate and Silicate Functional Groups on Drug Release Kinetics

HPLC analyses showed that the drug release kinetics were faster and greater for samples with a higher content of silicate functional groups on the surface and vice versa for samples with a greater content of phosphate functional groups. This is seen by the drug release kinetics of non-immersed samples where the cumulative, %, and deceleration of drug release in the first four hours decreased ($p < 0.05$) drug release from samples P-0 (1.521±.026 mg; 37.66±.89 %;-66.92 μg of Vanc/mL /hr^2) to P-331 (1.276±.016 mg; 33.46±.77 %;-34.07 μg of Vanc/mL /hr^2), respectively. On the other hand the pre-immersed samples experienced a faster and greater drug release than the non-immersed samples due to the increase in silicate functional groups bonding to Vanc functional groups. The values of cumulative, %, and deceleration of drug release in the first four hours for pre-immersed samples show an increase ($p < 0.05$) from samples P-0 (1.505±.014 mg; 33.59±1.35 %; -72.60 μg of Vanc/mL/hr^2) to P-331 (1.581±.057 mg; 42.27±1.51 %; -46.04 μg of Vanc/mL/hr^2). Furthermore, during the first 4 hours of burst release the percentage of drug released from the total amount of drug loaded for non-immersed samples P-0 was 41 % and for P-331was 26 %. After the 4 hours of Vanc release the amount of Vanc available for release for samples P-0 and P-331 was .898 mg and .945 mg, respectively. The same relationship was found for pre-immersed samples during the first 4 hours of burst release the percentage of drug released from the total amount of drug loaded for samples P-0 was 42 % and for P-331 was 30 %. After the 4 hours of Vanc release the amount of Vanc available for release for samples P-0 and P-331 was .873 mg and 1.106 mg, respectively. These results indicated the effect of phosphate content on decreasing the drug release rate. The drug release kinetics showed

that the release of phosphate ions from the surface of Cris prior to drug loading exposed active silicate functional groups that enhanced drug binding by physisorption which in turn facilitated rapid release kinetics. On the other hand, a slower drug release rate was observed as the phosphate functional groups increased on the material surface due to chemisorption. Furthermore, these results showed that as the amount of phosphate content increased the amount of drug released during the burst release stage decreased, while the drug available for release during the sustained release phase increased and vice versa for a higher silicate content. This trend in the release of Vanc was also demonstrated in the work of Daculsi et. al. with CDA and BCP bioceramics, where CDA (Ca/P=~1.57) samples had a higher content of phosphate functional groups than BCP (Ca/P=~1.54) [10-12]. Furthermore, it is also noted that in the studies of Daculsi et. al. samples of CDA (Ca/P=~1.57) and BCP (Ca/P=~1.54) have a substantially longer elution (100 minutes, and 3 to 7 days, respectively) of Vanc in comparison to the rapid drug elution of mesoporous silica samples SBA-15 (~10 minutes) and FDU-12 (~ 10 minutes) without any linker as found in the study by Carmona et. al [10-13].

CHAPTER 5: CONCLUSIONS

The results from this study showed that it is possible to engineer drug adsorption and release kinetics by modifying the surface functional groups of a bioceramic using silicate and phosphate functional groups. It was also shown that the exposure of silicate functional groups enhanced drug adsorption by physisorption due to the rapid release kinetics. While less drug adsorption and a slower drug release rate due to chemisorption was observed as the phosphate functional groups increased on the material surface. Furthermore it was shown that the sustained release profile can be engineered by controlling the phosphorus content of the bioceramic drug carrier. It was demonstrated that as phosphate content increased a smaller percentage of drug was released in the burst release stage, while for the sustained release a significantly greater amount of drug was available for release. Also that it is possible to enhance the burst release stage of a bioceramic drug carrier by increasing the silicate functional groups. It was shown that the presence of the silicate functional groups increased the % of drug released during the burst release stage and decreased the amount of drug released in the sustained release stage. Additionally, it was shown that a bioceramic with more silicate functional groups increased the rate of drug release and vice versa for samples containing more phosphate functional groups. Recommendations from this study would be to study the effect of other functional groups and drug combinations in order to build an understanding on how to control drug adsorption and release kinetics using other functional groups.

The knowledge of knowing how each functional group and drug combination effect drug binding and release kinetics can be documented in a database and be used in a clinical setting to tailor bioceramic DDS to cure diseases.

REFERENCES

1. Hoffman, A.S., *The origins and evolution of "controlled" drug delivery systems.* Journal of Controlled Release, 2008. **132**(3): p. 153-163.

2. Ummadi, S., et al., *Overview on controlled release dosage form.* International Journal of Pharma Sciences, 2013. **3**(4): p. 258-269.

3. Andersson, J., et al., *Influences of material characteristics on ibuprofen drug loading and release profiles from ordered micro-and mesoporous silica matrices.* Chemistry of Materials, 2004. **16**(21): p. 4160-4167.

4. Cosijns, A., et al., *Porous hydroxyapatite tablets as carriers for low-dosed drugs.* European Journal of Pharmaceutics and Biopharmaceutics, 2007. **67**(2): p. 498-506.

5. Kundu, B., et al., *Development of porous HAp and β-TCP scaffolds by starch consolidation with foaming method and drug-chitosan bilayered scaffold based drug delivery system.* Journal of Materials Science: Materials in Medicine, 2010. **21**(11): p. 2955-2969.

6. Lopez-Heredia, M.A., et al., *An injectable calcium phosphate cement for the local delivery of paclitaxel to bone.* Biomaterials, 2011. **32**(23): p. 5411-5416.

7. Paul, W., J. Nesamony, and C.P. Sharma, *Delivery of insulin from hydroxyapatite ceramic microspheres: preliminary in vivo studies.* Journal of biomedical materials research, 2002. **61**(4): p. 660-662.

8. Vallet-Regi, M., et al., *A new property of MCM-41: drug delivery system.* Chemistry of Materials, 2001. **13**(2): p. 308-311.

9. Zamoume, O., et al., *Macroporous calcium phosphate ceramic implants for sustained drug delivery.* Materials Science and Engineering: C, 2011. **31**(7): p. 1352-1356.

10. Gautier, H., G. Daculsi, and C. Merle, *Association of vancomycin and calcium phosphate by dynamic compaction: in vitro characterization and microbiological activity.* Biomaterials, 2001. **22**(18): p. 2481-7.

11. Gautier, H., et al., *Isostatic compression, a new process for incorporating vancomycin into biphasic calcium phosphate: comparison with a classical method.* Biomaterials, 2000. **21**(3): p. 243-9.

12. Obadia, L., et al., *Calcium-deficient apatite: influence of granule size and consolidation mode on release and in vitro activity of vancomycin.* Biomaterials, 2003. **24**(7): p. 1265-1270.

13. Carmona, D., F. Balas, and J. Santamaria, *Pore ordering and surface properties of FDU-12 and SBA-15 mesoporous materials and their relation to drug loading and release in aqueous environments.* Materials Research Bulletin, 2014. **59**: p. 311-322.

14. Doadrio, A.L., et al., *Mesoporous SBA-15 HPLC evaluation for controlled gentamicin drug delivery.* J Control Release, 2004. **97**(1): p. 125-32.

15. Xia, W. and J. Chang, *Well-ordered mesoporous bioactive glasses (MBG): a promising bioactive drug delivery system.* Journal of Controlled Release, 2006. **110**(3): p. 522-530.

16. Mir, M., et al., *Synthesis and characterization of calcium deficient apatite granules for drug eluting bone graft applications.* Ceramics International, 2014. **40**(7): p. 10719-10725.

17. El-Ghannam, A.R., *Advanced bioceramic composite for bone tissue engineering: Design principles and structure–bioactivity relationship.* Journal of Biomedical Materials Research Part A, 2004. **69**(3): p. 490-501.

18. AnTHOny, J., *BideAux, rA, BlAdH, KW, & niCHOlS, mC (1995) Handbook of Mineralogy. Silica, Silicates.* Mineral Data Publishing: Tucson, Arizona. **2**(1): p. 46.

19. Withers, R., J. Thompson, and T. Welberry, *The structure and microstructure of α-cristobalite and its relationship to β-cristobalite.* Physics and Chemistry of Minerals, 1989. **16**(6): p. 517-523.

20. Jordan, D. and P. Reynolds, *Vancomycin*, in *Antibiotics*. 1967, Springer. p. 102-116.

21. Robles Piedras, A.L., *Therapeutic drug monitoring of vancomycin.* 2009.

22. Salter, C.J., R.C. Mitchell, and A.F. Drake, *Infrared spectroscopic studies of vancomycin and its interactions with N-acetyl-D-Ala-D-Ala and N, N'-diacetyl-L-Lys-D-Ala-D-Ala.* Journal of the Chemical Society, Perkin Transactions 2, 1995(12): p. 2203-2211.

23. McCusker, L., et al., *Rietveld refinement guidelines.* Journal of Applied Crystallography, 1999. **32**(1): p. 36-50.

24. Shannon, R.t., *Revised effective ionic radii and systematic studies of interatomic distances in halides and chalcogenides.* Acta Crystallographica Section A: Crystal Physics, Diffraction, Theoretical and General Crystallography, 1976. **32**(5): p. 751-767.

25. Parise, J.B., et al., *Pressure-induced phase transition and pressure dependence of crystal structure in low (α) and Ca/Al-doped cristobalite.* Journal of applied physics, 1994. **75**(3): p. 1361-1367.

26. Etchepare, J., M. Merían, and P. Kaplan, *Vibrational normal modes of SiO2. II. Cristobalite and tridymite.* The Journal of Chemical Physics, 1978. **68**(4): p. 1531-1537.

27. Ocana, M., et al., *Polarization effects in the infrared spectra of α-quartz and α-cristobalite.* Physics and Chemistry of Minerals, 1987. **14**(6): p. 527-532.

28. Swainson, I., M. Dove, and D. Palmer, *Infrared and Raman spectroscopy studies of the α–β phase transition in cristobalite.* Physics and chemistry of minerals, 2003. **30**(6): p. 353-365.

29. Eichert, D., et al., *Nanocrystalline apatite-based biomaterials: synthesis, processing and characterization.* Biomaterials research advances, 2007: p. 93-143.

30. Eichert, D., et al. *Specific characteristics of wet nanocrystalline apatites. Consequences on biomaterials and bone tissue*. in *Key Engineering Materials*. 2004. Trans Tech Publ.

31. Rey, C., et al., *Physico-chemical properties of nanocrystalline apatites: implications for biominerals and biomaterials.* Materials Science and Engineering: C, 2007. **27**(2): p. 198-205.

32. Swet, J.H., et al., *A silica-calcium-phosphate nanocomposite drug delivery system for the treatment of hepatocellular carcinoma: In vivo study.* Journal of Biomedical Materials Research Part B: Applied Biomaterials, 2014. **102**(1): p. 190-202.

33. Dayanand, C., et al., *Structural investigations of phosphate glasses: a detailed infrared study of the x (PbO)-(1− x) P2O5 vitreous system.* Journal of materials science, 1996. **31**(8): p. 1945-1967.

34. Ye, H., X.Y. Liu, and H. Hong, *Characterization of sintered titanium/hydroxyapatite biocomposite using FTIR spectroscopy.* Journal of Materials Science: Materials in Medicine, 2009. **20**(4): p. 843-850.

35. ElBatal, H., et al., *Characterization of some bioglass–ceramics.* Materials Chemistry and Physics, 2003. **80**(3): p. 599-609.

36. Ming, C., Y. Greish, and A. El-Ghannam, *Crystallization behavior of silica-calcium phosphate biocomposites: XRD and FTIR studies.* Journal of Materials Science: Materials in Medicine, 2004. **15**(11): p. 1227-1235.

37. Pacheco, H., et al., *Tissue engineering scaffold for sequential release of vancomycin and rhBMP2 to treat bone infections.* Journal of Biomedical Materials Research Part A, 2014. **102**(12): p. 4213-4223.

APPENDIX A: PROTOCOL FOR X-RAY DIFFRACTION (XRD) WITH RIETVELD REFINEMENT

The following is a detailed protocol of how XRD diffraction with Rietveld Refinement was performed in this study using the PANalytical's X'Pert PRO Materials Research Diffractometer (PANalytical, Westborough, MA) and X'Pert HighScore Plus program. This protocol will go over sample preparation, XRD sample alignment, XRD sample analysis, and performing Rietveld Refinement. The first step in this protocol was to properly prepare the sample for XRD (λ=1.54059 Å) analysis:

1) First the Ceramic sample was ground into a very fine powder using an agate mortar and pestle. Grinding was performed until the powder began to stick to the surface of the mortar and pestle. The fine powder will allow for a better signal to noise ratio.
2) Next the sample was placed into the zero background holder (ZBH) in a manner such that the powder was a flat consistent medium in the ZBH cavity. The powder was pressed into the ZBH cavity using a flat surface and non-stick paper or film as in Figure 65. (Note: after pressing, the powder must be flush with the outer surface of the ZBH cavity.)

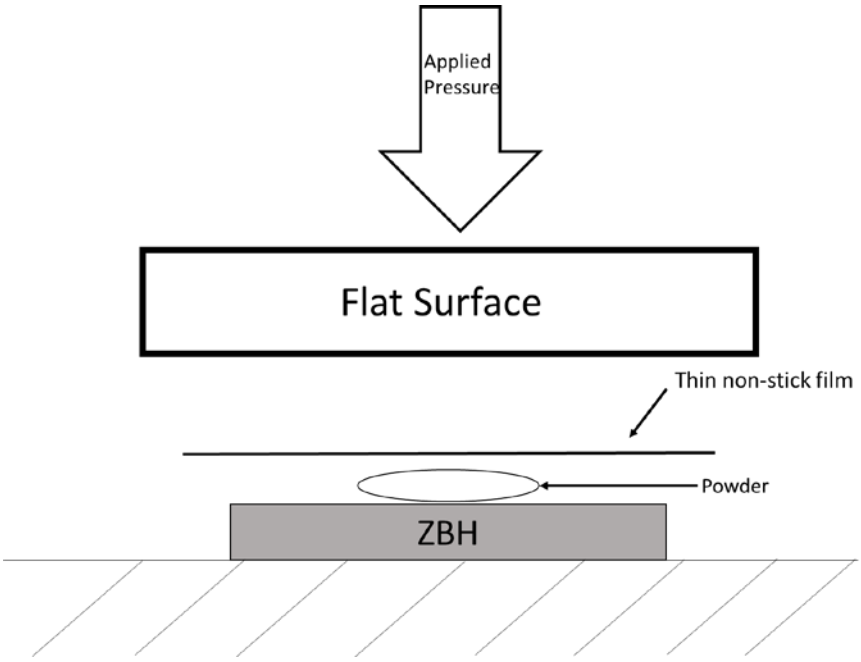

Figure 65: ZBH powder sample loading schematic

3) Next the X'pert Data Collector program was opened and set up as follows:
    a. The instrument configuration was set up by going to the instrument menu>selected Connect>selected configuration_1 and clicked on ok button
    b. the X-ray voltage and current was setup by going to the instrument settings tab and double clicked to bring up instrument settings window>selected X-ray tab, set voltage and current to 45kV and 40mA, respectively in increments (Note: turning on the voltage and current to 45kV and 40 mA in one step can damage the X-ray tube)

4) After the X'Pert Data Collector program has been setup the sample and X-ray beam alignment can be done as follows:
    a. The beam optics were changed in both the hardware and software:
        i. Incident beam: Divergence slit = 1/32^{o} , attenuator = Cu/Ni 0.2/0.02 mm manual, and do not switch was selected
        ii. Diffracted beam: receiving slit = 0.27 mm collimator, soller slit = soller slit 0.04 rad.
        iii. Under the tabs of incident beam optics and diffracted beam optics the change in hardware was set.
    b. The sample stage offsets were set to 0 in the instrument settings window by selecting position and setting all positions to 0. Afterwards ok was clicked to position the sample stage with the sample loaded.
    c. Next the straight beam alignment was done by the 2theta scan to find 0 position of 2theta (Note: this is only required for first sample):
        i. Select the measure menu>select manual scan and which brings up the prepare manual scan window.
        ii. In the prepare manual scan window set the scan axis to 2Theta, mode to continuous, range to 2^{o}, step size to 0.01^{o}, and time per step to 0.50 s.
        iii. Start was clicked and a manual scan window appeared to show the progress and results of the alignment.
        iv. Peak mode was selected by right-clicking the manual scan window and align was clicked to move the 2 theta to the center of the peak.

v. Next the 2 theta position was entered by going to user settings > selecting sample offsets> selecting set new zero.

d. Next the beam cut alignment by Z scan was done to align the sample surface to the focus of the diffractometer:

i. Select Z in the instrument settings window and set it to 8. (Note: this is to make surface sample surface is in the view of the diffractometer)

ii. In the prepare manual scan window set the scan axis to Z, mode to continuous, range to 4 mm, step size to 0.01^{o}, and time per step to 0.50 s and click start to begin scan.

iii. Afterwards use the move mode by right-clicking to align the cursor line to cut the beam signal in half.

e. Next the sample tilt alignment was done to align the sample surface with the straight beam:

i. In the prepare manual scan window the scan axis was set to omega, mode to continuous, range to 4^{o}, step size to 0.01^{o}, and time per step to 0.50 s and click start to begin scan.

ii. After the scan the peak mode was selected by right-clicking and align was clicked to move the cursor line to cut the beam signal in half.

iii. The sample offsets were changed under the user settings menu to set a new 0

f. Another beam cut alignment by Z scan may be done to finish up the alignment

5) After alignment the hardware optics were changed to the following:
    a. incident beam optics: Divergence slit = 1^o divergence fixed slit, attenuator = Ni 0.02mm attenuator
    b. Diffracted beam optics: receiving slit = none, soller slit = 0.04 rad.
    c. Change the settings in the software optics
6) The program scan was then set to the following parameters:
    a. Scan Axis = Gonio
    b. 2θ range = 15^o to 55^o
    c. time step = 2 seconds
    d. scan speed = 0.01 ^{o}/s
7) Once the scan was completed the file of the XRD pattern with extension .XRDML was saved onto a flash drive.
8) Next the .XRDML file can be opened on the X'Pert HighScore Plus program to perform Rietveld refinement. The following steps were followed before performing Rietveld refinement:
    a. view>desktop name> and select structures from drop down box
    b. customize>defaults>global parameter defaults and set background method and profile base width to 8 or more in refinement
    c. customize>program settings and select "show selected phase profile"
9) The following steps start Rietveld Refinement:
    a. file>open and select your experimental XRD pattern

b. file>insert and select the crystallographic phases that will be used for refinement
c. analysis>Rietveld>click start pattern simulations
d. analysis>Rietveld>refinement mode>select semi-automatic mode

10) Finally you are ready to do a Rietveld refinement in the X'Pert HighScore Plus program (note: only refine one parameter at a time when beginning; too many parameters can cause a bad refinement or the program to crash; Furthermore, to check if a refinement is being well done the R statistical factors can be checked by selecting the global parameters under the object inspector and selecting agreement indices; a good refinement is being done when R statistical factors are reaching a value of 10 or below):
    a. First the scale factor is refined by selecting it and clicking on the start refinement button
    b. The background was refined one parameter at a time (note: or you can automatically choose a background)
        i. Scale factor
        ii. Scale factor + flat background
        iii. Scale factor + flat background + coefficient 1
        iv. Scale factor + …..+….+……+1/x background
    c. Now that a background is available look at the data (R statistical factors and XRD pattern) to check if the refinement is good if not refine the peak positions by refining specimen displacement

d. To further check the quality of refinement go to view>additional graphics> select difference plot (note: the difference plot will show you the difference between the experimental XRD pattern and the standard)
e. With the previous refinement parameters selected refine specimen displacement of zero shift error to take into account shifting (note: never refine both at the same time)
f. Next start refining the peak profiles start refining Cagliotti parameters W,V, U one at a time
g. Next refine the peak shape 1 without refining any Cagliotti parameters
h. Next look at the lowest peak angles to determine if you need to refine peak profile asymmetry (note: repeat steps 6-8 refining one parameter at a time under profile parameters)
i. Refine the lattice parameters a, b, and c at the same time
j. Now you can start refining different parameters at the same time one by one

It is important to have a good signal to noise to perform Rietveld Refinement as this will lead to a better refinement. It is also important to check that the R statistical factors after a refinement are near or below 10 (values below 10 mean data is acceptable). Furthermore, it is important to repeat the Rietveld refinement a few more times just to make sure the results are consistent.

APPENDIX B: PROTOCOL FOR FOURIER TRANSFORM INFRARED (FTIR) SPECTROSCOPY WITH GAUSSIAN FITTING

The following is the detailed protocol of how FTIR analysis with Gaussian fitting was performed in this study using the Nicolet 6700 FTIR in the diffuse reflectance mode with the Omnic software. This protocol will go over sample preparation, KBR Background scan, sample analysis, and performing Gaussian fitting. The first step encompasses the background scan and sample preparation:

1) KBr, was grinded to a fine powder then loaded into the sample holder using a spatula to make a flat consistent medium inside the sample holder cavity. The KBr was used as the background and collected from 400 to 4000 cm^{-1} range after 64 scans at a 2 cm^{-1}. (Note: the KBr scan will tell you about the conditions inside the machine. If there is too much noise in the KBr background scan turn up the purge gas flow and allow the FTIR to purge for at least 15 minutes to clean the FTIR environment of any impurities that may be in the system.)
2) To analyze the samples, FTIR grade KBr was grinded in an agate mortar and pestle and loaded into the sample holder using a spatula. Afterwards the sample was loaded on top of the KBr already present in the sample holder. Infrared spectra for each sample was collected in the 400 to 4000 cm^{-1} after 200 scans at a 2 cm^{-1} resolution range. (Note: the KBR with the sample must be a flat consistent medium in order to produce a good quality spectra with a good signal to noise ratio. If your sample is not flat it will be noticed in the quality of the spectra.)

The following are steps that must be done to the FTIR spectra before Gaussian fitting:

1) The FTIR spectra must be normalized to the highest peak intensity
    a. process>select normalize frequency
2) The baseline must be corrected by selecting “Aut Bsln” on the tool bar to automatically correct baseline.

Now the Gaussian fitting may be performed as follows:

1) analyze>select peak resolve
2) Set the following parameters for the Gaussian fit:
    a. Find Peaks = Gaussian
    b. Noise target= 10
    c. full width half height (FWHH) =15 (note: you may choose your own FWHH, this was used, because it worked well with my study)
    d. base line = no baseline (note: only for solids)
    e. sensitivity= low
3) Afterwards select find peaks and then select fit peaks. (Note: the Gaussian fitting takes longer as the amount of spectra analyzed increases. It is advisable to analyze the spectra using Gaussian fitting in small portions.)

After Gaussian fitting was completed the area, FWHH, position, and height of peaks can be seen by selecting the peaks icon. The data of the peaks can by copied by selecting the clip board button and putting the data into a .CSV file for further analysis of the peaks on a different software. Furthermore the statistics of the Gaussian fitting can be seen by selecting statistics (standard error of or near .05 is acceptable). Additionally the residual between the fit and experimental spectra can be seen to show the difference between the

fit and data. As with the Rietveld Refinement it is advisable to perform the Gaussian fitting a few more times to ensure your results are consistent.